Investigations to improve CTC-based liquid biopsy in pancreatic ductal adenocarcinoma by screening high volume of blood

Inaugural dissertation

for the attainment of the title of doctor

in the Faculty of Mathematics and Natural Sciences

at the Heinrich Heine University Düsseldorf

presented by

Rosa Guglielmi

from Monopoli, Italy

Düsseldorf, April 2023

from the institute for Experimental Surgical Oncology
at the Heinrich Heine University Düsseldorf

Published by permission of the
Faculty of Mathematics and Natural Sciences at
Heinrich Heine University Düsseldorf

Supervisor: Prof. Dr. med. Nikolas H. Stoecklein
Co-supervisor: Prof. Dr. rer. nat. Hans Neubauer
Mentor: Prof. Dr. rer. nat. Matthias Kassack

Date of the oral examination: 14.11.2023

Part of the data in the present thesis are included in:

Guglielmi, R., Lai, Z., Raba, K., G. van Dalum, J. Wu, B. Behrens, A. A. S. Bhagat, W. T. Knoefel, R. P. L. Neves & N. H. Stoecklein. *Technical validation of a new microfluidic device for enrichment of CTCs from large volumes of blood by using buffy coats to mimic diagnostic leukapheresis products.* Sci Rep 10, 20312 (2020).

Personal contribution: conduction of the experiments, data analysis and manuscript preparation, for an overall contribution of 75%.

Nikolas H. Stoecklein*, Georg Flügen*, **Rosa Guglielmi***, Rui P.L. Neves*, Thilo Hackert, Emrullah Birgin, Stefan A. Cieslik, Monica Sudarsanam, Christiane Driemel, Guus van Dalum, André Franken, Dieter Niederacher, Hans Neubauer, Tanja Fehm, Jutta M. Rox, Petra Böhme, Lena Häberle, Wolfgang Göring, Irene Esposito, Stefan A. Topp, Frank A.W. Coumans, Jürgen Weitz, Wolfram T. Knoefel, Johannes C. Fischer*, Ulrich Bork*, Nuh N. Rahbari*. *Ultra-sensitive CTC-based Liquid Biopsy for Pancreatic Cancer enabled by Large Blood Volume analysis.* Mol Cancer 22, 181 (2023).

*These authors contributed equally.

Personal contribution: conduction of the experiments, data analysis and drafting of figures, for an overall contribution of 20%.

TABLE OF CONTENTS

ABSTRACT

Pancreatic ductal adenocarcinoma (PDAC) is one of the most lethal cancers worldwide. Surgical resection combined with systemic therapies remains the only approach with curative intent, but the rapid progression of the disease reduces the chance to detect patients in early stages, when the surgery would be more efficient. The potential of pancreatic circulating tumor cells (CTCs) as liquid biopsy could help to guide therapy.

The main aim of this thesis was to investigate whether screening of large blood volumes could improve CTC detection and characterization. In a first step, the value of diagnostic leukapheresis (DLA) in PDAC was tested. Compared to a conventional blood sample, DLA could significantly increase CTC detection. Interestingly, detection of CTCs was correlated with impaired overall survival. Moreover, PDAC CTCs could be isolated from positive samples and subjected to single cell genomic profiling. This revealed pathogenic mutations in hotspot regions of *KRAS* and *TP53* as well as copy number alterations (CNAs) typical for PDAC, confirming the malignant origin of the isolated marker-positive cells. Besides commonalties, the genomic data also revealed differences with the matched tumor tissue, supporting the notion that CTC-based liquid biopsies can provide additional information on the systemic disease. However, due to their high white blood cells (WBCs) background, current CTC-detection is technically restricted to a fraction (~5%) of whole DLA products, limiting the utility of the approach for clinical applications. Thus, another goal of this work was to test the performance of a label-free spiral microfluidic chip that potentially allows processing of whole DLA products. The data revealed the feasibility of the approach although a loss of 50% of enriched cells was noticeable. DLA biochip efficiently processed up to $400x10^6$ WBCs per run (equivalent to ~ 120 mL PB) and never clogged. Moreover, a two-cycles enrichment of samples originally containing $400x10^6$ WBCs resulted in the 99.98% of WBC depletion (~ 60,000 WBCs remaining in the enriched sample).

In conclusion, it was demonstrated that the screening of high volume of blood allows to detect and analyze pancreatic CTCs, contributing to move towards the use of CTC-based liquid biopsy in PDAC management.

LIST OF ABBREVIATIONS

ACCEPT	automated CTC classification, enumeration and phenotyping
ADM	acinar-to-ductal metaplasia
APC	allophycocyanin
BC	buffy coat
BRACA	breast cancer protein
CA19.9	carbohydrate-antigen 19-9
CAF	cancer-associated fibroblast
CD45	cluster of differentiation 45 (leukocyte common antigen)
CDKN2A	cyclin dependent kinase inhibitor 2A
CHR	chromosome
CK	cytokeratine
CNA	copy number alteration
CTC	circulating tumor cells
ctDNA	circulating tumor DNA
CTdR	celltracker deep red dye
CTG	celltracker green dye
CTO	celltracker orange dye
Cy5	cyanine5
DEP	dielectrophoresis
DFF	dean flow fractionation
DLA	diagnostic leukapheresis
DMSO	dimethyl sulfoxide
DVT	dean vortex trapping

EGFR	epidermal growth factor receptor
EMT	ephitelial to mesenchimal transition
EpCAM	epithelial cell adhesion molecule
EV	extracellular vescicle
FDA	food and drug administration
FR_DLA	frozen DLA cohort
FSC	forward scatter
GAP	GTPase-activating protein
GDP	guanosine diphosphate
GEF	guanine nucleotide exchange factor
GTP	guanosine triphosphate
Her2	human epidermal growth factor receptor 2
KRAS	Kirsten rat sarcoma virus
mDLA	mimicking-DLA
MNCs	mononuclear cell
mPC	metastatic pancreatic cancer
MUC1	mucin1 protein
NGS	next generation sequencing
NSCLC	non-small-cell lung carcinoma
OS	overall survival
PanIN	pancreatic intraepithelial neoplasia
PB	peripheral blood
PBS	phosphate buffered saline
PCR	polymerase chain reaction

PDAC	pancreatic ductal adenocarcinoma
PE	phycoerythrin
PeCy7	phycoerythrin-cyanine7
PFS	progression-free survival
QC	quality control
qRT-PCR	real-time reverse transcription PCR
RAS	rat sarcoma virus
RT	room temperature
S1	sample 1
S2	sample 2
SMAD4	small mother against decapentaplegic family member 4
SNV	single nucleotide variant
SSC	side scatter
TP53	tumor protein 53
VAF	variant allele frequency
W1	waste 1
W2	waste 2
WBC	white blood cell
WGA	whole genome amplification

1. INTRODUCTION

1.1 Pancreatic cancer

1.1.1 Epidemiology and etiology

Pancreatic cancer is the thirteen most frequent cancer worldwide (1). However, with 466,003 deaths in 2020 (2) and an overall 5-year survival rate less than 10% (3) it is the seventh leading cause of cancer-related deaths worldwide (1).

The high lethality of the disease can be related to different aspects. Patients rarely exhibit symptoms until an advanced stage of the disease, leading to a late diagnosis which reduces the chances for a successful treatment (4). Secondly, even when operable tumors are detected, the patients show a high metastatic recurrence after the surgical resection indicating that dissemination of the tumor occurs since early stages, long before the clinical manifest disease (5, 6).

According to anatomical and histological differences within the pancreas, different neoplasm subtypes can arise. Pancreatic ductal adenocarcinoma (PDAC) is the most common subtype (7), accounting for more than 90% of all pancreatic cancer cases (4).

Although the causes of pancreatic carcinoma are not yet fully known, there are identified risk factors as tobacco smoking, type 2 diabetes, obesity, alcohol abuse, age, ethnicity, family history and personal history of chronic pancreatitis (8). Furthermore, some genetic alterations that predispose to pancreatitis and some genetic mutations in BRACA1 and BRACA2 are associated with increased risk of PDAC (8).

1.1.2 Carcinogenesis of PDAC

Anatomically the pancreas is divided into a head, neck, body, and tail. Functionally, the pancreas comprises two compartments, the exocrine and the endocrine part, respectively (9). Histologically, the pancreas contains cells of exocrine (acinar cells), epithelial (ductal cells), and endocrine (α, β, δ, ε cells) origin (4). Based on the anatomical, functional and histological differentiation, different malignant tumor subtypes can arise (10). The PDAC arises from the exocrine compartment (11) and can grow in every anatomical region, although it is mostly found in the head of the organ (12). Under macro- and micro-environmental stimuli, as tissue damage and inflammatory or stress conditions, acinar cells transdifferentiate to more epithelial phenotypes (“ductal-like”) (figure 1) with varying degrees of cellular atypia and

differentiation (4, 13). During this process, which is called acinar-to-ductal metaplasia (ADM), acinar cells acquire "progenitor cell-like" features and are more susceptible to pro-oncogenic hits, which can lead to pancreatic intra-epithelial neoplasia (PanIN) (4). PanINs are usually small precursor lesions from which PDAC can arise (14). Subsequently, genetic and epigenetic dysregulations contribute to the further progression to invasive PDAC (15). Cancer cell invasion can induce a desmoplastic reaction, which is characterized by the presence of a dense stroma of cancer-associated fibroblasts (CAFs) and inflammatory cells (16). Activated CAFs, in turn, secrete factors that promote the cell proliferation and the metastasis (16). At diagnosis, the liver and lungs are the most common metastatic sites (17). *In vivo* models of pancreatic cancer progression demonstrated that in parallel to tumor formation at the primary site, the dissemination of PDAC cells out from the primary tumor and the seeding of distant organs occurs (18), giving a valid explanation to the evidence that the majority of patients with PDAC have already metastasis at diagnosis.

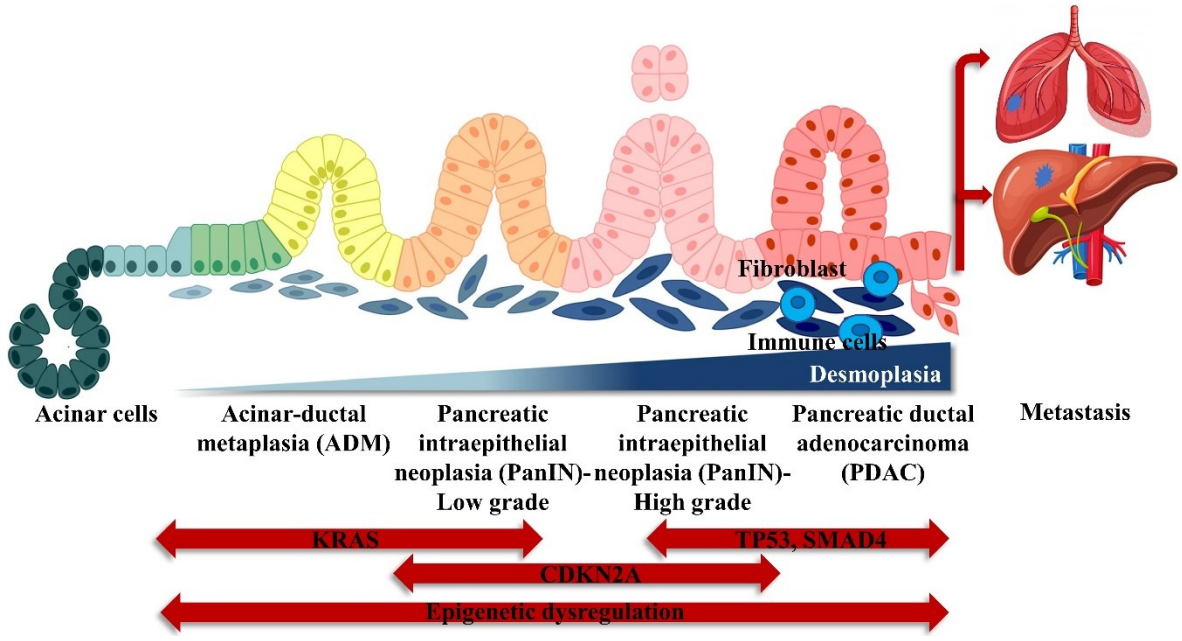

Figure 1. **Steps of PDAC carcinogenesis.** The formation of invasive PDAC is a multi-step process. Acinar cells transdifferentiate to "ductal-like" cells. Pro-oncogenic alterations can contribute to transform "ductal-like" cells into pancreatic intra-epithelial lesions (PanIN), and the precursor of PDAC develops. The accumulation of genetic and epigenetic changes contributes to the development of an invasive tumor, which mainly metastasize to the liver and lungs.
Image representing carcinogenesis steps was used and adapted from Orth et al. (4) under a Creative Commons Attribution 4.0 International License.

1.1.3 Genomic alterations: mutations in driver genes

Overt PDACs present significantly recurrent mutations mainly in four genes: KRAS oncogene and TP53, P16/CDKN2A and SMAD4 tumor suppressor genes (19-24), while mutations in additional protein-coding genes were reported at lower prevalence (≤10%) (23).

Point mutations in KRAS are found in over 90% of PDAC cases (24, 25). The KRAS proto-oncogene is part of the RAS family and encodes for a ~21 kDa small GTPase, which cycles between GTP-bound active and GDP-bound inactive states (26). The guanine nucleotide exchange factors (GEFs) promote the exchange of GDP for GTP, inducing a KRAS active state, while the GTPase-activating proteins (GAPs) induces the hydrolysis of GTP and the KRAS inactivation (26). Constitutive activation of RAS results in the persistent activation of various intracellular downstream signaling pathways and transcription factors inducing typical mechanisms of cancer as cell proliferation, migration, suppression of apoptosis (27). The most frequent KRAS mutations in human PDAC are point mutations causing amino acid substitutions in codon 12 and with lower frequency also in codons 13 and 61 (27-29) (table 1). These mutations can block the interaction between KRAS and GAPs, conferring a permanent activation of the KRAS protein, independently from extracellular stimuli (activating mutations). The presence of these mutations was demonstrated already in the very early stages of PanIN lesions (30, 31) and they were associated to the initiation of the carcinogenesis (32, 33) (figure 1). Nevertheless, other studies with mouse models highlighted the role of KRAS mutations also in the tumor maintenance (34).

Table 1. Frequently detected mutations in KRAS and TP53 genes in PDAC. The most frequent pathogenic missense mutations are detected in exon 2 and 3 of KRAS (27-29) and exon 5, 7 and 8 of TP53 (25, 35-41). CDS mutation: change in the nucleotide sequence; AA mutation: change in the peptide sequence.

Gene	Exon	CDS mutation	AA mutation
KRAS	2	c.34G>T	p.G12C
		c.34G>A	p.G12S
		c.35G>T	p.G12V
		c.35G>A	p.G12D
		c.38G>A	p.G13D
		c.37G>A	p.G13S
	3	c.183A>C	p.Q61H
TP53	5	c.524G>A	p.R175H
	7	c.742C>T	p.R248W
		c.743G>A	p.R248Q
	8	c.817C>T	p.R273C
		c.844C>T	p.R282W

TP53, the most frequent mutated gene in cancer (42), is the second most frequently mutated gene in PDAC and somatic mutations in TP53 occur in 70% of PDAC cases (23, 43, 44). TP53 encodes for p53, which is activated in response to stress signals and acts as a tumor suppressor, principally inducing growth arrest, apoptosis, cell senescence, DNA repair, metabolic adaptations (45). One of the mechanisms that allow this activity is the ability of the protein to bind the DNA and regulate the gene expression (46, 47). However, different mutations in TP53 can cause various effects, that can implicate a loss or a gain of function (48, 49). The most frequent mutations in TP53 are missense mutations (23) and in PDAC the most frequent missense mutations alter the codons 175, 248, 273, and 282 (25, 35-40, 50) (table 1), which are part of the DNA binding domain of the protein. Amino-acid substitutions in one or multiple of these codons cause conformational changes compromising the DNA binding and this was proposed as one of the mechanisms leading to p53 loss of activity as tumor suppressor (51). Mutations in TP53 (as well as in other genes as *P16*/CDKN2A, and SMAD4) have been associated with tumor progression and invasive carcinoma, and therefore proposed as later events in the PDAC carcinogenesis (33, 41, 52, 53) (figure 1).

1.1.4 Genomic alterations: copy number alteration

Beside the point mutations, larger genomic structural variations, i.e., amplifications and/or losses of DNA segments ≥ 1kb, were also identified in pancreatic cancer (54-56). Bulk whole genome sequencing revealed frequent copy number alteration (CNAs) in PDAC, which contribute to the complex mutational landscape of this cancer (19). Genome-wide DNA copy

number analyses revealed that the q-arm of chromosome 8 (Chr 8q), where the Myc oncogene resides, is the region most frequently affected by genomic gains, while chr. 9p is the region most frequently affected by genomic losses (54, 57). Additional gains have been observed in the chromosomes arms 6p, 12p, 18q and 19q, which contain cyclin D3, KRAS, GATA binding protein 6, protein kinase B, while additional losses were observed in chromosome arms 18q, 10q and 17p, which contain SMAD4, Phosphatase and Tensin homolog (PTEN) and TP53 (58). Many of these genes are known oncogenes or tumor suppressor. There are different hypotheses on the possible correlation of certain CNAs and genetic predisposition (55), disease progression (59) and poor prognosis (60) in PDAC. The dissection of CNA sub-clonal heterogeneity through the analysis of single CTCs might allow a better understanding of such mechanisms.

1.1.5 Diagnosis of PDAC

Patients with PDAC often present with non-specific symptoms, as weight loss, back pain, abdominal pain, and fatigue and are usually diagnosed already in advanced stages (61) Additionally, PDAC tends to disseminated and metastasize early, already when the tumor is considered small in size (<2cm) (62). Different methods for the diagnosis of PDAC are recommended by current guidelines and the decision of the most appropriate approach should be made in reference centers (61, 63, 64). Among the options, are the cross-sectional imaging, the endoscopic ultrasound combined with fine-needle aspiration, the histological evaluation of the surgery biopsy, and the screening of the CA19.9 as a serum biomarker (63). The aim of these methods is to identify the tumor, assess its spread and classify the tumor as metastatic, local advanced, borderline, or resectable. A proper classification of tumor stage is critical for the optimal delivery of stage-specific therapy (65).

Depending on the disease stage, histopathologic confirmation might be required to confirm malignant pancreatic lesions. A pathological confirmation is always required in locally advanced and metastatic PDAC (63). In these cases, KRAS-mutation analysis on cytopathological sections could increase the sensitivity and accuracy of the diagnosis, compared to cytopathology alone (66, 67). Nevertheless, each of the mentioned diagnostic strategies has its own limitations. The imaging, for example, can fail to detect small lesions, and in these cases the endoscopy with fine-needle aspiration biopsy is more sensitive (63). By contrast, endoscopic biopsies are challenging due to the anatomical position of the organ and might lead to false negative results due to the cannulation of stromal cells. Although the

classical biopsy remains the main option, this method is invasive and harbors the risk for tumor spread (63).

Furthermore, all these procedures do not guarantee an early diagnosis (68). Since it was demonstrated that the prognosis of patients with an early diagnosis improves after tumor resection compared to the prognosis of patients with unresectable tumor (69), additional strategies to early detect the tumor are urgently needed to improve the prognosis for PDAC patients. All together, these diagnostic limitations push towards the need to find approaches to complement the role of the current methods in order to improve the diagnosis and therefore also the prognosis. In this context, liquid biopsy is gaining an increasing interest (70). The liquid biopsy has been proposed as a promising tool for early detection of high-risk patients (71) and has the big advantage to be a noninvasive procedure, with no inherent risks to the patient.

In PDAC, highly specific tumor biomarkers are lacking (72). Currently, one of the most common blood-based biomarker which is used in the clinical routine of PDAC is the CA19.9 (73). However, its specificity and sensitivity are still a matter of debate. It was reported that CA19.9 has a sensitivity of 70–81% to diagnose pancreatic adenocarcinoma (74, 75), but high levels were also found in some benign forms of the disease (e.g. pancreatitis) and in other cancer types (e.g. colorectal cancer, gastric cancer, bladder cancer and uterine squamous cell carcinoma), raising doubts on the specificity of the marker (76).

Therefore, the validation of novel liquid biopsy derived biomarkers could contribute to improve the diagnosis in PDAC samples.

1.1.6 Treatment options in PDAC

To date, the surgical resection remains the only potential cure for PDAC. Pancreatic surgery combined with adjuvant treatment can improve the five-year survival up to around 30% for patients with resectable disease (69). In these cases, monotherapy with Gemcitabine is still used as adjuvant first line treatment (77, 78), despite recent evidences demonstrating better efficacy of a modified FOLFIRINOX (folinic acid, 5-fluorouracil, irinotecan and oxaliplatin) compared to Gemcitabine alone (79). However, most of PDAC patients are diagnosed in advance stage of the disease when the tumor has already metastasized and in these cases, a combined chemotherapy has been approved as first line therapy (FOLFIRINOX or Gemcitabine plus nab-paclitaxel) although the prognosis is still poor (78, 80, 81).

Unfortunately, only the 10-20% of the PDAC patients are detected early enough to qualify for a therapy with curative intention (82-84), while in the remaining cases only palliative treatments are offered. More recently, additional surgery during multimodal treatment has been extended to patients with unresectable PDAC, but the actual clinical benefits of resection have not yet been fully investigated (85). In these patients, the debate remains whether upfront surgery or neoadjuvant treatment is more beneficial (86).

Although advancements in the multimodal therapy, unfortunately PDAC shows a high chemotherapy resistance, partially explained by the extensive desmoplastic reaction, a poor vessel density, and hypoxia, which is common in PDAC (87, 88). Another reason, might be associated to the high level of inter- and intra- tumor heterogeneity in PDAC (89). In this context, the characterization of the molecular subtype may help to sort patients into definable and more uniform groups to better guide the treatment (19, 90, 91).

In the last decades, the potential of immunotherapy is gaining interest and many approaches aiming to trigger the immune system to attack cancer cells have been investigated. However, PDAC is a type of cancer that has a strong immunosuppressive microenvironment, making it challenging for single-agent immunotherapy to effectively treat the disease (92). Recent trials have focused on combining immunotherapy with standard chemotherapy to improve efficacy (93).

Other potential therapeutic targets are associated with altered genes, such as KRAS, TP53, CDKN2A, SMAD4, BRCA, APOBEC, and KDM6A (94). In particular, the KRAS gene is a focus of attention due to its high frequency of activating mutations and its critical role in PDAC growth and maintenance (34, 95). The use of inhibitors for KRAS and downstream components of the RAS pathway has been widely studied. However, the surface topology of the KRAS protein makes it a difficult drug target, hindering the design of high-affinity small-molecule antagonists (96, 97).

1.2 Liquid biopsy and CTCs

1.2.1 Introduction to liquid biopsy and CTCs

The potential utility of liquid biopsy in the cancer management is gaining an increasing interest as a complementary approach to the conventional tumor biopsy. Liquid biopsy assays have been studied as promising tools for diagnosis, prognosis and real-time monitoring of cancer progression and response to treatment (98-100). Liquid biopsies describe mainly blood

analysis, but this has been extended to the analysis of other body fluids (e.g. urine, saliva, spinal fluid) in a minimally invasive way (101), with negligible risks for the patient, at low costs and in short time. The nature of the approach could offer a chance to obtain relevant information in cases where a standard tumor biopsy is not feasible, such as when accessing the tumor location is difficult or when the origin of the tumor is unknown (102, 103).

Liquid biopsy of peripheral blood (PB) analyses in most cases circulating tumor cells (CTCs), circulating tumor-derived cell-free DNA (ctDNA), tumor derived cfRNA or tumor-derived extracellular vesicles (EVs) (100). Most studies report on the application of these analytes separately. Among these different biomarkers, CTCs are of particular interest because they can represent vital metastatic cells. Once that tumor cells have detached from the primary lesion, they can enter the bloodstream via intravasation (104-106) (figure 2A) and become CTCs. In the bloodstream, the main fraction of CTCs appear to undergo apoptosis before seeding in distant organs and only few cells seem succeed to metastasize (107). Recent findings suggest that CTCs, which travel in clusters or in association with neutrophils may have a greater contribution to the metastatic process compared to CTCs that travel as single cells and this seems to be associated with mechanical and immune features (108-110). In order to metastasize, CTCs need to extravasate into the surrounding tissue, find a suitable niche, and colonize (111) (figure 2B). Nevertheless, not all the surviving cancer cells disseminated to distant sites can initiate a metastasis. A fraction of cells can enter a quiescent state in their metastatic site and persist with the potential to reactivate and generate a metastatic lesion. This event is known as cellular dormancy and it is considered as one of the mechanism responsible for the failure of most therapeutic options targeting proliferating cells (112).

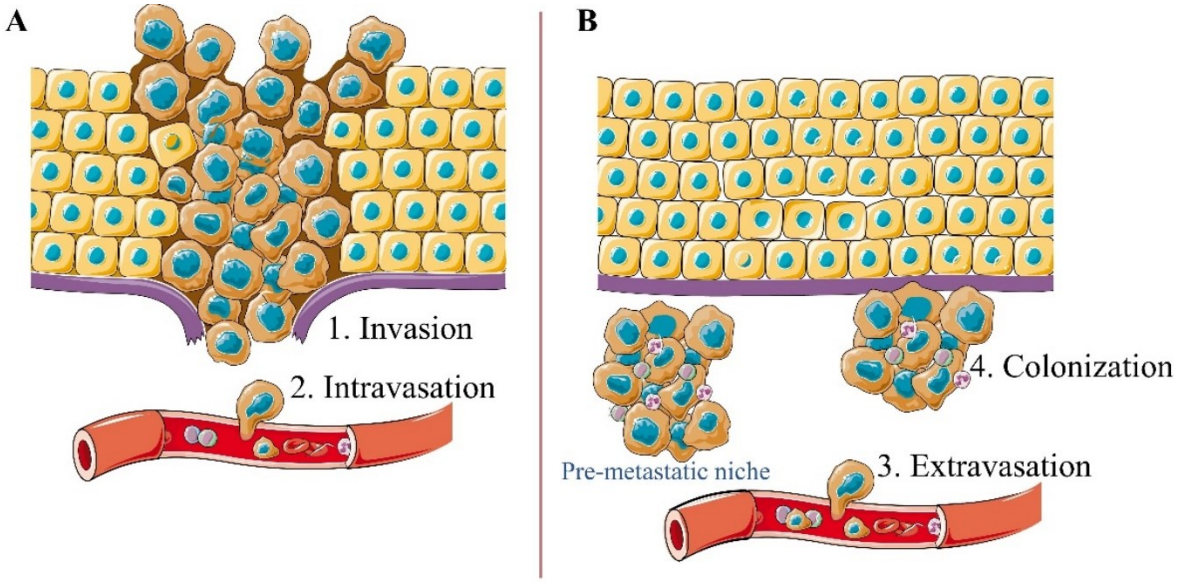

Figure 2. Metastatic cascade. (A) Tumor cells invade the local tissue and subsequently intravasate. **(B)** In the circulation some of them survive until reach distant organs, where they can extravasate. In the destination tissue, cancer cells start to divide and colonize and form a metastasis (113). *Created with the equipment from "Medical Specialities" attributed to Servier Medical Art by Servier, licensed under a Creative Commons Attribution 3.0 Unported License.*

Although CTCs are not currently used in clinical practice, there is high interest in these cells as tumor biomarkers. CTCs are typically detected in patient's blood sample, after a preliminary enrichment step that helps to reduce the number of background cells (figure 3). The diagnostic, prognostic and potentially predictive role of CTC enumeration has been demonstrated in patients with breast, lung, prostate and colorectal cancer (114-118). In addition, molecular characterization of CTCs offers the opportunity to profile tumor material at genomic, transcriptomic, proteomic and functional level, with the aim to better understand mechanisms of metastasis (119) and may help treatment decisions if clinical relevant targets are profiled (106). Over the years, many technologies have been developed with the aim to detect and isolate CTCs (120-122). However, a standardized integrated workflow that allows to detect, isolate, and genetically analyze CTCs is lacking.

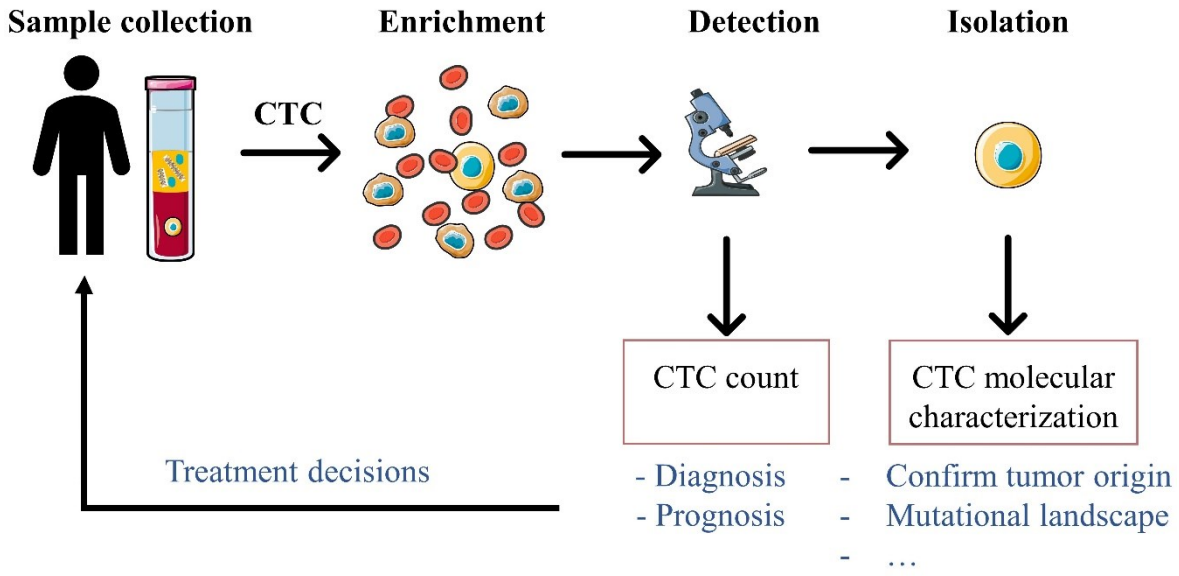

Figure 3. Circulating tumor cells based liquid biopsy: approach and utility. After blood collection, an enrichment approach should allow to increase the ratio between rare tumor cells and background cells, in order to help CTC detection. With the aim to detect CTCs, the target cells should be labelled. CTC detection allows for enumeration, but it could also allow cell isolation. CTC enumeration has been proposed as a diagnostic, prognostic and predictive tool. CTC isolation offers the chance to access genetic information and investigate tumor biology. Together, enumeration and molecular characterization might allow better treatment decisions and personalized therapies.
Created with the equipment from "Laboratory Equipment" attributed to Servier Medical Art by Servier, licensed under a Creative Commons Attribution 3.0 Unported License.

The detection of CTCs is technically very challenging for two main reasons. The first one is that these cells are extremely rare in circulation, compared to the blood cells (typically ~ 1 CTC per 10^8 blood cells). The second reason is that CTCs are very heterogeneous, both in terms of their biophysical characteristics (e.g. size, deformability) and phenotype (e.g. protein marker expression). Although CTCs are considered to be larger compared to WBCs (123), their size can vary over a wide range (124) while expression analyses (at protein and mRNA level) suggest that the phenotype of CTCs can change dynamically and different sub-population can co-exist (125, 126). The presence of these phenotypes is associated with important mechanisms proposed to explain the progression of cancer metastasis: the epithelial-mesenchymal transition (EMT) and its reversal mesenchymal-epithelial transition (MET) (126). During the EMT, tumor cells loose apicobasal polarity and cell-cell adhesions with disruption of the basolateral membrane and they acquire a mesenchymal phenotype by transiently expressing distinct mesenchymal markers (127, 128). These mechanisms generate cells that can express typical epithelial markers, as the cell surface marker epithelial cell

adhesion molecule (EpCAM) and the cytoplasmatic cytoskeletal proteins (CKs), but also cells that lost the epithelial markers and express mesenchymal-typical markers (as N-cadherin and vimentin), or a combination of both resulting in hybrid epithelial–mesenchymal CTCs (129, 130). In the last decade, it is gaining attention also the possible role of EMT to generate cells with the traits of cancer stem cells (CSC) (131, 132) constituting a subset of CTCs with a stronger potential to initiate metastasis (133).

1.2.2 Strategies to enrich circulating tumor cells

The low frequency in the blood and the heterogeneous phenotype of CTCs challenge the detection methods. Therefore, a key methodological step to help CTC detection is a preliminary enrichment step (figure 3). This approach aims to increase the ratio between tumor cells and background blood cells (134). CTC enrichment can be done with different methods, which are commonly grouped in molecular-based and biophysical-based (figure 4). Based on these methods, different technologies have been developed.

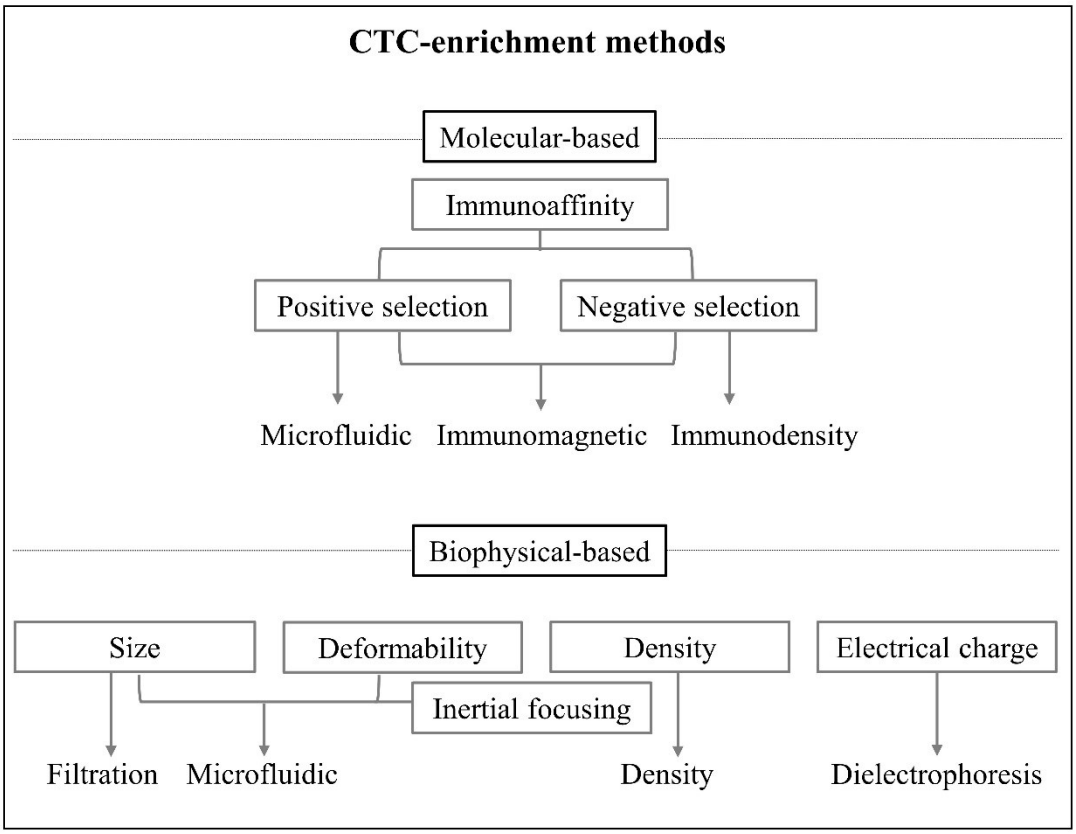

Figure 4. Methodological approaches to enrich CTCs. CTCs can be enriched based on their molecular or biophysical properties and different technologies have been developed to profit from those features to separate CTCs from the blood cells.

1.2.2.1 Molecular-based CTC enrichment

Several technologies have been developed to enrich CTCs with an immunoaffinity-based approach, by targeting either CTC surface antigens to directly capture the tumor cells (positive selection), or antigens which are not expressed by CTCs to deplete non-cancerous cells (negative selection) (121) (upper panel, figure 4). The most immunoaffinity-based technologies use antibodies against EpCAM and CD45, but some devices allow the users to introduce additional antibodies against tumor-associated antigens. The technologies based on immunocapturing can be sub-grouped in immuno- magnetic, -density and microfluidic methods.

For immunomagnetic enrichment, the antibodies can be coupled to magnetic ferrofluid (e.g. CellSearch® system) or microbeads (e.g. MACS® microbeads, Miltenyi Biotec, Germany, for positive selection (135) or EasySep, StemCell™ Technologies, Canada, for negative selection (136)) to allow the cell separation in a magnetic field.

Different technologies adopt immunomagnetic for CTC capturing (134), however CellSearch® system (Menarini Silicon Biosystems Inc., USA) is considered as the gold standard for CTC enumeration in metastatic breast, prostate and colorectal cancer (137-139) and it was clinically validated and approved by the Food and Drug Administration (FDA).

The CellSearch® system consists of two instruments: the CellTracks® Autoprep® system (Autoprep), and the CellTracks® Analyzer II (CTAII). The enrichment phase is performed by the Autoprep. The system captures CTCs based on the expression of epithelial markers. The ferrofluid is coated with anti-EpCAM antibodies and the cells that have bound the ferrofluid-conjugated antibodies are pulled to the magnets to be separated from the rest of cells (140) (positive selection). After enrichment, CTCs are also immunofluorescently labelled within the Autoprep to be later detected by image analysis at CTAII. According to CellSearch®-CTC selection criteria, a CTC is phenotypically defined as a nucleated cell, larger than 4 microns, EpCAM+, and/or CK+ (mainly CK 8, 18, and 19), and lacking the leukocyte common antigen (CD45−) (115, 141).

As an alternative, an immunodensity-based approach is available for negative selection (i.e. RosetteSep (StemCell™ Technologies)) (136). RosetteSep utilizes cocktails of tetrameric antibody complexes (anti- CD2, -CD16, -CD19, -CD36, -CD38, -CD45, -CD66b and -glycophorin A) to bind simultaneously leukocytes and RBCs and form cellular rosettes with higher density compared to the other cells. These aggregates can precipitate after density gradient centrifugation and they can be removed (134).

Further, different technologies have been developed to combine microfluidics and immunocapture. In these devices antibodies are immobilized on the surface of microfluidic channels while the blood flows at controlled slow flow rates to allow binding of the cells to the antibodies (121) (e.g. CTC-Chip (142, 143), HB-Chip (144), (Massachusetts General Hospital, USA)). With the aim to improve magnetic-based separation for CTC capture, magnetic and microfluidic strategies were combined. The result are systems where the sample is subjected to magnetic field while passing through microfluidic channels to maximize the effect of magnetic field in the sample (134) (e.g. i-Chip (Massachusetts General Hospital) (145), IsoFlux^{TM} system (Fluxion Biosciences, Inc., USA) (146)).

However, immunocapturing-based enrichment has limitations. For example, EpCAM-based methods might miss the capture of some CTCs that lost the expression of epithelial antigens in favor of mesenchymal antigens as consequence of the EMT (147, 148). Additionally, positive enrichment immunoaffinity-based methods usually require sample centrifugation steps that can cause CTC loss (121).

1.2.2.2 Biophysical-based CTC enrichment (ClearCell® FX system)

Extensive studies investigated the biophysical differences between CTCs and normal blood cells in terms of cellular size, density, deformability capacity and electrical membrane properties (123, 149). Based on these biophysical differences, different technologies have been developed to help the CTC enrichment.

Based on the finding that CTCs are larger (ranging from 17 µm to 52 µm) than RBCs (6-8 µm (150)) and WBC (7-20 µm) (123, 151-153), a simple strategy to enrich CTCs based on these size differences is the membrane filtration (e.g. ISET (154, 155)). The blood is pushed to pass through the pores of a membrane (typically 8 µm (156)) either under controlled pressure or by centrifugation, and, ideally, larger cancer cells should be retained on the membrane while smaller blood cells should pass through. The filtration principle was also used to build 3D-geometries, consisting in two layers of pore membrane and with the aim to preserve the cell viability (e.g. 3D-microfilter (157), SB microfilter (158)). However, filtration methods have some limitations, such as the possible clogging of membrane pores and the low purity, because many background cells are also retained on the membrane due to an overlapping size range between WBC and tumor cells (159, 160). Additionally, after

enrichment, the enriched cells remain stuck in the filter surface and their detachment is very challenging which hinders their isolation for downstream analyses.

Another method to enrich CTCs is based on differential cell density (161). For that, the sample is placed on the top of a separation medium and centrifuged to separate tumor cell from blood cells. The RBCs and neutrophils (density of >1.077 g/mL) pellet at the bottom while the CTCs and mononuclear cells (density of <1.077 g/mL) separate on the top of the gradient medium (Ficoll-Paque, Percoll) (123). However, the use of gradient media is not specifically intended for CTC enrichment, and this strategy is usually not very efficient in terms of CTC capturing and purity. Therefore, different technologies have been developed based on density gradient centrifugation with the aim to improve the CTC enrichment efficiency. For example, OncoQuik® (Greiner Bio-One, Germany) (162, 163) couples the density gradient centrifugation with filtration, which help to capture the CTCs on a membrane.

Microfluidic systems have been developed to enrich CTC based on differences in cell size and deformability (Parsortix^{TM} system (Angle North America, Inc., PA) (164)), and some of those use hydrodynamic forces and inertial focusing to separate CTCs (e.g. Vortex Technology (Vortex Bioscences, Inc., USA), ClearCell FX system (Biolidics Ltd, Singapore)) (165-167). Recently, Parsortix^{TM} system was FDA-cleared for gathering CTCs from metastatic breast cancer patients (168).

Compared to filtration- or density-based approaches, these technologies are considered as more gentle to separate CTCs from the background cells, better preserving the cell viability for downstream analyses, and they suffer less of clogging problems (169). The performance of spiral chips for processing standard blood samples has been previously reported (170, 171). The ClearCell® FX system allows a separation of the tumor cells from the blood cells based on differences in sizes and stiffness, according to the Dean Flow Fractionation (DFF) principle (165, 171-175). The system channels the sample, at a defined flow rate, through a spiral microfluidic channel with rectangular cross-section, the CTChip FR1 (figure 5). While flowing through the chip, blood cells, which tend to be smaller than cells from solid tumors, are more heavily influenced by the secondary Dean vortex which drags them to a position near to the outer wall of the microfluidic channel. In parallel, the larger tumor cells are more strongly influenced by the generated inertial lift forces and migrate to a position near to the inner wall. At the end of the spiral, the channel is branched out into two separate outlets and

because of the different positioning of the blood cells and tumor cells in the channel, the two populations can be recovered separately (176).

In the last years, technologies that rely on electric cell membrane properties were developed (177). During the tumor development, tumor cells modify their shape, nuclear/cytoplasm ratio and protein expression, acquiring changes in the polarity and electrical charge when suspended in a solvent. Because these properties are different in CTCs and WBCs, dielectrophoresis (DEP) principle can be used to separate these cell types (178). DEP allows for the directed movement of polarizable particles in a non-uniform electric field, and can therefore be used to manipulate the movement of particular types of cells in suspension based on the cellular membrane properties. Some technologies have been developed to combine the use of DEP and microfluidics (179).

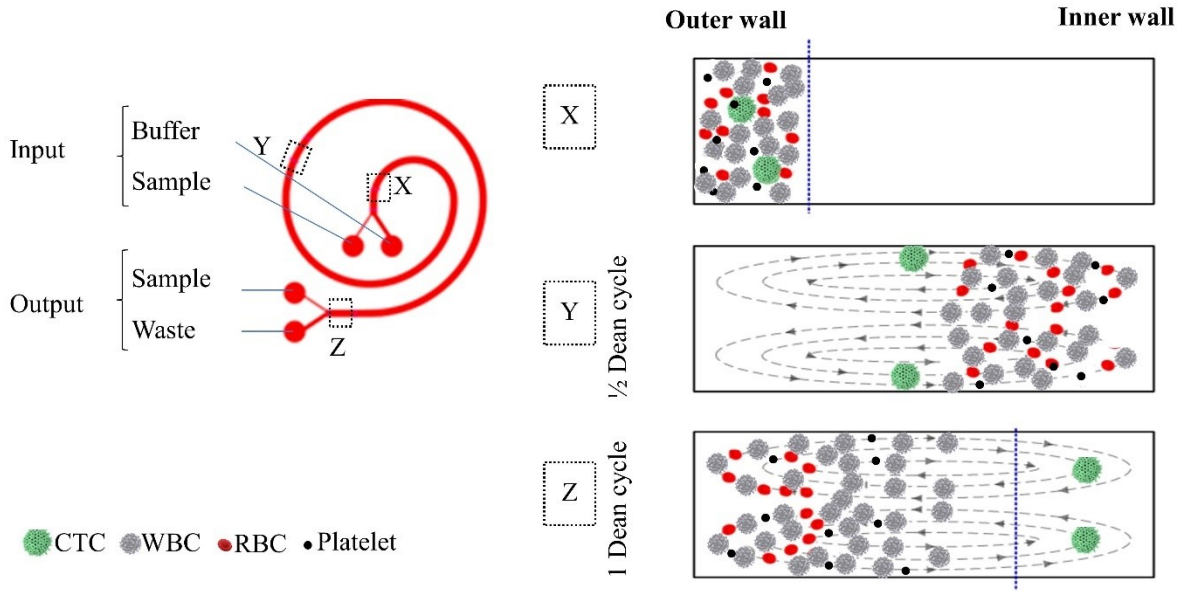

Figure 5. Spiral microfluidics and cell separation within CTChip FR1.
The left figure panel shows the schematic design of CTChip FR1: the buffer and the sample are directed into two separate input tubes; the CTC enriched fraction and the waste flow into two separate output tubes. The cross section of the chip (right panel) shows the positions of the blood cells (in white and red) and CTCs (in green) at three different positions along the chip flow (X, Y, Z of the schematic design).
Reused from Guglielmi et al. (176), Copyright 2013 by Creative Commons CC-BY-NC-ND.

1.2.3 Strategies to detect CTCs

No enrichment method can provide pure CTCs and after enrichment, the CTC-enriched samples still contain a fraction of leukocytes, which hinders CTC detection (180). In order to identify CTCs among the WBC background, a phenotypic profiling is required.

The detection of the expression of epithelial proteins, a hallmark of most epithelial malignancies (181-184), is currently the most abundantly used approach to distinguish epithelial CTCs from the mesenchymal blood cells. A typical method is the use of fluorescently labelled antibodies against CKs (e.g. CK8, CK18 and CK19) as positive markers, anti-CD45 as exclusion marker labeling WBCs, and DAPI for nuclear staining. Through multicolor image analysis with a fluorescence microscope or flow cytometry, CTCs can be detected as CK+/CD45-/DAPI+ cells (185).
However, epithelial markers on CTCs, such as EpCAM and CKs, may be downregulated as consequence of EMT and become undetectable (186-188) hindering CTC detection with the risk of false negative results. Several studies indicate that the use of additional markers might represent an advantage to increase the number of CTC detected (106, 121, 189). For example, the introduction of additional tumor associated markers (e.g. anti-Her2, -EGFR, -MUC1) or mesenchymal markers (e.g. vimentin or N-cadherin) could improve the detection of CTCs (180, 190).

In many protocols, the immunostaining for CTC detection is a post-enrichment step that is performed separately. This step usually requires several centrifugations and sample manipulation, which can increase the chance of CTC loss (188). To limit this problem, a possible solution could be the implementation within the enrichment technologies of an *in-situ* staining and an integrated imaging system, following the example of the CellSearch® system. Although the immunodetection is the most common approach used especially in Clinical Laboratory Improvement Amendments (CLIA)-certified molecular diagnostics laboratories (191), there are alternative methods, which might bypass the risk of false negative results. In this context, gene expression analysis has been used for CTC detection. Indeed, Real Time PCR (qRT-PCR) is a highly sensitive technique that allows to simultaneously analyze dozens of markers and detect even rare transcripts associated with CTCs (192). However, such molecular technique does not allow to isolate intact CTCs.

1.2.4 Clinical significance of CTC enumeration in PDAC using CellSearch®

The potential of the enumeration of CTCs (in particular with the CellSearch® system) as prognostic biomarkers has been widely investigated in different tumor entities. To date, CTC enumeration is accepted as prognostic and monitoring tool for breast (115, 193), prostate (116, 194) and colorectal (195, 196) cancer. However, in PDAC, heterogenous results are reported (197) and the number of studies is limited, which increases the uncertainty of the potential clinical value of CTCs in this tumor entity.

Table 2. Collection of data obtained from CellSearch®-based studies published between 2008 and 2021 and evaluating the prognostic role of CTCs in PDAC. Data were extrapolated from the 8 studies with the aim to collect information on the detection frequency and enumeration of CTCs at different stages of PDAC and their correlation with the prognosis (154, 198-203).

STUDY	PATIENT (number)	DETECTION RATE (%)	CTC/7.5 mL blood (median)	STAGE	PROGNOSIS
Kurihara et al., 2008	26	57%	16.9	IV	worse OS
Khoja et al., 2012	54	39%	0	IV	towards decreased OS
Bidard et al., 2013	29	5%	2.7	III	worse OS
Earl et al., 2015	45	20%	1	II–IV	worse OS
Bissolati et al., 2015	20	45%	3	IIa and b	no correlation to OS/PFS
Dotan et al. 2016	48	48%	4.9	mPC (IV)	no correlation to OS
Okubo et al., 2017	65	32.3%	1	III–IV	worse OS
Hugenschmidt et al., 2021	98	7%	1	IIb	worse CSS

Initial studies using CellSearch® Assay in PDAC have confirmed the presence of CTCs, but with significantly lower overall numbers (median of 2 CTC/7.5mL of blood) and detection frequency (range 5-57%) (table 2) (154, 198-203) compared to other epithelial tumors (115). These low counts and discrepant frequencies impact negatively the (discriminatory) power of CellSearch-CTCs as biomarkers. Nevertheless, with some exceptions (203), the majority of the studies showed that in metastatic patients (with non-resectable tumor) CTC positivity reflected a significant or a trend to poorer progression-free survival (PFS) and overall survival (OS) than what is observed in CTC-negative patients (198, 199, 201, 202, 204, 205) (table 2). No correlation was found in patients at resectable stage IIa and b (200). Of note, a consensual cut-off number for CTCs used to define patient positivity/negativity has not been established yet and different cut-off values have been used in different studies evaluating CTCs in PDAC

(206), which makes difficult to compare the results. However, the low CTC numbers and detection frequencies observed in PDAC patients suggest that lower cut-off value might be considered to discriminate patients with a good or poor prognosis.

The low numbers and detection rates of CellSearch-CTCs in PDAC could be partially explained by the heterogeneous expression of EpCAM protein on the CTC surface (154, 207, 208), and by the fact that a downregulation of EpCAM takes place during EMT and this is a crucial step for PDAC progression at early stages (209). These features highlight that EpCAM-based methods might not be efficient enough for pancreatic CTC capturing.

In addition, it has been hypothesized that the hepatic filtration during the portal circulation transit could also contribute to trap CTCs and therefore reduce the chance to detect cells in the peripheral blood, as already observed in colorectal carcinoma (210-212). The portal venous circulation is the main way for hematogenous dissemination of PDAC CTCs, which have direct access into the low-pressure flow of portal circulation where they can quickly reach hepatic tissue. Thus, some studies proposed CTC enumeration from portal venous blood as a strategy to increase the chance to find CTCs and identify patients at risk for hepatic metastasis (213, 214).

1.2.5 Strategies to isolate CTCs for downstream analysis

The analysis of CTCs at single cell level is acquiring increasing interest to investigate the mutational landscape of progressing cancers and open a window into tumor heterogeneity (215, 216). To access the molecular profile of individual CTCs, they need to be first isolated as single cells, and this is technically challenging. After enrichment and phenotypical characterization, the population of target cells is still contaminated by WBCs (217). Depending on the number of contaminating WBCs and the type of labeling used to detect CTCs, the most appropriate method has to be selected for the target cell isolation. The cell isolation can be performed manually or integrated in a semi- or fully-automated technology (218).

The manual approach, i.e. micromanipulation, consists of detecting the CTC under a fluorescent microscope and the operator guides a micropipette to suction the single cells and place them in the desired reservoir (218). This strategy is economically convenient, but very laborious. More recent technologies were developed to introduce some automation. For

example, the CellCelector™ (ALS, Germany) offers the possibility to automatically scan the entire source plate and analyze the images to detect and tag target cells to be picked by a high-precision robotic arm (217). This strategy is compatible with many of the major biophysical- (219) and molecular-based (including immunomagnetic (220)) CTC enrichment technologies.
An alternative strategy is provided by the DEPArray™ system, which combines microelectronics and microfluidics in a highly automated platform, to enable the isolation of single cells or pools of cells (221). After a preliminary immunostaining and volume reduction, the cell suspension is loaded in a microfluidic cartridge which contains an array of individually controllable electrodes, each with embedded sensors. This circuitry enables the creation of DEP cages around the cells, which can be visualized and subsequentially selected by a browser software to be gently moved into a holding chamber for isolation and recovery. This strategy can be integrated in workflows downstream to many of the biophysical and immunological-based (including immunomagnetic (221)) CTC enrichment technologies.
Flow cytometry is also one other strategy to sort CTCs from the background co-enriched cells. It has been already shown that FACS sorting is a very efficient and cost-effective way to detect and isolate CTCs (222), discriminating the cells based on the expression of several markers, their size and granularity. However, this approach does not offer the chance to visualize the cell and observe its morphology, which might hinder the selection. FACS sorting showed compatibility with the major immunological-based CTC enrichment technologies (including immunomagnetic (222)).

1.2.6 Diagnostic leukapheresis to increase the CTC yield

A major obstacle to unlock the potential of CTC-based liquid biopsy is their extreme low concentration in the peripheral blood, which complicates their detection. This becomes especially problematic if only 10 mL of blood (typical volume of standard clinical samples) is analyzed. An approach that could increase the CTC yield would be to screen larger blood volumes and the theoretical basis for this approach have been explored (223-226). The diagnostic leukapheresis (DLA) was established with this purpose (227). DLA is a shorter leukapheresis (LA), a method that is used to separate mononuclear cells (MNCs) from liters of blood and it has various applications in the clinics (228, 229). During the LA procedure, the blood is continuously extracorporeally processed (figure 6A) to enable a density-based cell separation of MNCs with a density of 1.055–1.08 g/mL (227). As the density of epithelial cells falls in the range of MNCs, LA could allow a co-enrichment of CTC and the MNCs

(227) (figure 6B). During the DLA procedure around 2.5 L of blood are processed and its MNC content is concentrated in approximately 40 mL with around 10^8 WBC /mL (230, 231). DLA has been reported as a clinically safe method that reliably enables higher detection of CTCs (227, 232). It was initially introduced by the HHU Düsseldorf (227), and in the meantime it has been validated by different groups and a European multicenter study (230, 233, 234).

The high blood cell concentration makes the processing of the complete DLA product for CTC enumeration extremely challenging. So far, the most effective method for CTC detection in DLA samples is the CellSearch® system (230), where $2x10^8$ MNCs (approximately only 5% of the total DLA product) can be analyzed. Considering the assay costs and the sample-load capacity, the CellSearch® approach is not a feasible alternative to process a whole DLA product. Alternative strategies are still required to process higher volumes of DLA and unlock the full potential of the DLA.

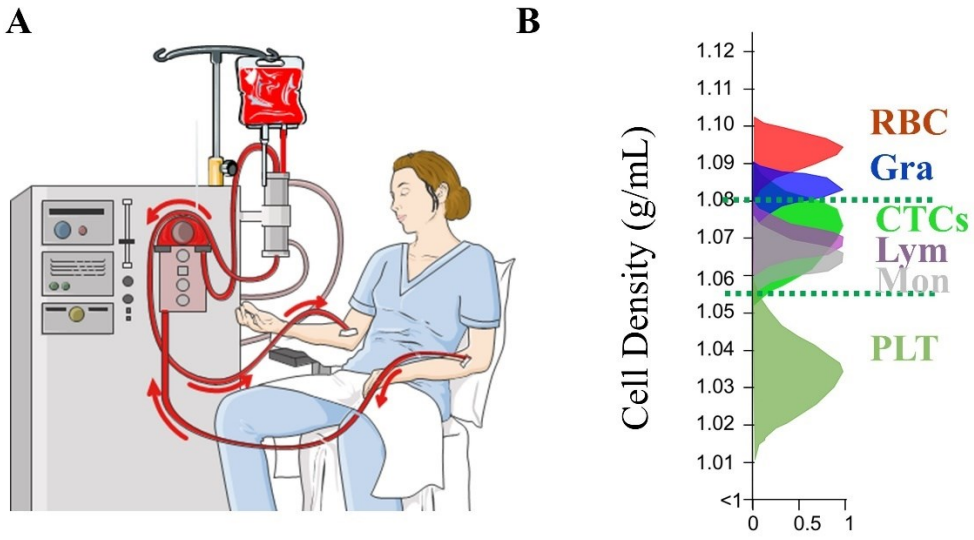

Figure 6. Diagnostic leukapheresis procedure. (A) Representation of the procedure of diagnostic leukapheresis executed on patient.
Adapted from "Medical Equipment" attributed to Servier Medical Art, under a Creative Commons Attribution 3.0 Unported License.
(B) Density of hematological cells and CTC. The plot shows that the CTC-density range mainly overlaps with the density range of Lymphocytes and Monocytes (d = 1.055–1.08 g/mL). Therefore, this density range can be used to separate together CTCs and MNCs from the rest of blood cells.
Adapted from Stoecklein et al. (232) and used with permission from Taylor & Francis.

2. AIM OF THE STUDY

Despite an increased understanding of the biology of PDAC and modern therapies, this malignancy is still characterized by an extremely poor prognosis. Prognostic biomarkers that can help treatment decisions and new therapeutic targets could improve the clinical outcome of PDAC patients. Prognostic value of CTCs has been already proved in different tumors and the possibility to molecularly characterize CTCs at single cell level has been considered as a good opportunity to dissect the heterogeneous biology of the tumor and move towards a more personalized therapy (115, 116, 194, 235-237). However, a major obstacle that limits the use of pancreatic CTCs for clinical and research purposes is their extreme rarity and difficult accessibility. The main aims of my work were:

- To investigate whether the screening of large blood volumes could improve CTC detection in PDAC patients and evaluate the prognostic impact of pancreatic CTCs. The strategy was to analyze a fraction of patient derived DLA product using CellSearch® system and compare the results with those obtained after the analysis of matched PB.
- To investigate whether both fresh and cryopreserved DLAs could improve the characterization of pancreatic CTCs.
- To test the performance of a label-free spiral microfluidic chip (DLA biochip) to process samples with increasing cell load and demonstrate the potential for the up-scalable DLA biochip to process complete DLA products, enabling high-volume CTC-based liquid biopsies.

3. MATERIAL AND METHODS

3.1. Cell culture

Human cell line cells of different tumor origin were cultured and used to model CTCs in spike-in experiments and to validate the strategy for mutation analyses by targeted NGS. Hup-T4, Capan-1 and MIA PaCa-2 were used as human pancreatic cancer cell model (all from Leibniz Institute DSMZ- Germany), Sk-BR-3 (Leibniz Institute DSMZ, Germany) and MDA-MB-231 (kindly provided by the Department of Obstetrics and Gynecology, University Hospital of the Heinrich-Heine University Düsseldorf, Germany) as human breast cancer cell model, and LNCaP (kindly provided by the Institute of Urology of the Heinrich-Heine University Düsseldorf) as human prostate cancer cell model. Hup-T4 was cultured in MEM Eagle (PAN-biotech Aidenbach, Germany), containing EBSS, NEAA, 1 mM Sodium Pyruvate, 2 mM L-Glutamine, 1.5 g/L NaHCO3, and supplemented with 20% fetal bovine serum (FBS) (Gibco, Germany); CAPAN-1 in RPMI1640 (PAN-biotech, Germany) supplemented with 20% fetal bovine serum (FBS) (Gibco, Germany); MIA PaCa-2 in Dulbecco's MEM (PAN-biotech, Germany) supplemented with 20% FBS and 2.5% horse serum (PAN-biotech, Germany); Sk-BR-3 in McCoy´s 5A modified (Gibco, Germany), containing high glucose, L-Glutamine, bacto-peptone and 2.2 g/L NaHCO3, and supplemented with 10% FBS (Gibco, Germany); LNCaP in RPMI1640 containing L-Glutamine, 2 g/L NaHCO3 (PAN-biotech, Germany) and supplemented with 10% FBS (Gibco, Germany); MDA-MB-231 in RPMI1640 (Gibco, Germany) containing 2 mM L-Glutamine, supplemented with 10% fetal bovine serum (FBS) (Gibco, Germany) and 20mM HEPES (Gibco, Germany). 1% penicillin-streptomycin was added to all culture media and the cells were maintained in a humidified incubator at 37 °C with 5% CO2.

For passaging or to prepare the cells for experiments, the cells at a confluency of 60-80% were detached with 0.25% trypsin/EDTA (Sigma-Aldrich, Merck KGaA, Germany) at 37 °C for 2–5', trypsin reaction was stopped by adding the respective supplemented medium and centrifuging at 800 g for 4'. The pellet was resuspended in fresh medium for further culture or in PBS for other analyses. Periodic profiling of short tandem repeats (STRs) was done to verify the identity of the cell lines. The STR data were analyzed on the online DSMZ Profile Database (www.dsmz.de/fp/cgi-bin/str.html).

3.1.1 Cell size measurements

Because the efficiency of the enrichment methods that we wanted to test is directly dependent on the size of the cells, we assessed the mean diameters of Hup-T4, LNCaP and Sk-BR-3 tumor cell harvested from cell culture and leukocytes isolated from buffy coat. The cells were pre-labelled with 0.2 µM CellTracker Green CMFDA Dye (CTG) (ThermoFisher Scientific Inc., USA) according to manufacturer's instruction for a sharper definition of the cell contour under microscopy. Then, a small fraction of each cell type was transferred into one 14mm-field of a 3-field adhesive microscope slide (Erie Scientific LLC, USA). Each slide field was automatically scanned (LabView 8.6 - CellSpotter 2.7.3) in an Eclipse E400 epi-fluorescence microscope (Nikon, Japan) at 20X with Cy3 fluorescence filter and in bright field. Afterwards, n = 22 Sk-BR-3 cells, n = 28 Hup-T4 cells, n = 25 LNCaP cells and n = 28 WBCs were randomly selected from different image frames to be analyzed with ImageJ software (https://imagej.nih.gov/ij/download.html). The drawing function was used to trace the cell diameter, and the measuring tool was used to determine its length in pixels. Subsequently, the values were converted in µm, using as conversion factor 1 pixel = 0.34 µm at 20X magnification.

3.2 Diagnostic Leukapheresis of PDAC patients

Diagnostic leukapheresis (DLA) and peripheral blood (PB) samples were obtained from 46 patients (24 women and 22 men) with a mean age of 66 years, treated for PDAC between 2011 and 2019 at the Department of General, Visceral and Pediatric Surgery in the University Hospital of the Heinrich-Heine University Düsseldorf (Germany), as part of a study done in collaboration with the University of Heidelberg. Part of the data collected within this study are used in *Stoecklein, N.H., Fluegen, G., Guglielmi, R. et al.,* Mol Cancer (2023) (238). The project was approved by the Ethics Committee of the Medical Faculties of the Heinrich-Heine University Düsseldorf and Ruprecht-Karls-University Heidelberg, and it was performed accordingly to Good Clinical Practice guidelines. All patients provided written informed consent. DLA (DLA cohort) and PB (PB cohort) samples were obtained from each patient prior of surgery. DLA was performed at the Department of Transplantation Diagnostics and Cell Therapeutics in University Hospital of the Heinrich-Heine University, Düsseldorf (Germany) in patients with appropriate venous access and no history of increased bleeding tendency.

The tumors of all 46 patients were staged by the pathologists according to the TNM classification of malignant tumors as described in the seventh edition of the Union for International Cancer Control (UICC) (239): 31 tumors were classified with stage I-III, the remaining 15 tumors were classified with stage IV (table 10). Thirty-four patients were also grouped according to their N stage: 31 patients showed locoregional metastasis (N+), three patients did not show locoregional metastasis (N-). Survival data were updated until 2020.

3.2.1 Calculation of DLA efficiency

The efficiency of each DLA procedure was determined by calculating the collection efficiency of MNCs. This was calculated based on the DLA product generated and the analysis of corresponding PB sample. For that, complete blood cell counts were obtained from the DLA samples (after the DLA procedure) and from PB samples (before the DLA procedure), using a CELL-DYN Ruby hematologic analyzer (running software version 2.3ML) (Abbott, USA).

The MNCs collection efficiency was calculated as follow:

$$MNC\ collection\ efficiency = \frac{[MNC\ in\ harvest\ (per\ mL)\ X\ Volume\ of\ DLA\ product\ (mL)]}{[MNC\ before\ harvest (per\ mL)\ X\ Volume\ of\ PB\ processed\ \ (mL)]}$$

3.2.2 Freezing and thawing of DLA products

For each of the 46 patients, one aliquot of the DLA product containing 200x10^6 WBCs was freshly analyzed with CellSearch® system (DLA cohort), while the rest was frozen in aliquots containing 100x10^6 WBCs (FR_DLA cohort).

For freezing, the DLA product was first centrifuged at 200g for 10' and supernatant was aspired. The pellet was diluted to a final WBC concentration of 100x10^6/mL, and each 1 mL-aliquot was mixed with 1 mL of freezing medium consisting of 45% RPMI1640, 45% HSA and 10% DMSO (Sigma-Aldrich, Merck KGaA, Germany) in cryovials. The cryovials were then placed for 24h at -80 °C in a Mr. Frosti freezing container which guarantees a cooling rate of 1 °C/min, and then transferred to liquid nitrogen for long term storage.

For thawing DLA products for CellSearch® analysis, the DLA product contained in one cryovial was rapidly thawed in a 37 °C water bath, while the cap was briefly loosened to allow pressure release. After complete thawing, the content was transferred directly into a CellSearch® conical centrifuge tube (Menarini Silicon Biosystems Inc, USA), diluted up to 8

mL with a PBS containing 15 mM EDTA and the entire volume of fixative from one CellSave preservative tube (Menarini Silicon Biosystems Inc, USA), and incubated for 30' at RT before CellTracks® Autoprep® system run.

The impact of our cryopreservation/thawing method on tumor cell loss was tested with spike-in experiments in the context of the Master Thesis project of V. Raba (Department of Experimental Surgical Oncology). For that, a defined number of CTG (ThermoFisher Scientific Inc., USA) pre-labelled Hup-T4 cells were manually spiked in $100x10^6$ WBCs, the same content of 1 mL DLA product. WBCs were isolated from buffy coats (BC) obtained from the blood donation center of the Institute for Transplantation Diagnostics and Cell Therapeutics from the University Hospital of the Heinrich-Heine University, Düsseldorf (Germany). Healthy donors provided written informed consent for the use of surplus blood products for research purposes. Buffy coats were prepared by qualified operators at the blood donation center according to standard protocol used in the clinics and were provided in bags containing citrate as anticoagulant.

After receiving the BC, 15 mL were pipetted on top of Ficoll-Paque (GE Healthcare, Sweden) for density gradient WBC separation and isolation (more detailed protocol will be described in the chapter "Mimicked DLA product"). The obtained WBC-enriched fraction was washed twice with PBS and the sample was concentrated to $100x10^6$ WBC/mL.

The cultured cells were spiked in triplicate using different BCs (biological replicates) and each spiked-in BC was frozen as described above and stored in liquid nitrogen until usage. An aliquot of 100 µL was taken prior freezing and stained with 4 µL of anti-CD45/PE-Cy7 (ThermoFisher Scientific Inc., USA) as WBC marker, and 50 µL (of a 1:200 dilution in PBS) of the nuclear dye DRAQ5 (ThermoFisher Scientific Inc., USA). The stained samples were analyzed with flow cytometry in a FACSCanto II (BD Biosciences, USA). Each frozen spiked-in BC was thawed as described above and 100 µL were stained and analyzed in the same way as for the aliquot of sample before freezing. DRAQ5 was detected upon excitation at 640 nm, whereas CD45-PeCy7 and CTG upon excitation at 488nm. In order to determine the number of CTG positive Hup-T4 cells before and after freezing, 50 µL of CountBright™ absolute counting beads (Invitrogen, USA) (0,52 x 10^5 beads/50 µL) were added to the sample prior flow cytometry analysis. Hup-T4 and counting beads were detected and the total number of target cells in the sample was determined as:

$$\frac{cells\ count}{beads\ count}\ X\ beads\ concentration.$$

The calculated number of Hup-T4 cells detected was compared to the number of spiked-in cells, in order to determine the cell recovery rate (%).

3.3 CellSearch® analysis of PB and DLA samples

The number of CTCs in the PB and DLA samples was determined using the CellSearch® system with the CellSearch® Circulating tumor cell kit (Menarini Silicon Biosystems Inc, USA), containing all the reagents to allow a ferrofluid-based CTC capture and an immunofluorescent cell staining. All the enrichment and labeling steps are performed within the CellTracks® Autoprep® instrument. Here, after the capturing of EpCAM+ cells, CTCs are stained with anti-CKs antibodies conjugated with Phycoerythrin (PE), anti-CD45 antibody conjugated with Allophycocyanin (APC), and DAPI as nuclear marker. The output sample is recovered in a cartridge located within the Magnest Cartridge holder, which is then loaded into the CellTracks® Analyzer II (CTAII) instrument. This instrument scans the cartridge content, acquires the images and pre-selects DAPI+/CK+ events, bigger than 4 μm, which are presented to the operator as an image gallery. The gallery was reviewed manually in post-processing mode at the CTAII. Additionally, CTCs were also scored from the galleries using the open-source imaging software ACCEPT for Automated CTC Classification, Enumeration and Phenotyping (240, 241). CTCs were scored using the full detection tool with the following settings: mean fluorescence intensity DNA >100; mean fluorescence intensity CK >20, mean fluorescence intensity CD45 ≤20, size CK ≤500 μm^2, size DNA >20, DNA overlay CK >0.5. ACCEPT-selected DAPI+/PE+/APC- events, which were then reviewed by an operator for CTC selection (semi-automated CTC selection).

PB samples were collected directly into CellSave preservative tubes and stored at RT until use. Within 96h after blood collection, a volume of 7.5 mL was transferred into 15 mL conical centrifuge tube, diluted up to 14 mL with the dilution buffer (Menarini Silicon Biosystems Inc, USA) and centrifuged at 800 g for 10' without brake to allow the plasma separation. The prepared sample was processed by the CellTracks® AutoPrep® system according to manufacturers' instructions for "CTC samples".

Aliquots containing approximately $200x10^6$ WBCs of fresh DLA samples were diluted with the CellSearch dilution buffer up to 7.5 mL in a CellSave preservative tube and stored at RT until use. The content of the tube was transferred into a 15 mL conical centrifuge tube and processed by CellTracks® AutoPrep® system according to manufacturers' instructions for

"control samples". This strategy allowed to process the DLA samples without any additional centrifugation for plasma removal as would be required if sample would be processed as "CTC samples".

For each DLA product, the concentration of MNC in DLA, the concentration of MNC in PB and the processed DLA volume were used to calculate the equivalent PB volume analyzed by CellSearch® according to the following formula (227):

$$Equivalent\ PB\ volume = \frac{MNC_{DLA}\ Concentration\left(\frac{n}{mL}\right) X\ DLA\ Volume\ (mL)}{MNC_{PB}\ Concentration\ \left(\frac{n}{mL}\right)}$$

Each thawed DLA sample (prepared as described in sub-chapter 3.2.2) was processed with CellTracks® AutoPrep® system according to manufacturers' instructions for "control samples". The output samples were analyzed using CTAII and the image galleries were reviewed manually in post-processing mode at the CTAII.

The sample preparation and the CellSearch® system processing of PB and fresh DLAs until 2017 were performed by qualified operators in the Department of Obstetrics and Gynecology, University Hospital and Medical Faculty of the Heinrich-Heine University Düsseldorf, while samples collected after 2017 and cryopreserved DLA products were processed by qualified operators in the Department of General, Visceral and Pediatric Surgery in the University Hospital of the Heinrich-Heine University Düsseldorf, Germany.

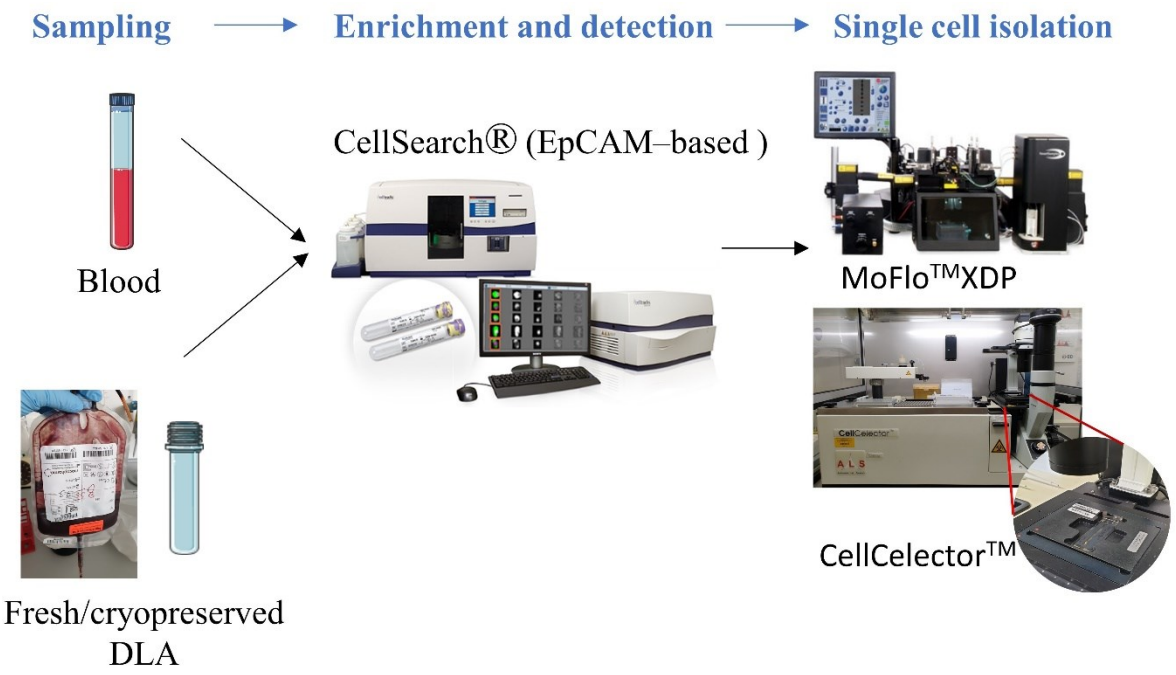

Figure 7. Workflow for CTC enrichment, detection and isolation from patient derived blood, fresh and cryopreserved DLA. PB, fresh and cryopreserved DLA samples were prepared to be processed by CellSearch® for CTC enrichment and detection. Subsequently, the CellSearch® cartridge was eluted and the content was analyzed by flow cytometry and/or CellCelector™ for single CTC isolation. The zoom-in on the mechanical stage of the microscope integrated in the CellCelector™ shows a slide placed on the MagnetPick™ adapter.

3.4 Isolation of CTCs and WBCs from DLAs after CellSearch® enrichment

After CS-enrichment, the content of the cartridge was eluted using extra-long pipette tips pre-coated with 2% BSA and transferred either to a Falcon 5 mL Polystyrene Round-Bottom Tube (BD Bioscience, USA) for isolation of single WBC and CTCs by flow cytometry or deposited on a glass slide for isolation by micromanipulation (figure 7).

3.4.1 Flow cytometry

The MoFlo™ XDP sorter (Beckman Coulter, Germany) was used for the flow cytometry analysis and single cell isolation. As first, the entire content of the cartridge (around 375 µL) was transferred into a Falcon 5 mL Polystyrene Round-Bottom Tube (BD Bioscience, USA),

then, the inner walls of the cartridge were washed two times with 150 µL PBS 1X, which were also transferred into the same tube to maximize the cell recovery.

Immediately prior the analysis, 6 µL of the DNA intercalating Propidiumiodide (PI) were added to the sample to re-stain the nuclei. The gating strategy to discriminate the different populations was based on what reported by Neves et al. (222), but slightly re-adapted to also include events with a lower intensity in PE (CKs+ cells), a modification based on preliminary analyses.

CTCs were defined as high positive in the PI channel, positive in the PE channel and negative in the APC channel (nucleated/CK+/CD45-), WBCs were defined as high positive in the PI channel, positive in the APC channel and negative in the PE channel (nucleated/CK-/CD45+). All the detected CTCs and five WBCs per each sample were isolated by the instrument directly into empty 0.2 µL PCR tubes and frozen at -20 °C until use.

3.4.2 Micromanipulation

The CellCelector™ micromanipulator was used as alternative to flow cytometry to detect and isolate CTCs from frozen DLA samples after CS-enrichment. The CellCelector™ consists of an inverted epifluorescence microscope (CKX41, Olympus) connected to a CCD camera (XM10-IR, Olympus, Japan) and a robotic arm with a glass capillary of 30 µm in diameter for the cell picking (CellCelector™ software 3.0).

To guarantee a good cell dispersion, the content of the cartridge was loaded unto two glass slides placed on magnetic holders on the motorized stage of the microscope (figure 7). To maximize the cell recovery, the inner wall of the cartridge was washed two times with 150 µL PBS 1X which were deposited on the same slides. Before the analysis, the cells were allowed to settle at least for 15'.

The slides were automatically scanned using the following parameters: cell diameter ranging from 5 to 40 µm; exposure time of 20 ms for DAPI, 300 ms for PE and 500 ms for APC; magnification of 40X. Then, the images of software- pre-selected events were reviewed by the operator to score CTCs. CTCs were defined as DAPI+/CK-PE+/CD45-APC- cells, presenting an intact-cell morphology in bright field (BF). The position of selected cells was automatically recorded for subsequent isolation using the mechanical arm. The glass capillary aspired the cell in a volume ranging from 20 to 100 nL and deposited it into an empty PCR tube.

3.5 Molecular characterization of isolated cells

In order to confirm the tumor origin of the cells isolated from PDAC patients, somatic mutations and chromosomal copy number alterations were assessed. Single cells were processed according to the workflow presented in the figure 8.

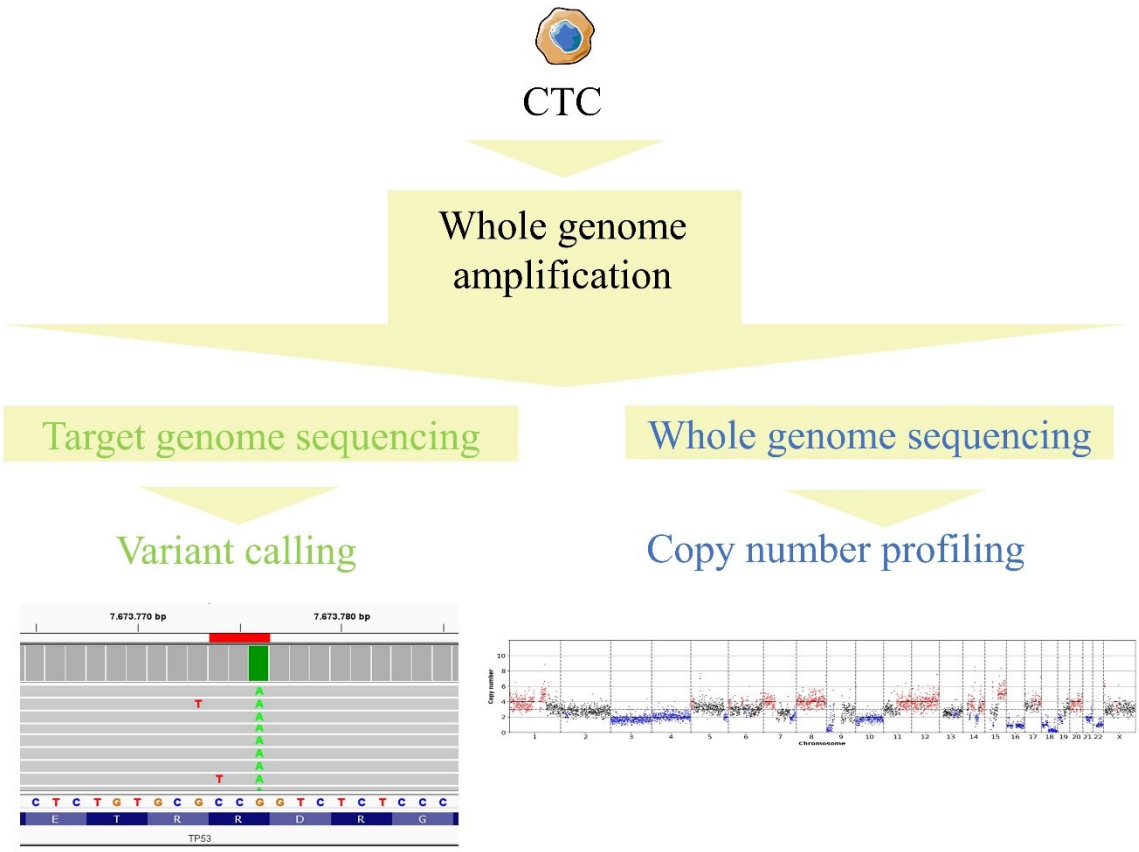

Figure 8. Workflow for molecular characterization of single CTC. CTCs were isolated as single cells according to the methods described above. Subsequently, the DNA content was amplified with a protocol of Whole Genome Amplification adapted for single cells. The WGA product was used both to detect somatic point mutations, with a target NGS-genome sequencing approach, and for copy number profiling, with a whole NGS-genome sequencing.

3.5.1 Whole genome amplification

The DNA from single cells was amplified to obtain a sufficient genomic material for a comprehensive analysis of the whole genome. Whole genome amplification (WGA) was performed according to the single-tube protocol initially described by Klein et al. (242), later adapted by Stoecklein et al. (243), and which is now commercialized as Ampli1 (Menarini Silicon Biosystems S.p.A., Italy).

As first step, every cell isolated was incubated with 3 µL of a reaction mix containing: 1 µL picking buffer (Igepal (Sigma Aldrich, Merck KGaA, Germany) 0.5% in PBS 1X), 0.2 µL One Phor All (OPA) buffer (prepared by diluting 12.5 g Tris-acetate, 50 mL Magnesium acetate and 50 mL Potassium acetate in 500 mL distilled water), 0.13 µL Tween 20 (Sigma Aldrich, Merck KGaA, Germany) 10%, 0.13 µL Igepal 10%, 0.26 µL Proteinase K 10 mg/mL (Roche Diagnostic, USA) and 1.28 µL water.
The sample was incubated for 10h at 42 °C in a Thermal Cycler for PCR (C1000, BioRad, USA) for protein digestion by cleavage of the peptide bonds, and then for 10' at 80 °C to inactivate the protease. Next, 2 µL of "digestion mix" were added to each sample for the enzymatic cell DNA fragmentation at 37 °C for 3h. Digestion mix contained 0.2 µL MseI endonuclease 50 U/µL (New England Biolabs Inc., USA), which recognizes the sequence 5'-T^TAA-3', 0.2 µL OPA buffer and 1.6 µL distilled water. The restriction enzyme was inactivated at 65 °C for 5'.
Meanwhile, two DNA oligonucleotides with complementary sequences (table 3) were annealed by incubating 0.5 µL OPA buffer, 0.5 µL LIB1 oligo 100 µM, 0.5 µL ddMSE11 oligo 100 µM and 1.5 µL water. The pre-annealing PCR program starts at 65 °C and cool down to 15 °C with ramps of 1 °C min^{-1}. Annealing generates a double-stranded DNA oligonucleotide with a 5' TA overhang compatible with that created by the MseI restriction enzyme.

Table 3. Sequence of the oligonucleotides used as adaptors (WGA protocol).

Oligonucleotide name	**Sequence**
ddMse11	5'-TAACTGACAGCdd-3'
LIB1	5'-AGTGGGATTCCTGCTGCTGTCAGT-3'

Subsequently, 3 µL of the annealed adapters, 1 µL T4 DNA ligase (Thermo Fisher Scientific, USA) and 1 µL ATP 10 mM (Roche Diagnostic, USA) were added to each MseI-digested single cell genome and the mix was incubated at 15 °C overnight to allow the ligation between the double-stranded adapters and the 5' TA overhangs of the MseI-digested DNA fragments. As last step, each adapter-ligated fragment was amplified by a PCR. Fot that, an "amplification mix" was prepared by mixing 3 µL Expand Long Template buffer 1 (Roche Diagnostic, USA), 1 µL DNA PolMix (Roche Diagnostic, USA), 2 µL dNTPs 10 mM each (GE healthcare) and 35 µL water. Each sample was incubated with 40 µL of "amplification mix" according to the following PCR cycling protocol:

Table 4: PCR cycling protocol for the amplification of the ligated products (WGA protocol).

Cycles	Temperature	Time
1	68 °C	3'
	94 °C	40"
14	57 °C	30"
	68 °C	1'30" + 1"/cycle
	94 °C	40"
8	57 °C	30" + 1 °C/cycle
	68 °C	1'45" + 1"/cycle
	94 °C	40"
22	65 °C	30"
	68 °C	1'53"+ 1"/cycle
1	68 °C	3'40"
	4 °C	∞

At this point, the DNA was stored at -20 °C. In each experiment, isolated Sk-BR-3 cell line cells were included as positive control and nuclease-free water as negative control.

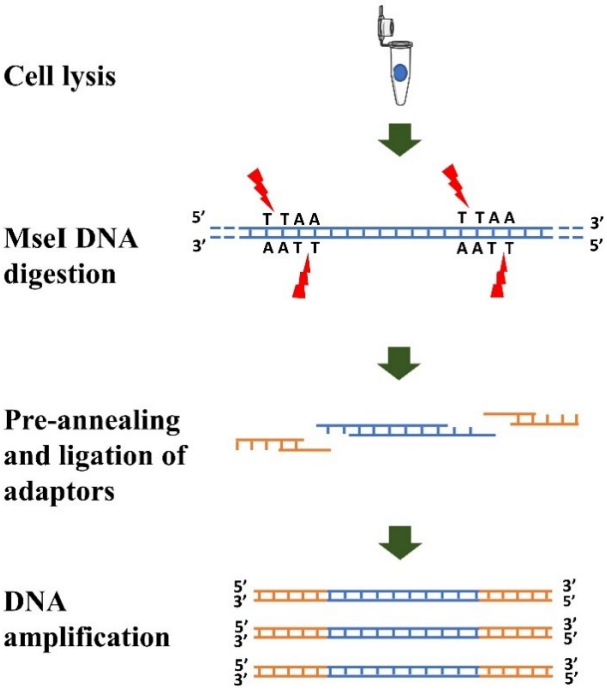

Figure 9. Whole genome amplification steps. The scheme represents the main steps of WGA starting from single cell lysis. The genome is then digested through MseI restriction endonuclease that recognize 5'-T^TAA-3' to generate fragments which are subsequently ligated to pre-annealed adapters. At the end, adapter-specific primers allow to amplify the DNA fragments.

3.5.2 Multiplex PCR-based DNA quality control

In order to verify the integrity of the WGA DNA library, a 6-fragment multiplex-PCR (QC-test) was performed as previously described (244). For that, 0.5 µL of WGA product were amplified using 5 µL DreamTaq Green PCR master mix (Thermo Fisher Scientific, USA), 1 µL primer mix (detailed in the table 6) and 3.5 µL water, according to the following PCR cycling protocol:

Table 5. Multiplex-PCR cycling protocol.

Cycles	Temperature	Time
1	95°C	2'
33	95°C	30"
	60°C	40"
	72°C	1'
1	72°C	5'
	4°C	+∞

To assess the success of this multiplex PCR, 10 µL of the amplified products were loaded on an 1.5% agarose (Sigma-Aldrich, Merck KGaA) gel prepared in TBE and containing 0.01 % gel red (Biotium Inc., USA) As a marker, 6 µL of 100 bp DNA Ladder (Thermo Fischer Scientific Inc, USA) were used. The gel was run for 45' at 150 V and afterwards, it was visualized in a Versadoc imaging system (Bio-Rad). five out of six bands are expected from fully successful WGA products, corresponding to amplicons of 111 bp, 232 bp, 288 bp, 358 bp and 401 bp. The 175 bp amplicon should not be detected, since it contains a MseI restriction site, and its presence would indicate an incomplete enzymatic digestion.
Human female reference DNA 0.2 µg/µL (gDNA) (Agilent, USA) and nuclease-free water were used always as positive and negative internal control respectively.

Table 6. Primers used to assess the integrity of the WGA library with a multiplex-PCR method (QC-test). The used concentration and the amplicon size are reported for each case. F: forward; R: reverse.

Gene	Primer sequence	Concentration (µM)	Amplicon size (bp)
LAMC1	F: TCTGCTTTGGGCATTCTTCT R: TTCTAACAGGTTGGGGGATG	0.2	111
CADPS	F: CCCCACCCTTCTTCACTACA R: GTGTGCACATACCACCGAAG	0.08	175
GRIK5	F: CTAGCTCCCACCAACCTCAG R: CTCGATGATCCCGTTGATCT	0.2	232
NEK9	F: GCAGGAGGGAACCTGTATGA R: CAGGAAAGAAAGCCCACAGA	0.1	288
PICK1	F: TCGTATGCTGGAGTCCTGTG R: GGGATGGCTTTGTTGAGGTA	0.08	358
DNAH9	F: GGGTCTCATCACCAGCATTT R: GCCATCTTCCACATGGTCTT	0.08	401

3.5.3 Detection of point mutations with NGS targeted sequencing

Single nucleotide variants (SNVs) in a total of five hotspot genomic regions located in KRAS exon 2 and 3 and TP53 exon 5, 7 and 8 (19, 24) were sequenced with an amplicon-based NGS deep sequencing.
Before applying it to patient derived CTCs, the procedure was validated in cell lines known to harbor mutations in the analyzed hotspot regions: MDA-MB-231 (heterozygous G13D in

KRAS exon 2; homozygous R280K in TP53 exon 8); CAPAN-1 (homozygous G12V in KRAS exon 2; A159V in TP53 exon 5); Sk-BR-3 (homozygous R175H in TP53 exon 5); MIA PaCa-2 (homozygous G12C in KRAS exon 2; R248W inTP53 exon 7).

3.5.3.1 Primer design

The primers used were designed using Primer-BLAST (https://www.ncbi.nlm.nih.gov/tools/primer-blast/) adopting the following parameters to efficiently amplify the WGA products: the absence of a MseI restriction site within the target DNA sequence and a PCR product size below 200 bp. Each primer pair sequence was flanked on its 5' terminus by an oligonucleotide adapter (Tag1 for the forward and Tag2 for the reverse primers) that provided a binding site for universal MID Dx primers for Illumina systems to be used later (Multiplicom, part of Agilent, USA). The adaptor-primer oligonucleotides were synthesized by Metabion (Germany). Upon arrival, primers were reconstituted with water to a concentration of 100 µM (stock solution) and stored at -20 °C until use.

Table 7. Adapter-primer used to amplify specific regions in KRAS (exon 2 and 3) and TP53 (exon 5, 7 and 8) genes. The amplicon size is reported for each case. F: forward; R: reverse.

Gene	Adapter-Primer sequence	Amplicon size (bp)
KRAS Ex2	F: 5'-AAGACTCGGCAGCATCTCCA-TTGGATCATATTCGTCCACAA-3' R: 5'-GCGATCGTCACTGTTCTCCA-CCTTATGTGTGACATGTTCTAATATAGT-3'	168
KRAS Ex3	F: 5'-AAGACTCGGCAGCATCTCCA-CCTTCTCAGGATTCCTACAG-3' R: 5'-GCGATCGTCACTGTTCTCCA-CCACCTATAATGGTGAATATC-3'	192
TP53 Ex5	F: 5'-AAGACTCGGCAGCATCTCCA-CTACAGTACTCCCCTGCCCT-3' R: 5'-GCGATCGTCACTGTTCTCCA-CACCATCGCTATCTGAGCA-3'	193
TP53 Ex7	F: 5'-AAGACTCGGCAGCATCTCCA-GACTGTACCACCATCCACTA-3' R: 5'-GCGATCGTCACTGTTCTCCA-AGAAATCGGTAAGAGGTGGG-3'	192
TP53 Ex8	F: 5'-AAGACTCGGCAGCATCTCCA-TGCCTCTTGCTTCTCTTTTC-3' R: 5'-GCGATCGTCACTGTTCTCCA-CTTGCTTACCTCGCTTAGTG-3'	179

3.5.3.2 Library preparation for NGS target sequencing.

The library was prepared with a KAPA2G Fast Multiplex Mix (F. Hoffmann-La Roche, Switzerland) in two PCR rounds: the first PCR for the amplification of the target regions and the second PCR for the sample barcoding. The reagents' volumes were adapted according to the protocol detailed by Franken et al (245).

A first PCR was performed to amplify each of the five target regions in five separate reaction tubes. Each reaction contained 0.5 µL of WGA product, 1 µL of 10 µM target-specific primer pair mix (pre-dilution:10 µL reverse primer and 10 µL forward primer in 80 µL of water) (table 7), 5 µL of KAPA2G Fast Multiplex Mix and 3.5 µL of water for a final volume of 10 µL. The reaction was performed according to the following PCR program:

Table 8. PCR cycling program for the first and second amplification step of the library preparation for NGS target sequencing.

Cycles	Temperature	Time
1	98°C	3'
30	98°C	45"
	56°C	45"
	72°C	1'
1	72°C	5'
	4°C	+∞

The second PCR was performed to obtain a barcoded sample. Reaction contained 0.5 µL of each of the five first-PCR products (total 2.5 µL template), 1 µL of MID Dx primer for Illumina systems (0.5 µL of reverse primer and 0.5 µL of forward primer) (Multiplicom, part of Agilent, USA), 10 µL of KAPA2G Fast Multiplex Mix and 6.5 µL of water, for a total volume of 20 µL. Each primer consists of a sequence motif binding to the previously used adapter-adapter, a unique multiplex identifier (MID), and a P5 or P7 adapter for sequencing in the MiSeq platform. This second PCR reaction was performed according to the PCR program as shown in table 8.

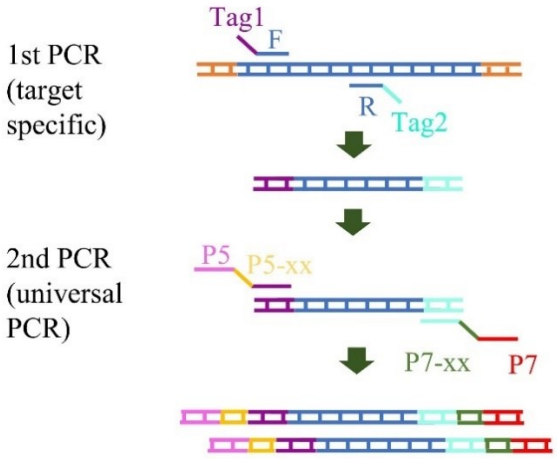

Figure 10. Library preparation steps for target NGS.

3.5.3.2.1 Evaluation of the first PCR amplification with gel electrophoresis.

In order to verify whether the target regions were successfully amplified using the specific primer, the products of the first PCR were loaded into a 1.5% agarose gel prepared in 1X TBE and containing 0.01% of GelRed. Based on the total length of the primers and the amplicon, products of 208 bp were expected for KRAS exon 2 amplification, products of 232 bp were expected for KRAS exon 3 and TP53 exon 7 amplifications, products of 233 bp were expected for TP53 exon 5 amplifications, and products of 219 bp were expected for TP53 exon 8 amplification (figure 11). For the samples where no amplification was achieved for one of the regions, the first amplification was repeated one time. The samples which did not show an amplification of any of the target regions were not further processed. The samples which showed an amplification of all the target regions, or a partial amplification (1-4 target regions amplified) were further processed for library preparation and sequenced.

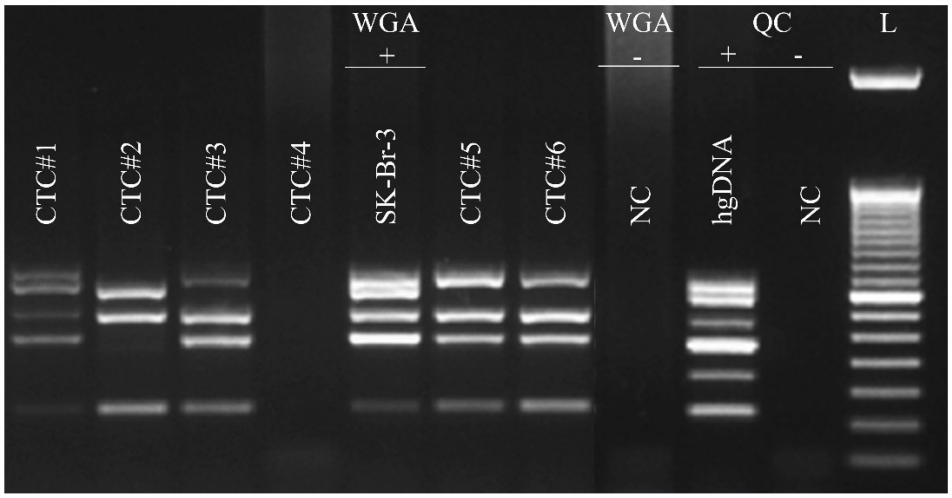

Figure 11. Representative gel electrophoresis to confirm the specificity of the amplification after the first PCR cycle of the target NGS protocol. The smallest amplicons (208 bp) were detected for KRAS exon 2 amplification; similar size amplicons (232 and 233 bp) were detected for KRAS exon 3, TP53 exon 5 and TP53 exon 7 amplification, and intermediate size amplicons (219 bp) were detected for TP53 exon 8 amplifications.

3.5.3.2.2 DNA purification and quantification.

The final PCR products were purified using Agencourt AMPure XP beads (Beckmann Coulter, USA) according to the manufacturer's protocol.

Purified libraries were quantified with the Qubit 2.0 Fluorometer (Thermo Fisher Scientific Inc., USA) according to the manufacturer's Protocol of the Broad Range Quant-iT dsDNA Assay Kit (Thermo Fisher Scientific Inc., USA). Each indexed library was diluted to a concentration of 0.043 pM, with the aim to pool equimolar amounts of the 96 samples loaded into the MiSeq system (Illumina, CA).

3.5.3.3 Sequencing on MiSeq Illumina platform and data analysis

The indexed libraries were sequenced in 151 bp paired-end reads mode to a median coverage depth of 3,056×. In each sequencing run, at least one WBC DNA library was included. For the data analysis, each of the two FASTQ files generated from one sample were loaded on the Galaxy web platform, available on the public server usegalaxy.org (246) and the reads were

aligned against the entire human reference genome (h38) with the Bowtie2 tool (Galaxy Version 2.3.4.3), choosing "paired-end reads" and default alignment parameters.
The process generates files.bam and files.bai. Bam file contains the index-able representation of nucleotide sequence alignments and bai file is the index file which must be found in the same directory as the bam file. In order to browse the alignment to detect single nucleotide mutations, the file.BAM was open in IG Viewer (Version 2.3.25) (247). As criteria for mutation calling, each identified mutation was covered by >100 reads and had a variant allele frequency (VAF) >5%. To exclude germ-line mutations, mutations found in CTCs must be absent in the patient-matched WBCs (three to five WBCs per patient analyzed).

3.5.4 Single cell copy number profiling

3.5.4.1 Whole genome library preparation for Illumina

With the purpose to analyze the copy number profile at genome-wide level and confirm the cancer nature of the isolated cells, whole genome libraries for NGS were prepared from WGA products using the Ampli 1 LowPass Kit for Illumina (Menarini Silicon Biosystems Spa, Italy) according to manufacturer's instruction and as previously described (248). The method is based on a ligation mediated PCR WGA and uses hybrid PCR primers (including barcoded adaptors compatible with Illumina platforms on the 5' end, and primary WGA universal adaptor on the 3' end) (248). The protocol consists in three main steps: the first barcoding reaction with Ampli 1 D7xx index adapter, the second barcoding reaction with Ampli 1 D5xx index adapter and the final library amplification. Each step is followed by a purification step with SPRIselect beads (Beckman Coulter).
A dual-indexed whole genome library was prepared from cell-DNA in which point mutations were detected or from cell-DNA isolated from samples in which CellSearch-detected CTCs were morphologically intact and showed a particularly strong signal in PE.
For each WGA product, all the reaction steps from first barcoding reaction up to the final library purification were performed in the same well of a 0.2 mL PCR plate (96-well format). After last purification, the library was eluted in a clean well within the same PCR plate.

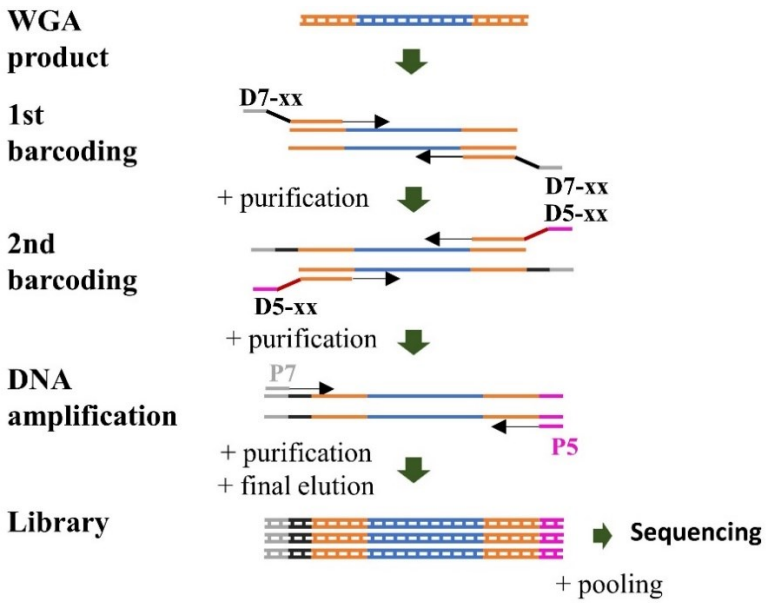

Figure 12. Library preparation steps for whole genome NGS to explore the CNA profile.

3.5.4.1.1 qPCR for library quantification

A real-time qPCR method was used to quantify the libraries. For that it was used the SYBR green-based KAPA Library Quantification Kit for Illumina® Platform (Roche Diagnostics, USA) according to the manufacturer's instructions. Each library was preliminary diluted 1:10,000. All the reactions were prepared in duplicate in a 96-well plate, and these were run in a G8830A AriaMix Real-Time PCR system (Agilent, USA) according to the following cycling protocol:

Table 9. qPCR program set in the AriaMix Real-Time PCR system (Agilent, USA**) for the quantification of the NGS libraries before whole genome sequencing.**

Cycles	Temperature	Time
1	95°C	5'
35	95°C	30"
	60°C	45"

Six DNA standards present in the KAPA Library Quantification Kit were included in each run for absolute quantification of library products. The average Cq values of the DNA standards were plotted against their log10(concentration in pM) provided by the manufacturer to generate a standard curve, which was then used to interpolate the concentration of each library.

3.5.4.1.2 Size determination of the libraries with Bioanalyzer

To determine the average fragment size of the libraries, the sequencing libraries were diluted to a concentration of 5 nM and analyzed in a Bioanalyzer (Agilent, USA) using the High Sensitivity DNA Kit (Agilent, USA) following the manufactures' instruction. All the fragments with size between 200 and 3,500 bp were considered to determine the average size. Libraries with an average size ~ 700 bp were considered as optimal.

3.5.4.2 Whole genome sequencing and data analysis

After converting the average Cq value (n= 2) of each library to concentration (in pM) using the standard curve, libraries were pooled in equimolar amount aiming to obtain a pooled library of 4nM. The concentration of the prepared pool was verified in a new qPCR with the he KAPA Library Quantification Kit for Illumina Platforms as described in sub-chapter 3.5.4.1.1. The pool was then further diluted to 10-20 pM and sequenced with the MiSeq (MiSeq reagent kit V3, Illumina) in 151 bp single reads mode.

For the data analysis it was used a pipeline established in the research laboratory within the Department of General-, Visceral- and Pediatric Surgery. In this pipeline, Burrows-Wheeler Aligner tool (BWA) was used to align the sequences to the hg19 reference genome. Alignments were randomly sub-sampled closer to 200k reads. The aligned sequences were used to call the CNAs using the R package QDNAseq11.0 with a window size of 500kb bins. Quality control (QC) criteria were applied on each cell including Inter-Quartile range (IQR <0.35) and derivative log ratio spread (DLRS <0.35). All the CTCs that passed the QC criteria were used to generate copy number states (Gain/Normal/Loss) in CTCs by transforming the log2 ratios. The log2 values 0.25 and -0.25 were used as a threshold to determine gain and loss respectively from normal copy-number states. After the examination of all the CN profiles with the respective copy number states, a deletion of few segments in chr6 was observed in all the CTCs. These deletions were considered as an artifact from the amplification method and therefore, they were filtered out for further analysis. All the CTCs which passed QC were used for hierarchical clustering analysis in R.

Furthermore, the percentage of aberrant genome (PAG) was calculated both for CTCs and WBCs. The PAG calculated from the WBCs data set helped to choose a threshold to classify aberrant profiles.

CNA segments files were loaded into Progenetix and the plotting function was used to generate CNA frequency plots.

3.6 Molecular characterization of tissue samples

In order to compare the genetic profiles of single CTCs with the corresponding tumor, mutations in hotspot regions and CNA profiles were also analyzed in matched tumor tissues.

3.6.1 Selection of tissue sections, DNA extraction and quantification

Thin sections (5-10 µm) from tumor tissue blocks fixed in 4% buffered formaldehyde solution-embedded in paraffin (FFPE) were provided by the Institute of Pathology, Heinrich-Heine-University and University Hospital of Düsseldorf. The sections stained with hematoxylin and eosin (H&E) were examined by certified pathologists to score the tumor-stroma ratio and only sections with ≥50% tumor tissue were selected. For each section, the pathologist labelled the area of interest and performed microdissection to scrape off the unwanted (non-tumorous) cells. The remaining fraction (mainly containing tumor cells) was used for DNA extraction. Genomic DNA was extracted manually using the Qiagen Blood and Tissue Kit (Qiagen Inc, USA) according to the manufacturers' protocol. Subsequently, the DNA concentration was measured with Qubit™ dsDNA BR Assay Kit (Thermofisher Scientifics, Inc., USA) according to the manufacturers' instructions. The genomic DNA from eight samples and matched quantification data were provided by the Institute of Pathology, Heinrich-Heine-University and University Hospital of Düsseldorf.

3.6.2 Detection of point mutations with target NGS

From seven out of eight samples the target sequencing library was prepared according to the two round PCR protocol already described above (see sub-chapter 3.5.3.2), using between 9 and 100 ng of DNA (~ 2µL) in the first PCR. For patient #7, because no tumor tissue was available, the mutation profile was provided by the Institute of Pathology, Heinrich-Heine-University and University Hospital of Düsseldorf. This profile was generated with a multiplex-PCR based approach, using the Ion AmpliSeq™ Cancer Hotspot Panel v2 (Thermofisher Scientifics Inc, USA) according to the manufacturers' instruction (covering 207 amplicons from 50 oncogenes and tumor suppressor genes).

3.6.3 Copy number alteration profiling with NGS

3.6.3.1 Quality control of the DNA fragmentation

Formalin-fixation can cause fragmentation and chemical modifications in DNA, which could compromise the NGS applications. Prior the NGS library preparation, the DNA integrity was assessed to decide whether a preliminary fragmentation step could be skipped to avoid unnecessary steps that could affect the quality of the sample. With this purpose, the DEPArray FFPE QC Kit (Menarini Silicon Biosystems Spa, Italy) was used. The assay is based on qPCR, using two different primer pairs that produce amplicons of 54 bp and 132 bp. The quality of DNA (expressed as a QC score) is inferred by the difference in quantification cycles (Cq) obtained for the two amplicons. The reactions were prepared according to manufacturers' protocol and run in a G8830A AriaMix Real-Time PCR system (Agilent, USA). The data was analyzed to determine the QC score values for each sample following the manufacturers' instruction.

3.6.3.2 DNA library preparation

For the detection of CNAs in tumors, Illumina-compatible DNA libraries were prepared with the DEPArray LibPrep kit (Menarini Silicon Biosystem Spa, Italy). This kit is recommended when starting from human genomic DNA purified from FFPE samples with low tumor content (<15%) or with low DNA input.

Samples with a QC value higher than 0.15 were preliminary processed for DNA fragmentation with the Sonicator system M220 (Covaris LLC, USA), following the instruction of the DEPArray LibPrep kit manufacturer. Depending on the sample availability, a DNA amount from 30 to 100 ng was fragmented. After fragmentation, the DNA was processed for a first enzymatic reaction at 37 °C for 10', to dephosphorilate the fragment ends. In a second reaction, the fragment ends were repaired and polished. In the third step, the P7 adapter was ligated at the 3' end at a temperature of 25 °C for 15' and in the fourth reaction the P5 adapter containing a unique barcode was ligated at the 5'end at 40 °C for 10'. The obtained products were amplified with the KAPA HiFi HotStart ready Mix (2X) (Roche Diagnostics, USA) and the universal primer pair contained in the DEPArray LibPrep kit.

3.6.3.2.1 qPCR library quantification and size determination with Bioanalyzer

To accurately quantify and to assess the quality of the NGS libraries prepared for sequencing on Illumina platform, a qPCR-based quantification and a Bioanalyzer-based size determination were performed as already described in the sub-chapters 3.5.4.1.1 and 3.5.4.1.2 (see above).

3.6.3.3 Whole genome sequencing and data analysis

Eight libraries were pooled in equimolar amount to obtain a final pool of 4 nM and further diluted to 12 pM prior to be loaded and sequenced with the MiSeq system in 151 bp single reads mode.

The data were processed with the same pipeline described in the sub-chapter 3.5.4.2, but considering the percentage tumor content in original sample (given by the tumor-stroma ratio).

3.6.3.4 STR analysis of CTCs and tumor tissues

STR-analysis of CTCs and matched tumor tissue (when available) was performed to confirm the common origin of the samples. The STR analysis was performed by the Department of Legal Medicine, Heinrich-Heine University of Düsseldorf, as a fee-for-service.

3.7 Labelling of cell line cells

In order to label the cell line cells prior to the spike-in experiments, the cell line cells were washed with PBS 1X and then incubated for 30’ at 37 °C with the proper incubation media. This media was prepared by adding either 0.2 µM CTG, 1 µM CellTracker Orange CMTMR Dye (CTO) (ThermoFisher Scientific, Inc., USA), or 0.5 µM CellTracker Deep Red Dye (CTdR) (ThermoFisher Scientific, Inc., USA) to 5 mL of the appropriate growing medium (see chapter 3.1) without FBS. The cells were then washed one time in PBS 1X, harvested by centrifugation and used for the experiments.

3.8 Mimicked DLA product

Mimicked DLA (mDLA) were blood products prepared from fresh BCs and with a similar cell content to DLA products that were used for testing new protocols and applications. For convenience, buffy coats within two hours after collection (typically 60mL) were initially transferred from their original bag into Falcon tubes. A 1 mL aliquot was analyzed with the CELL-DYN Ruby hematologic analyzer (running software version 2.3ML) (Abbott, US) to record a complete blood count and a WBC differential analysis.

Afterwards, we performed a density gradient centrifugation of the BC to isolate WBCs. For that, 15 mL of BC were gently pipetted on top either of 15 mL Ficoll-Paque PLUS (d = 1.077 ± 0.001 g/mL; GE Healthcare, Sweden) or 15 mL Ficoll-Paque PREMIUM (d = 1.084 ± 0.001 g/mL; GE Healthcare, Sweden) in 50 mL conical tubes, and centrifuged at 800 g for 15' without break. Then, the WBC ring was collected and transferred into a clean tube for a washing step with PBS/0.01M EDTA. The pellet was then resuspended in 30 mL PBS and 1 mL aliquot was analyzed with the hematologic analyzer as before. Lastly, the mDLA volume was adjusted to a final concentration of $100x10^6$ WBC/mL.

3.9 Spike-in mDLA samples

To optimize the CTC enrichment process in the new DLA biochip, spike-in experiments were done with cell culture cells from different tumor types. All of them were pre-labeled with Hoechst 33342 nuclear dye (ThermoFisher Scientific Inc., USA) and one of three cytoplasmic dyes according to the protocol described in chapter 3.8. Hup-T4 were pre-labelled with CTO, Sk-BR-3 with CTG and LNCaP with CTdR, washed one time in PBS 1X and subsequently re-suspended in 7.5 mL PBS 1X to be fixed in Cell-free DNA BCT tubes (Streck, USA) for 1 hour.

The MoFlo^{TM} XDP flow sorter was used for the fluorescence-activated cell sorting (FACS) of the pre-labelled cells into mDLA products as following: 1,000 cells of each cell line in $50x10^6$ WBCs equivalent to ~15 mL of peripheral blood (experimental condition 1); 4,000 cells of each line in $200x10^6$ WBCs equivalent to ~60 mL of peripheral blood (experimental condition 2) and 8,000 cells of each line into $400x10^6$ WBCs equivalent to ~120 mL of peripheral blood (experimental condition 3) (176) (figure 13).

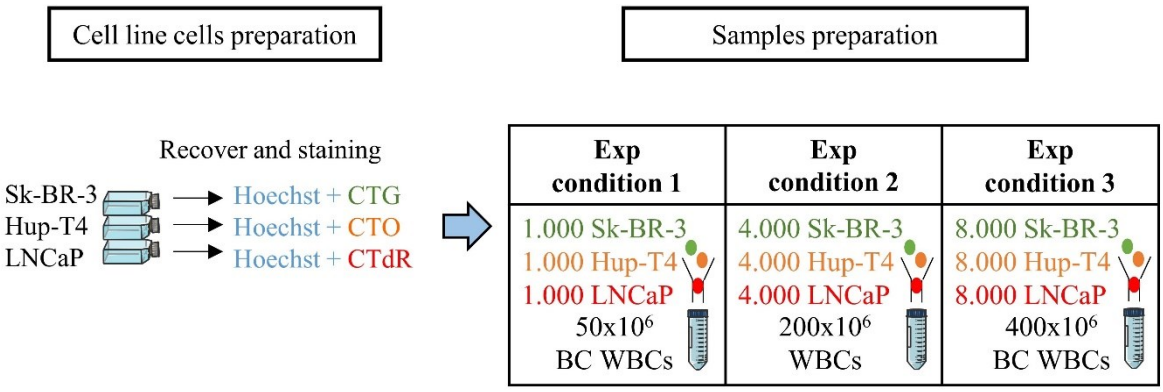

Figure 13. Spike-in experiments setup. Cells from culture were harvested and pre-labeled with Hoechst 33342 as nuclear staining and one of three different cytoplasmic dyes: CellTracker Orange CMTMR Dye (CTO); CellTracker Green CMFDA Dye (CTG); or CellTracker Deep Red Dye (CTdR). 1.000, 4.000 and 8.000 cells from each differentially pre-labelled cell line were spiked with flow cytometry respectively into $50x10^6$, $200x10^6$ and $400x10^6$ WBCs obtained as mDLA products. *Used from Guglielmi et al. (176), Creative Commons Attribution 4.0 International License.*

3.10 Tumor cell enrichment with CTChip® FR1

The ClearCell® FX system (Biolidics Ltd, Singapore) and the respective CTChip FR1 were prepared for the enrichment of tumor cells. Enrichment was done following the instructions of the manufacturer and each sample was loaded at the input straw and processed with the "Standard Protocol" for 54'. mDLAs samples prepared and spiked as described above (exp condition 1: $50x10^6$ WBC and exp condition 2: $200x10^6$ WBC) were diluted up to 4 mL with ClearCell® FX Resuspension Buffer (Biolidics Ltd, Singapore) while the sample containing $400x10^6$ WBC (exp condition 3) was directly processed. To test the performance of the CTChip FR1 with mDLA products, for each cell line we performed three replicates in experimental condition 1 and four replicates in experimental conditions 2 and 3 (33 experiments in total).

3.11 Tumor cell enrichment with DLA biochip

DLA biochip system was prepared according to the manufacturer's instruction. The chip was manually connected with a syringe through the input channel. The two output channels were

inserted in collecting tubes ("waste" or "sample") (figure 14B). Spiked-in mDLAs (exp condition 1, 2 and 3) were diluted up to 20 mL with PBS containing 2% of Diluent Additive (Biolidics Ldt, Singapore) and 0.01M EDTA. The chip was first primed with PBS containing 2% of Diluent Additive and then the diluted mDLA product was loaded in a 20 mL syringe (Injekt Solo, Braun) using a teflon tip. The syringe was placed on a 2-channels syringe pump and the sample was then channeled through the chip with a flow rate of 2.1 mL/min for the first enrichment cycle (cross-section of the chip is represented in figure 14A). The output sample (S1) (~4 mL) and the output waste (W1) (~16 mL) were both recovered in two 50 mL Falcon tubes. To calculate the output ratio the two tubes were weighted before (W_i and S_i) and after (W_f and S_f) the enrichment cycle and the ratio was calculated as $Or1 = \frac{(Wf-Wi)}{(Sf-Si)}$. The S1 was re-diluted up to 20 mL with PBS containing 2% of Diluent Additive (Biolidics, Singapore) and 0.01M EDTA and loaded again into the syringe for a second enrichment cycle through the same chip. The second output sample (S2) (~ 4 mL) and the second output waste (W2) (~ 16 mL) were recovered respectively in a 15 mL and a 50 mL Falcon tubes (figure 14B) and were weighted to calculate the output ratio ($Or2$) as before.

Output ratio is considered optimal in the range between 3.7 and 4.1, according to manufacturer's indications.

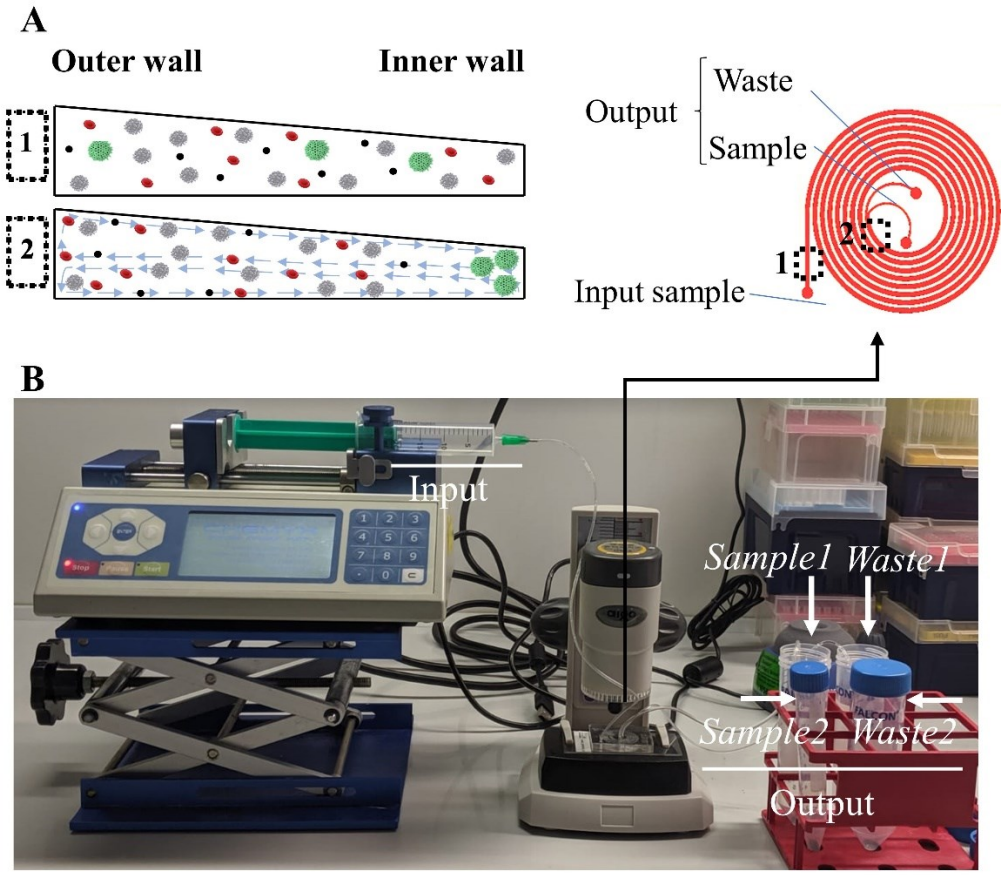

Figure 14. DLA biochip: system and workflow. (A) (Left panel) Cross section of the microfluid channel with representation of the blood cells (in grey and red) and CTCs (in green) at position 1 and 2 (as in the right panel). (Right panel) Representation of the DLA biochip showing the input slot for the pre-diluted sample and the output slots for CTCs enriched fraction and the contaminating fraction. *Reused from Guglielmi et al.* (176), *Copyright 2013 by Creative Commons CC-BY-NC-ND.*
(B) DLA biochip connected to the syringe (input) and the tubes (output). The syringe containing the diluted sample is loaded into the syringe pump and connected to the DLA biochip. This one is placed onto a portable microscope which is connected to a computer for monitoring the cellular flow through inside the chip. The sample is channeled to the chip output, which forks into two channels: the enriched fraction is collected in the 15 mL sample tube, while the contaminating fraction is collected in the 50 mL waste tube.

3.12 Analysis of spiked mDLA samples after enrichment

The spiked-in mDLA samples prepared as described in sub-chapter 3.9 were enriched with the CTChip FR1 chip or the DLA biochip and recovered in 15 mL Falcon tubes. Then, the samples were centrifuged at 500 g for 10' and supernatant was removed leaving around 500 µL and were immediately loaded on a MoFlo^{TM} XDP flow cytometer for the enumeration of the tumor cells enriched.

For the detection of intact cells, Hoechst^{pos} cells were discriminated from Hoechst^{neg} cells. Then, intact cells were discriminated based on their size and granularity measured respectively as the height of Forward (FSC-Height) and Side Scatter (SSC-Height) signals. Subsequently, the single cells were discriminated from clusters using the width of the Side Scatter signal (SSC-Width). The tumor cells were then defined based on the cell tracking dyes signals as follow: Hup-T4 as CTO^{pos} cells; Sk-BR-3 as CTG^{pos} cells; and LNCaP as CTdR^{pos} cells.

After DLA biochip enrichment, WBCs remaining in the S1 fraction (fraction after the first enrichment cycle) were enumerated using the CELL-DYN Ruby hematologic analyzer (running software version 2.3ML) (Abbott, US). Because S2 samples (fraction after the second enrichment cycle) were entirely analyzed by flow cytometry for tumor cell enumeration, the enumeration of WBCs using the hematologic analyzer could not be performed. As alternative, 18 additional spiked-in mDLA samples (six per experimental condition) were prepared according to the experimental set up described in sub-chapter 3.9 and were processed with the DLA biochip (two enrichment cycles). After enrichment and volume reduction to approximately 500 µL, each sample tube was immediately loaded on a MoFlo^{TM} XDP flow cytometer, and the sample was entirely analyzed to measure the WBC content. The gating strategy for detecting WBCs shows that intact cells were selected (based on their size measured as the FSC-Height signal) and then Hoechst^{neg} events were excluded. Instead, cell aggregates were not excluded using the SSC-Width signal.

The tumor cells recovery rate (expressed in percentage) was determined as the ratio between the number of cells detected by flow cytometry after enrichment and the number of initially spiked cells. Furthermore, a global mean tumor cell recovery rate was determined for each technology as the mean of the recovery rates of all three cell lines cells in all three experimental conditions. The global mean tumor cell recovery rate was used to compare the recovery rate efficiency of the two chips.

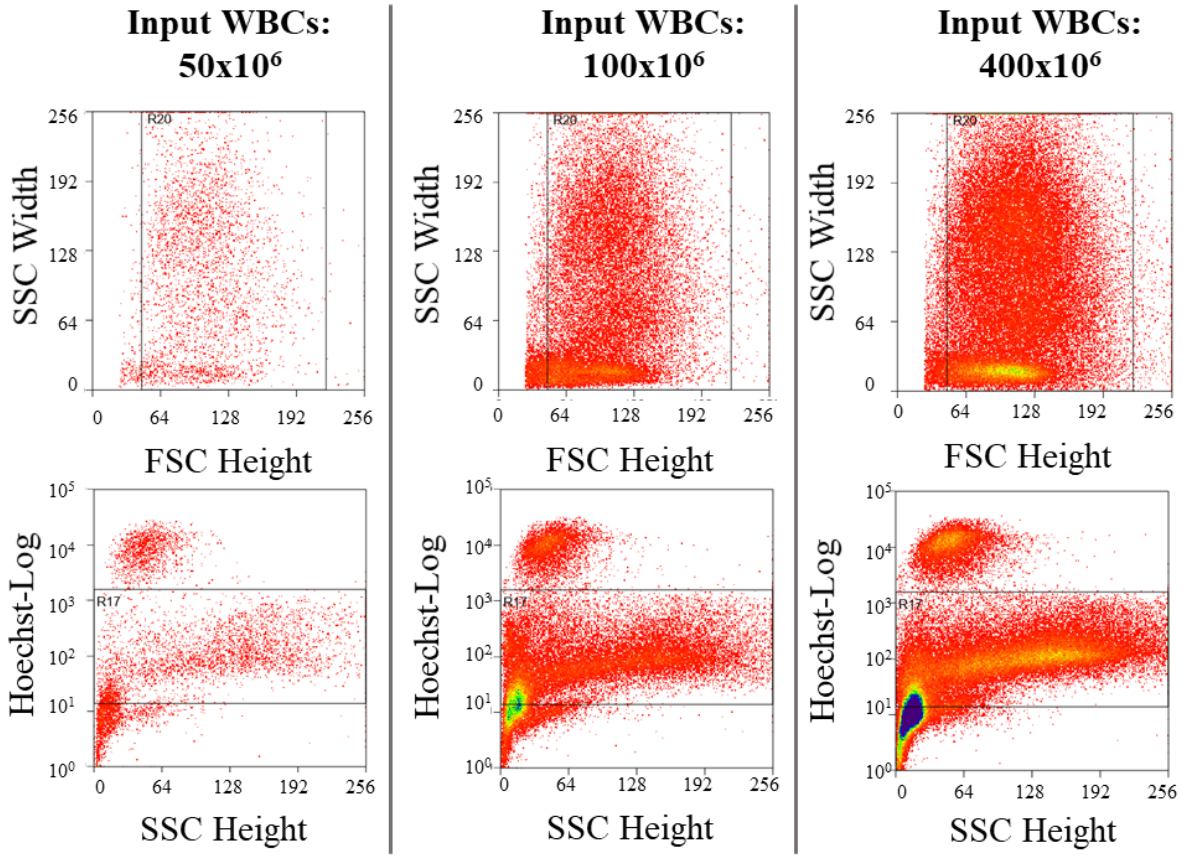

Figure 15. Representative flow cytometry analysis to determine the WBC fraction after two rounds of enrichment with DLA biochip. The plots represent the gates used to identify intact (upper plots) and Hoechst negative (bottom plots) cells, for each of the experimental conditions (mDLA products with $50x10^6$, $200x10^6$ and $400x10^6$ WBCs).
Adapted from Guglielmi at al. (176), Creative Commons Attribution 4.0 International License.

4. RESULTS

4.1 Analysis of PDAC DLA samples

4.1.1 Clinical parameters and blood parameters related to DLA and its efficiency in PDAC patients

DLA is a safe procedure that can be performed without noticeable side effects (227, 231). As part of the routine practice clinical parameters before and after the procedure were recorded and can provide useful indications on the tolerance of the procedure by each individual patient. In the present work, 49 patients were selected for DLA, but in three patients, the procedure was not possible due to a difficult venous access. The procedure was well tolerated by all the remaining 46 patients and did not lead to significant change either of the systolic ($p = 0.561$ by paired t-test,) or diastolic blood pressure ($p = 0.77$ by paired t-test,). After the procedure, the median heart rate did not change significantly ($p = 0.297$ by paired t-test,).

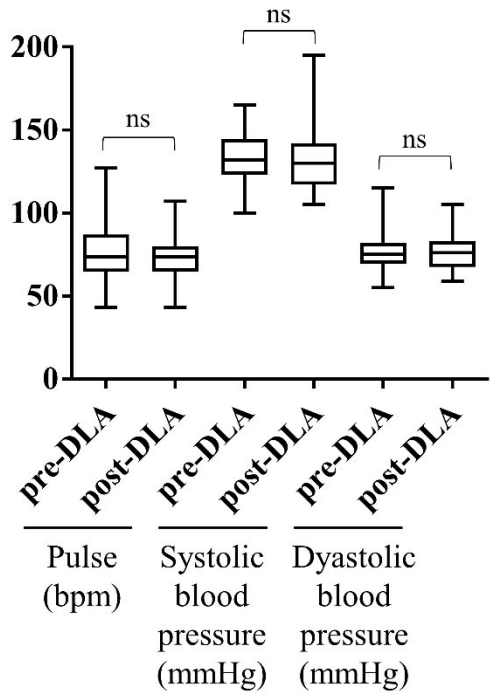

Figure 16. Heart rate, systolic and diastolic blood pressure registered before and after DLA procedure. After DLA procedure, median heart rate, systolic and diastolic blood pressure did not change significantly (respectively: $p = 0.297$, $p = 0.561$ and $p = 0.77$ by paired t-test).
Data are part of Stoecklein, N.H., Fluegen, G., Guglielmi, R. et al., Mol Cancer (2023) (238).

The volume of blood processed was recorded for each patient (Figure 17A). During the DLA procedure the median volume of blood processed was 2,673 mL (769-5,765 mL) and the

generated DLA products had a median volume of 47.5 mL (10-100 mL) (figure 17A). The DLA procedure allowed us to obtain products 25 times more concentrated in MNCs and 11 times more concentrated in WBCs compared to matched PB samples (figure 17B).

Considering that DLA procedure primarily targets MNCs, their counts in DLA and matched PB samples were used to further evaluate the DLA procedure. The mean efficiency of MNC collection was 45.4% (range 8-71%) (figure 17C). In breast cancer, a MNC collection efficiency above a threshold of 30% was previously used to indicate an efficient DLA procedure (231). In our patient cohort, the MNC collection efficiency was <30% for five patients (grey dots, figure 17C). However, all DLA samples were processed for CellSearch® CTC analysis.

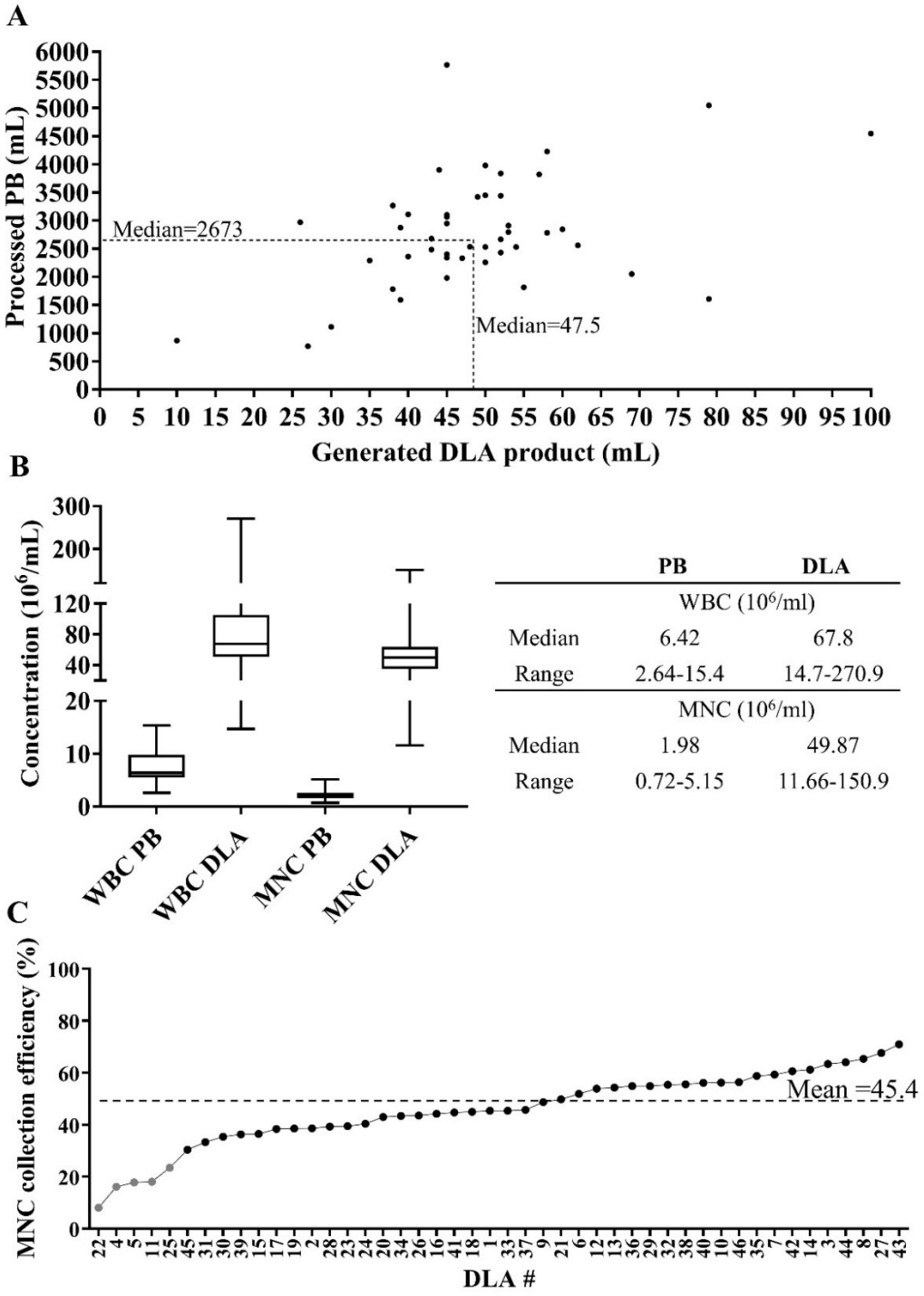

Figure 17. Efficiency of DLA in PDAC patients. (A) Correlation between volume of PB processed and the volume of DLA product generated. The volume of blood which flow out from the body (inlet blood volume) was measured for each patient to register the amount of blood processed. The dotted lines represent median values. **(B) Concentration of WBCs and MNCs in PB and DLA samples.** Box plots show the median values with interquartile range. Whiskers represent total range. Values are reported in the right panel **(C) MNC collection efficiency in DLA procedure.** Each dot represents an individual DLA sample. The dotted line indicates the mean MNC collection efficiency. The grey dots indicate DLAs with a MNC collection efficiency below the threshold of 30%.

Data are part of Stoecklein, N.H., Fluegen, G., Guglielmi, R. et al., Mol Cancer (2023) (238).

4.1.2 CTC enumeration in DLA products: CellSearch® manual count and ACCEPT analysis

From each DLA product, an aliquot containing ~ 200x10^6 WBCs, equivalent to a median of 2.9 mL of DLA product was screened for CTCs using CellSearch®. This DLA volume is equivalent to a median PB of 69.62 mL (range: 20.51 -156.1 mL). After CellSearch® sample processing, each gallery of images obtained from CTAII and containing candidate CTCs was manually analyzed to classify the CTCs (CS_Detection). Thirty-seven percent of the patients (17/46) were positive for CTCs, and 28% of the patients (13/46) had more than one CTC. No CTC was detected in 63% of the patients (29/46). Additionally, the images galleries of all samples were exported for semi-automated CTC enumeration by ACCEPT. ACCEPT identified DAPI+/PE+/APC- events and subsequently an operator manually reviewed and selected CTCs (ACCEPT_Detection). Fifty seven percent of the patients (26/46) were positive for CTCs, and 46% of the patients (21/46) had more than one CTC. No CTC was detected in 43 % of the patients (20/46). The results indicate that ACCEPT detected CTCs in a higher number of patients (p = 0.0016, by Fisher's exact test) (figure 18A). However, the number of CTCs enumerated by the two methods (CS_Detection and ACCEPT_Detection) was not significantly different (p = 0.182, by Wilcoxon matched-pairs signed rank test) (figure 18B).

A

		ACCEPT_Detection	
		Detected	Not Detected
CS_Detection	Detected	15	2
	Not detected	11	18

B

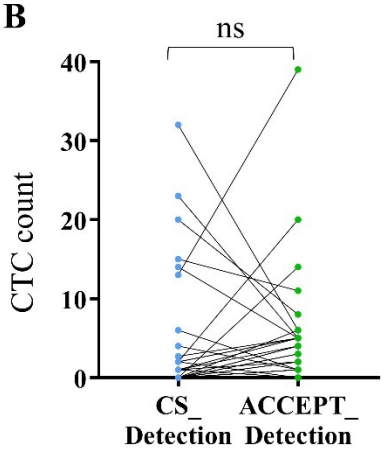

Figure 18. CTC detection and enumeration in DLA products by CellSearch®-manual count and ACCEPT analysis. (A) Number of patient samples in which CTC were detected or not detected by the two methods. **(B)** CTC count obtained for each individual sample with the two methods. p = 0.182 by Wilcoxon matched-pairs signed rank.

4.1.3 CTC enumeration in DLA and matching PB

From each DLA patient, 7.5 mL of matched PB sample was also analyzed for CTCs in the CellSearch® system. With the aim to evaluate the capacity of DLA to increase the CTC yield and the detection frequency in PDAC patients, we compared the number of CTC detected in the 46 DLA products and in the matching PB samples. An average of 0.08 CTC/mL was detected in PB, while a mean of 1.29 CTC/mL in DLA (>16 times more) and this difference was statistically significantly (P <0.0001, by Wilcoxon matched-pairs signed rank test) (figure 19A). The number of CTC/mL of DLA was multiplied for the entire volume of the produced DLA to calculate the total number of CTCs potentially detectable in each DLA product if entirely analyzed. This resulted in a mean CTC number of 54.56 CTCs/DLA product, which is 90 times more than the number of CTCs found in the standard PB samples. Furthermore, analyzing only 198.6x10^6 WBCs of the DLA products (corresponding to only 6% of the complete product) CTCs were detected in 56.5% (26/46) DLAs while only in 17.4% (8/46) PB samples being this difference also statistically significant (p = 0.0002, by Fisher's exact test) (figure 19B).

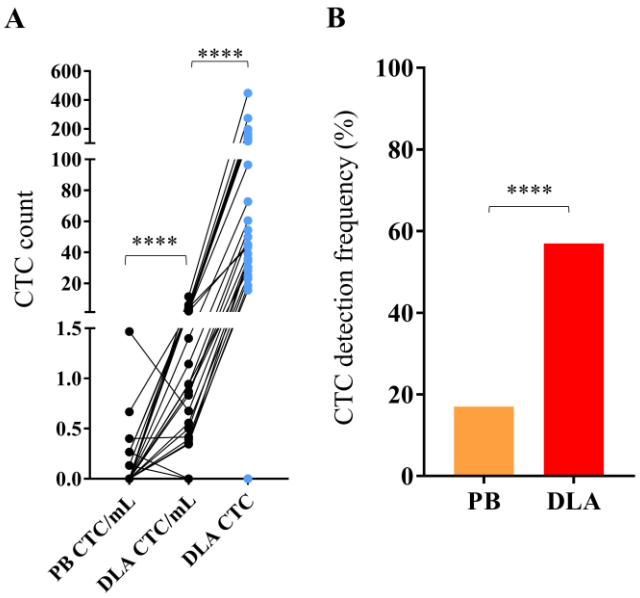

Figure 19. CTC detection in DLA products and matched PB samples. (A) CTC count. The DLA CTC/mL was calculated dividing the number of CTC counted in each DLA product by the corresponding DLA volume processed by CellSearch®. The PB CTC/mL was calculated dividing the number of CTC counted in each PB sample by 7.5 mL processed by CellSearch®. p <0.0001 by Wilcoxon matched-pairs signed rank test. The DLA CTC count was extrapolated by multiplying the CTC detected in 1 mL for the entire volume of DLA product. **(B) Detection frequency in matched PB and DLA samples.** p = 0.0002 by Fisher's exact test.
Data are part of Stoecklein, N.H., Fluegen, G., Guglielmi, R. et al., Mol Cancer (2023) (238).

4.1.4 Correlation between CTC detection and disease stage

Next, I investigated whether the CTC detection frequency and counts found in PB and DLA samples would correlate with the tumor-associated clinicopathological characteristics of the patients (Table 10). It was found that the presence of CTCs did not correlate with the lymph node metastasis, both in PB and DLA ($p = 0.313$ and $p = 0.54$ respectively, by Fisher's exact test).

However, the detection frequency was clearly higher in M1 (UICC stage IV) compared to M0 (UICC stage I-III) patients in both PB and DLA samples. In DLA samples, the detection frequency increased significantly from M0 to M1 patients (45.1% vs 80%, $p = 0.031$, by Fisher's exact test). In both patient groups M0 and M1, there was a significant higher detection frequency in DLA compared to PB samples (figure 20A).

In PB it was calculated a median of 0 CTC/100x10^6 WBCs both in M0 and M1 patients, and therefore a statistical analysis could not be performed. In DLA it was calculated a median of 0 CTC/100x10^6 WBCs (mean = 0.008) in M0 patients and 0.025 CTC/100x10^6 WBCs (mean = 0.021) in M1 patients, showing that the CTC count in DLA correlated positively with the progression of the disease ($p = 0.005$, by Mann-Whitney U test) (figure 20B).

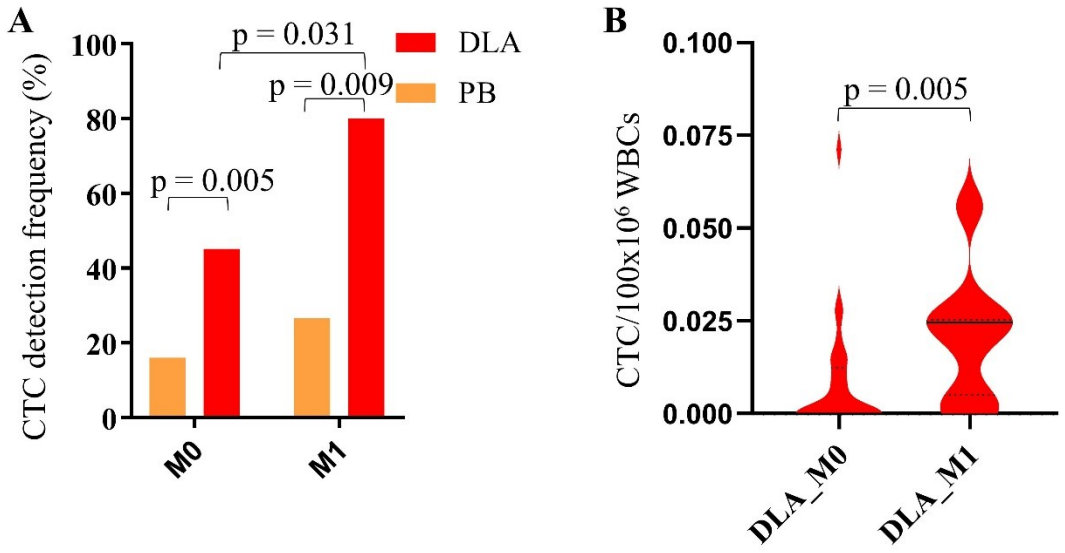

Figure 20. CTC detection and correlation to clinicopathological parameters. (A) CTC detection frequency in DLA and matching PB, both for M0 and M1 patients. P values by Fisher's exact test. **(B)** Number of CTC/100x10^6 WBCs detected in DLA samples in M0 and M1 patients. Horizontal line represents mean.

Data are part of Stoecklein, N.H., Fluegen, G., Guglielmi, R. et al., Mol Cancer (2023) (238).

Table 10. Summary of clinicopathological data from all patients. The clinicopathological data are reported for PB cohort, DLA cohort (patients undergoing the DLA procedure from which PB was also collected and analyzed for CTC enumeration) and FR_DLA sub-cohort (patients undergoing the DLA procedure from which cryopreserved DLA was processed to count, isolate and genetically characterize CTCs).
Data are part of Stoecklein, N.H., Fluegen, G., Guglielmi, R. et al., Mol Cancer (2023) (238).

		# PB cohort (%)			**# DLA cohort (%)**			**# FR_DLA cohort (sub-cohort from DLA cohort) (%)**	
		Total	**CTC+**		**Total**	**CTC+**		**Total**	**CTC+**
Total patients		46 (100)	8 (17)		46 (100)	26 (57)		16 (100)	12 (75)
Sex	**F**	24	6 (25)		24	15 (63)		9	7 (78)
	M	22	2 (9)		22	11 (50)		7	5 (71)
Surgical intervention	**Curative**	36	5 (14)		36	20 (56)		10	8 (80)
	Palliative	10	3 (30)		10	6 (60)		6	4 (67)
Tumor status (UICC stage)	**I**	2	0		2	1 (50)		0	0
	II	25	4 (16)		25	12 (48)		5	4 (80)
	III	4	0		4	1 (25)		1	0
	IV	15	4 (27)		15	12 (80)		10	8 (80)
Metastatic stage	**M0**	31	4 (13)		31	14 (45)		6	4 (67)
	M1	15	4 (27)		15	12 (80)		10	8 (80)
Lymph node status	**N-**	3	1 (33)		3	1 (33)		0	0
	N+	31	3 (10)		31	19 (61)		9	7 (78)

4.1.5 CTC detection and overall survival

The correlation between the presence of CTCs and the survival rate was explored. For the analysis, CTCs detected from DLA products where both the numbers and frequency of CTCs are higher were used. Kaplan-Meier analysis revealed a shorter overall survival for DLA-CTC+ patients compared to DLA-CTC- patients ($p = 0.0163$, by Log-rank test) (figure 21A). A shorter overall survival for DLA-CTC+ patients compared to DLA-CTC- patients was also observed in the subgroup of patients operated with curative intent ($n = 36$; $p = 0.026$, by Log-rank test). Kaplan-Meier analysis was also applied to the subgroups M0 and M1. As expected, M0_CTC- patients showed the best OS but interestingly, M0_CTC+, M1_CTC- and M1_CTC+ patients had similar OS (figure 21B).

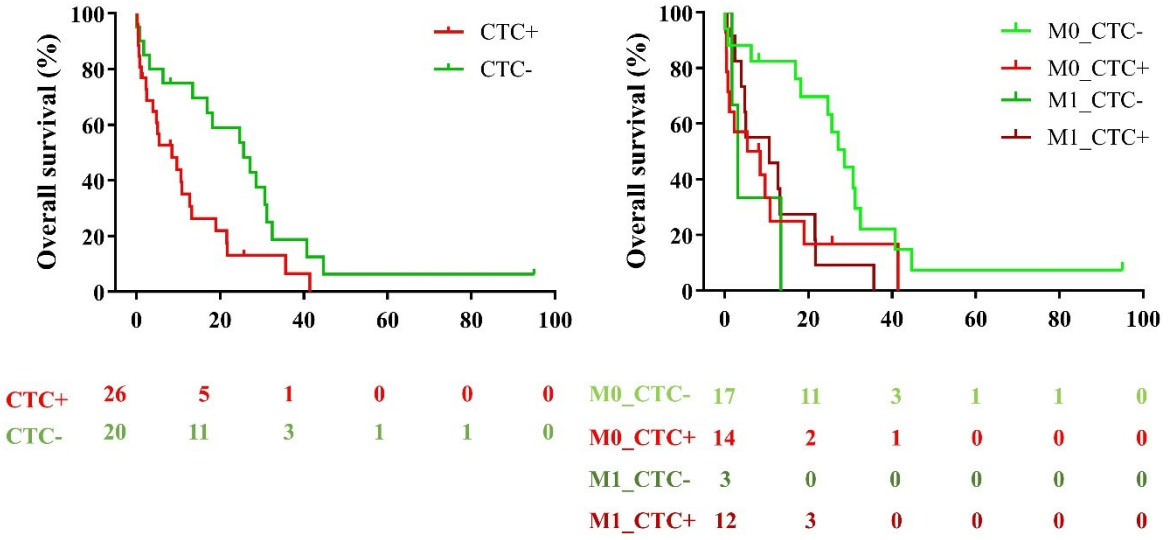

Figure 21. DLA-CTCs and overall survival. Kaplan-Meier survival analysis curves shows the time from blood draw in months (range 0-95 months). **(A)** Kaplan-Meier survival analysis of all 46 patients, subgrouped in CTC+ and CTC-. **(B)** Kaplan-Meier survival analysis of all 46 patients, subgrouped in M0_CTC-, M0_CTC+, M1_CTC- and M1_CTC+ patients. Patients who were still alive at the time of last contact were censored.
Data are part of Stoecklein, N.H., Fluegen, G., Guglielmi, R. et al., Mol Cancer (2023) (238).

4.1.6 Isolation of CTCs with flow sorting

For the latest two patients enrolled in the DLA cohort, samples were processed with the CellSearch® system and subsequently analyzed with the Moflo^{TM} XD flow cytometer with the aim to isolate single CTC. From patient #5, 3 CTCs candidate and 5 WBCs were isolated. From patient #6, 8 CTCs candidate and 5 WBCs were isolated.

4.2 Analysis of cryo-preserved PDAC DLA products to detect, isolate and characterize CTC

For each DLA product, only a fraction containing ~ 200x10^6 WBCs (corresponding to around 6% of the total volume) was analyzed for CTCs immediately after the DLA procedure, while the remaining fraction was cryopreserved in aliquots for later analyses. However, before analyzing cryopreserved patient samples, preliminary tests were necessary to evaluate the impact of the DLA cryopreservation on tumor cell loss. For testing purposes, mimicked DLA (mDLA) products were used.

4.2.1 Establishment of mimicked DLA product

Because DLA products represent precious patient material for detection of CTCs (227, 232) and the access to these samples is limited, for testing new protocols and applications were generated blood products with similar cell content to DLA products. These blood products are here referred as mDLA samples, and were generated from BCs, since BCs are concentrated in WBCs and they are available in large amount for research purposes from blood banks or commercial providers.

The blood cell profiles of unprocessed BCs and DLAs were first compared to see if the BC could be used without any further processing. BC collected from healthy donors (n = 18) had on average higher red blood cell (RBC) fraction ($p < 0.0001$, by Mann-Whitney U test), similar platelet fraction ($p = 0.72$), and lower WBC fraction ($p < 0.0001$) compared to patient-derived DLA products (n = 26) (figure 22A). Moreover, a significant difference in the prevalence of each WBC population between DLA products and BCs was observed (figure 22B). In particular, the monocytes were significantly less prevalent in BC than in DLA ($p < 0.0001$, by Mann-Whitney U test) and contrariwise the neutrophils were more prevalent ($p < 0.0001$, by Mann-Whitney U test). Aiming to obtain samples better mimicking DLAs, the BCs were processed by density gradient centrifugation using Ficoll-Paque PLUS 1.077 g/mL to enrich the mononuclear cells, which have a density between 1.067 and 1.077 g/mL, and the Ficoll-Paque PLUS 1.084 g/mL (1.05-1.08 g/mL) to include more granulocytes, which have a density higher than 1.080 g/mL) (249). Surprisingly, no significant difference between WBC composition after centrifugation with the two different media could be observed (by Mann-Whitney U test) and both media resulted in a WBC composition similar to DLA products (figure 22C), indicating that both could be used alike to produce suitable mDLA products. In BCs, after Ficoll centrifugation (BCs-Ficoll), basophil count was still lower compared to DLA products ($p = 0.0153$, by Mann-Whitney U test) (figure 22B), but due to the extremely low prevalence of this population, the result was considered not relevant.

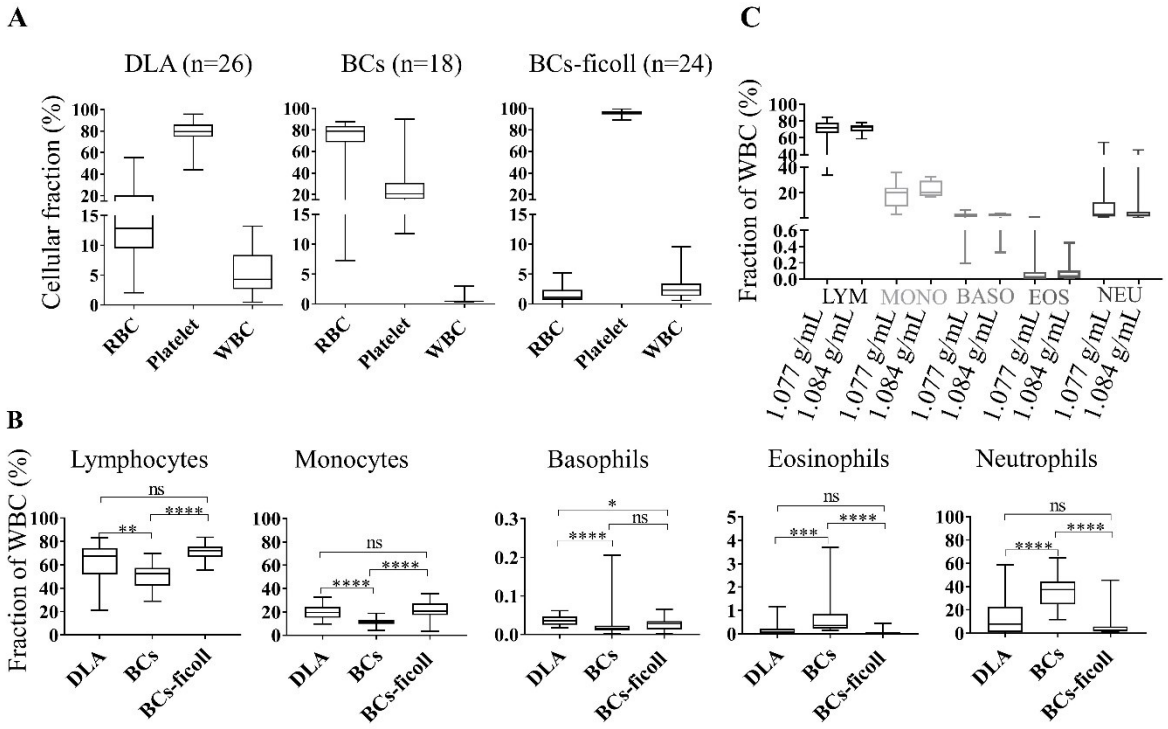

Figure 22. Blood cell composition in DLA samples, unprocessed and processed buffy coats.
(A) Percentage of RBC, platelet and WBC in DLA, BC and BC-ficoll. **(B)** Percentage of five individual populations of WBCs in DLA, BC and BC-ficoll. **(C)** Percentage of WBCs determined after processing BCs with Ficoll-Paque PLUS 1.077 g/mL and Ficoll-Paque PLUS 1.084 g/mL.
Box plots show the median values with interquartile range. Whiskers represent total range. *p <0.05; **p <0.01; ***p <0.001; ****p <0.0001, by Mann-Whitney U test.
Adapted from Guglielmi et al. (176), Creative Commons Attribution 4.0 International License.

4.2.2 Thawing of mDLA

To evaluate the impact of the DLA cryopreservation on tumor cell loss, the recovery rate of pre-labelled Hup-T4 and Capan-1 cells was determined after the thawing of spiked frozen mDLA samples. The number of spiked-in cells (before freezing) was compared with the number determined after thawing to calculate the recovery rates. A mean recovery rate of 66% ± 3 % (n = 9) was calculated for Hup-T4 and a mean recovery rate of 61% ± 6% (n = 9) for Capan-1. The recovery rates of the two cell lines were statistically different (p = 0.029, by unpaired t-test). The global mean recovery rate considering the two cell lines was 64% ± 5%.

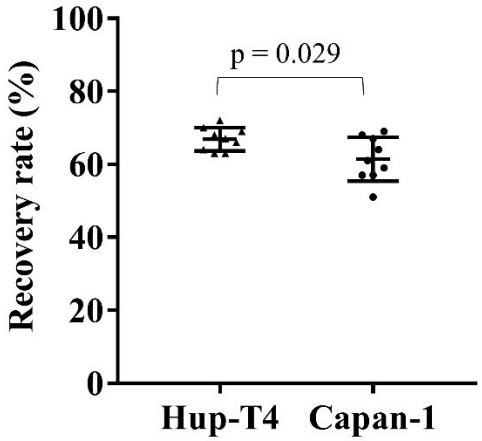

Figure 23. Tumor cell recovery rate determined in mDLA after sample thawing. Pre-labelled Hup-T4 and Capan-1 cells were spiked-in mDLA before freezing. In thawed samples, the number of cells was determined using flow cytometry and then compared with the number of spiked-in cells to calculate the recovery rates (%). p = 0.029, by unpaired t-test.

4.2.3 CellSearch® CTC analysis of cryopreserved patient-derived DLA samples

Cryopreserved DLA aliquots from 16 CTC+ patients were processed with the CellSearch® system for CTC detection (FR_DLA cohort, n = 16). For each patient of the FR_DLA cohort, the CTC count of freshly analyzed DLA products was available and this allowed to have a reference to compare the cell recovery from cryopreserved samples. Aiming to adopt similar scoring criteria, the galleries from the frozen samples (figure 24, left panel) were compared with the ones from the freshly analyzed samples (figure 24, right panel).

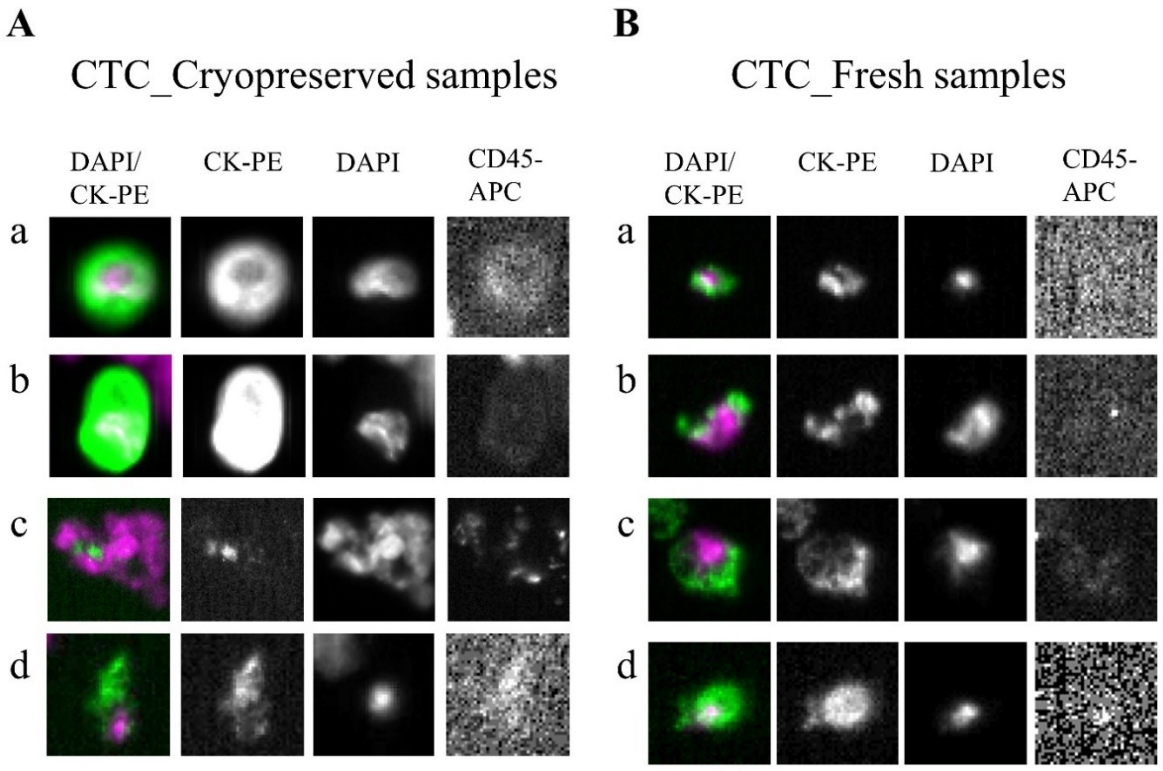

Figure 24. Representative images from CTCs obtained with CTAII. The four columns depict from left to right: Nuclear DAPI staining (purple)/cytokeratin (CK)-PE (green) overlay, CK-staining, nuclear DAPI staining and CD45-APC staining. **(A)** Left panel shows representative images from CellSearch-processed cryopreserved DLA samples from 4 different patients. **(B)** Right panel shows CellSearch-processed fresh DLA samples from one patient.

Although CTC classification in frozen samples was more challenging due to the higher frequency of WBC-aggregates which could mask some CTCs (figure 24, left panel, c) and cells with fragmented CK (figure 24, left panel, d), CTCs could be detected in 75% of 16 frozen samples (12/16) (figure 25A), and the detection frequency was not statistically

different (p = 0.101, by Fisher's exact test). A median of 2.5 CTCs per $100x10^6$ WBCs (range: 0.5-16 CTCs/$100x10^6$ WBCs) was calculated in fresh samples and a median of 1.85 CTCs/$100x10^6$ WBCs (range: 0-11 CTCs/$100x10^6$ WBCs) in the matched frozen samples (n = 16). The CTC count was not significantly different in fresh samples compared to frozen samples (p = 0.07, by Wilcoxon matched-pairs signed rank test) (figure 25B).

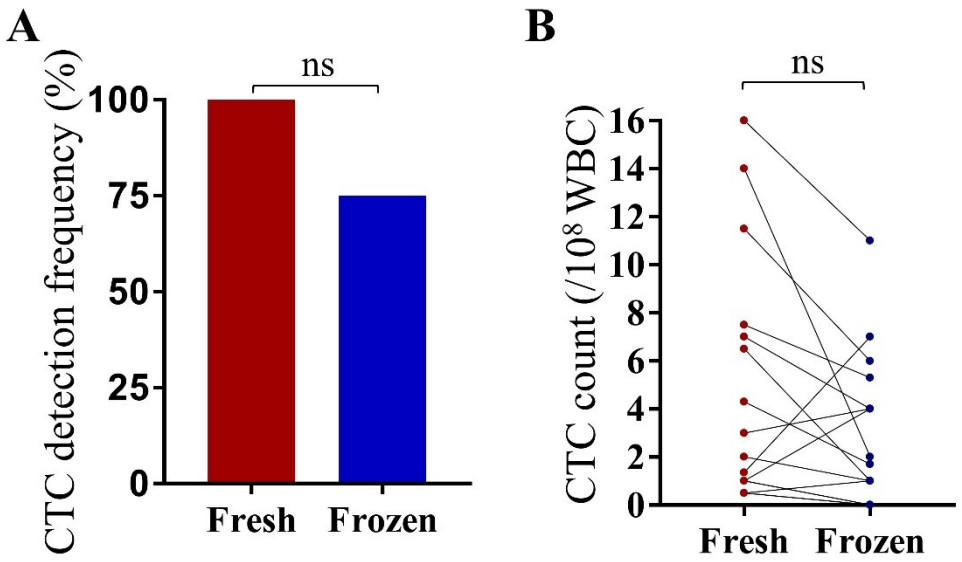

Figure 25. CellSearch-CTC detection in fresh and cryopreserved DLA products. (A) CTC detection frequency in matched fresh and frozen DLA samples (n = 16). **(B)** Number of CTCs detected in matched fresh and frozen DLA samples. All CTC counts were normalized for 10^8 WBCs analyzed.

4.2.4 CTC isolation with flow sorting and micromanipulation

After detection of CTCs with CellSearch® system in thawed DLA samples of 12 patients of the FR_DLA cohort, the enriched samples were further processed to isolate single tumor cells. Cell isolation was performed from a total of 14 CellSearch-enriched samples (two additional aliquots were processed for patient #1). A total of 102 potential CTCs (from 13 DLA aliquots obtained from 11 patients) were isolated with the MoFlo™ XD flow cytometer with a median of five cells/patient, and a total of four potential CTCs (from one DLA aliquot obtained from patient #1) were isolated by CellCelector™ micromanipulation (figure 26A, B). For each patient sample, five single WBCs were also successfully isolated either with flow

sorting or micromanipulation. The number of cells isolated by flow sorting was 1.9-fold higher than the number of the cells detected by CellSearch® (figure 26C).

A

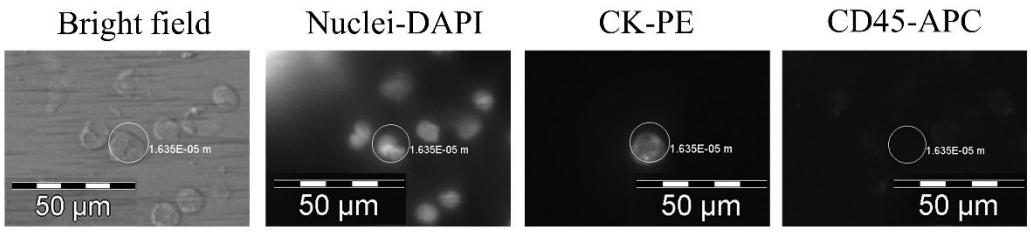

B

	CTC_Total		CTC_Per patient	
	Total count	QC bands ≥1	Median count	Range
CS_Detected	57	na	2	0-11
FACS_Isolated	102	88	7	0-31
CellCelector_ Isolated	4	3	4	4
Tot_Isolated	106	91	5	0-31

C

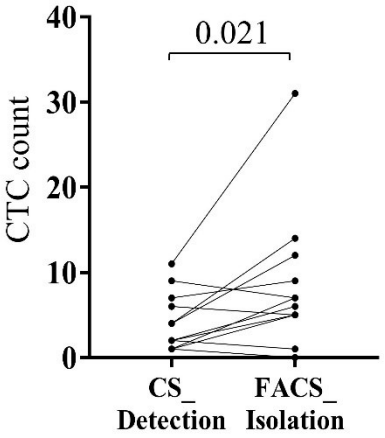

Figure 26. CTCs detected and isolated from thawed DLA samples of PDAC patients. (A) Representative CTC candidates isolated using CellCelector™ micromanipulator. Glass slides were scanned at a magnification of 40X, in each of the following channels: bright field for cell morphology visualization, DAPI for nuclei, PE for cytokeratins, APC for CD45. CTCs were defined as cells with intact morphology and DAPI+/PE+/APC-. **(B)** The table summarize the number of CTCs detected by CellSearch® system analysis and the number of CTC candidates isolated either with flow sorting or micromanipulation. Results are also reported as the median CTC count (with range) for each patient sample. **(B)** Counts of CellSearch-CTCs and CTC candidates detected by flow cytometry for individual patient samples. p = 0.021, by Wilcoxon matched-pairs signed rank test.

4.3 Molecular characterization of single cells isolated from fresh or cryopreserved PDAC DLA samples and matched tumors

4.3.1 Genome quality evaluation of WGA products of single cells isolated from fresh or cryopreserved PDAC DLA samples

The single cells isolated from the fresh or cryopreserved DLA samples were genomically characterized to validate their value as molecular tumor surrogates.

As a first step, the whole genome of each single isolated cell was amplified using a whole genome amplification (WGA), and a quality control check of the WGA procedure was performed. The quality control helps to predict the success of downstream analytical methods through the determination of the number of PCR amplicons, which indicates the presence of specific DNA fragments in the WGA library (figure 27A). From the initial 117 potential CTCs isolated (106 CTCs from cryopreserved DLAs and 11 CTCs from fresh DLAs), a medium to high quality of the WGA product (more than two PCR amplicons observed with the QC test) was observed in around the 71% of cells (83/117), while a low genomic quality (one or two QC-PCR amplicons) was observed in around the 12% of cells (14/117) (figure 27B). All the 97 CTCs from these both fractions were subsequently analyzed to detect point mutations in hotspot regions by targeted NGS, while only cells with a medium to high DNA quality and/or with at least a SNV detected (n = 31) were selected for more comprehensive chromosomal copy number profiling by whole-genome low coverage NGS. As shown by the black column in the graph of figure 27B, 17% (20/117) of the potential CTCs did not show any PCR amplicon with the QC test (e.g., CTC#4, figure 27A) and DNA from these cells was not further processed for molecular characterization.

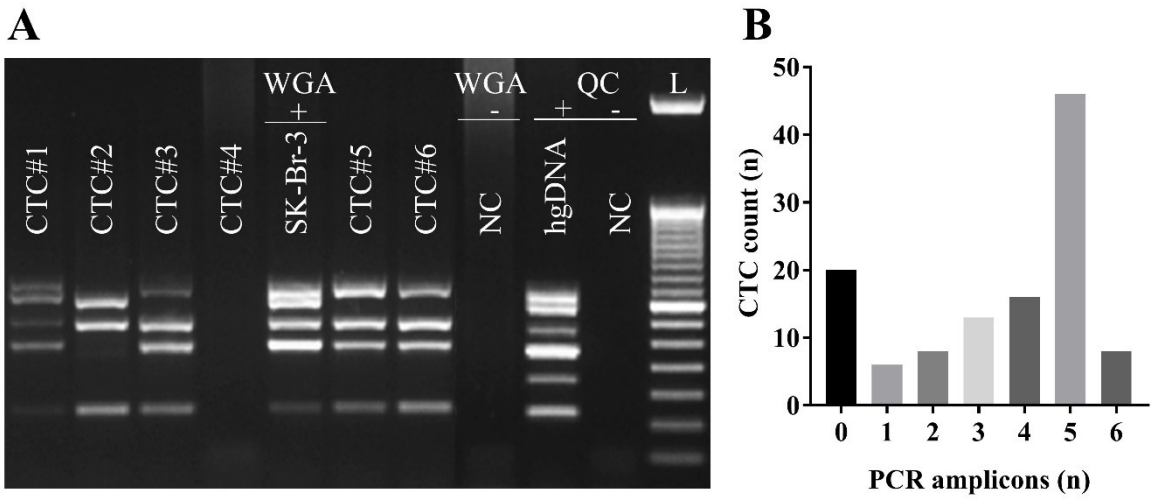

Figure 27. Evaluation of single cell genome quality after WGA. **(A) Representative gel electrophoresis of QC multiplex PCR products.** Amplified DNA samples from six patient-derived potential tumor cells (CTC#1-6). One SK-BR-3 cell serving as WGA positive control (WGA+), and DNA and nuclease-free water serving as WGA negative control (WGA- NC) of the WGA reaction. Commercial human genomic DNA (hgDNA) was used as positive control (QC+) and water was used as negative control (QC- NC) of the QC-PCR reaction. The presence of more than 2 PCR amplicons indicated a medium to high genomic quality. L: 50bps ladder. **(B) Genome quality of the 117 single cells isolated from fresh and cryopreserved PDAC DLA samples.** Bar graph shows the number of cells with 0, 1, 2, 3, 4, 5 and 6 amplicons obtained after QC multiplex PCR.

4.3.2. Detection of KRAS and TP53 point mutations

Point mutations in KRAS and TP53 are crucial events of PDAC carcinogenesis (32, 33), and specific point mutations are frequently detected in hotspot regions of these genes. For this study, the isolated CTCs and matched tumor tissue was analyzed for the presence of mutations in the hotspot genomic regions located in KRAS exon 2, KRAS exon 3, TP53 exon 5, TP53 exon 7, TP53 exon 8.

Out of the 97 CTCs screened, a total of 26 cells from seven patients (Pt #1-7) showed at least one SNV, with an allele frequency >5% (table 11). Globally, 12 SNV types were detected, of which 10 are predicted as being pathogenic and two with an unknown pathogenicity prediction (table 11). The potential pathogenicity of the detected point mutations was evaluated using a FATHMM scores ≥0.9 as criteria for pathogenicity (COSMIC: http://cancer.sanger.ac.uk/cosmic).

In CTCs of two patients (patient #1 and #7) the mutation KRAS G12V (c.35G>T) was detected. Interestingly, in patient #1, this mutation was present as homozygous (VAF = 100%) in one CTC, and as heterozygous (VAF = 50%) in the other CTC. In patient #7, the same mutation was present as homozygous in six CTCs, while in 1 CTC the G12V mutation was detected with a VAF = 16%. Although the presence of low frequent SNVs in codon 13 and 61 was investigated (27-29) (table 1), no mutations in those codons were detected. However, in two cases, mutations in KRAS exon 3 with an unknown pathogenicity were detected: KRAS D33N (patient #6), KRAS I55T and KRAS T58A (patient #7). In patient #7, one cell showed concomitant mutation in KRAS exon 3 (KRASI55T) and TP53 exon 7 (TP53 M246T), but in no cases, concomitant mutations in KRAS exon 2 and in TP53 were observed. In six patients, only mutations in TP53 were detected. Patients #2, #3 and #5 harbored the mutations TP53 P151R, TP53 R273C and TP53 R282W respectively, which are among the highly frequent missense mutation in TP53 occurring in PDAC patients (25, 35-40, 50). In four patients, less frequent mutations in TP53 were annotated: P112R, Q165*, R174G, T230A, M246T, L252P, E258G. Nevertheless, each of these mutations except R174G are reported as pathogenic.

Table 11. Summary of SNVs and CNA detected in CTCs and tumors. *Data are part of Stoecklein, N.H., Fluegen, G., Guglielmi, R. et al.,* Mol Cancer (2023) (238).

Patient ID	Sex	CTC(C) ID or Tumor(T) ID	SNV (KRAS)	SNV (TP53)	VAF	Prediction	CNA profile
Patient #1	F	C9917	G12V	0	50	pathogenic	aberrant
		C9918	G12V	0	100	pathogenic	aberrant
		C16328	NA	P112R	31	pathogenic	aberrant
		T 727	G12R	P151 R	21,25	pathogenic	aberrant
Patient #2	F	C10597	0	P151R	100	pathogenic	not aberrant
		T 723	G12V	R175H	8, 9	pathogenic	not aberrant
Patient #3	M	C10602	0	R273C	5	pathogenic	not aberrant
		C10603	0	R273C	12	pathogenic	not aberrant
		T 728	0	P278H	45	pathogenic	aberrant
Patient #4	F	C11123	0	R174G	31	unknown	not aberrant
		T 725	G12V	0	31	pathogenic	aberrant
Patient #5	F	C11351	0	R282W	100	pathogenic	failed
		C11352	A59G	E258G	30, 31	pathogenic	failed
		T 724	G12R	R175H	7, 7	pathogenic	not aberrant
Patient #6	F	C11569	0	L252P	16	pathogenic	not aberrant
		C11570	0	T230A, Y87H	16,19	pathogenic	not aberrant
		C11571	0	T230A, Y87H	25,25	pathogenic	not aberrant
		C11572	0	T230A, Y87H	13,16	pathogenic	not aberrant
		C11573	0	Y87H	20	pathogenic	aberrant
		C11575	0	T230A, Y87H	16,11	pathogenic	aberrant
		C11576	0	T230A, Y87H	23,23	pathogenic	not aberrant
		T 730	G12D	0	13	pathogenic	aberrant
Patient #7	F	C12201	G12V	0	100	pathogenic	aberrant
		C12202	G12V	0	100	pathogenic	aberrant
		C12204	G12V	0	100	pathogenic	aberrant
		C12207	T58A	0	14	unknow	not aberrant
		C12214	0	Q165*	21	pathogenic	not aberrant
		C12219	I55T	M246T	17,28	unknown, pathog.	not aberrant
		C12222	G12V	0	100	pathogenic	aberrant
		C12226	G12V	0	16	pathogenic	aberrant
		C12228	G12V	0	100	pathogenic	aberrant
		C12229	G12V	0	100	pathogenic	aberrant
		T 924-20	G12V	0	1.76	pathogenic	na
		T 924-20	G12D	0	0.48	pathogenic	na
		T 924-20	0	D186N	1.12	pathogenic	na
		T 924-20	0	R273H	1.38	pathogenic	na
		T 924-20	0	E285K	1.25	pathogenic	na
Patient #8	F	C10589	0	0	na	na	aberrant
		T 726	0	0	na	na	not aberrant
Patient #9	M	C11105	0	0	na	na	not aberrant
		T	na	na	na	na	na
Patient #10	M	C11116	0	0	na	na	failed
		C11117	0	0	na	na	aberrant
		C11118	0	0	na	na	failed
		T	na	na	na	na	na

When available, tumor tissue sections with a tumor content >50% were used for DNA isolation (figure 28) and SNV analysis. In patient #1, KRAS G12R and TP53 P151R were detected in the tumor tissue but not in the CTCs. Peculiar of this case was the difference in the nucleotide substitution of KRAS codon 12, between CTC and tumor: c.35G>T (translated in the G12V substitution) in CTC and c.34G>C (translated in the G12R substitution) in the tumor. Indeed, patient #2 and #4 harbored KRAS G12V in the tumor DNA, but not in the CTC. KRAS G12R was also observed in tumor DNA from patient #5, which did not harbor any mutations in codon 12 of KRAS in CTC DNA. In patient #6, KRAS G12D was detected only in tumor tissue. TP53 P151R was detected in tumor DNA from patient #1, but it was not detected in CTCs isolated from the same patient. Tumor DNA from patient #2 and #5 harbored the mutation TP53 R175H, but neither of them harbored that mutation in CTCs.
In patient #8, no SNV was detected in the tumor tissue neither in CTCs.
The data showed that the mutational profiles of KRAS and TP53 were often discordant between CTC and matched tumor tissue. Since the mutations detected in CTCs are not expected to originate in the germline, in parallel, the absence of each mutation was verified in WBC from the same patient (one to four WBC per patient) to exclude that the CTC-mutations were artefacts of WGA and NGS. In every case, the mutations detected in CTCs were not detected in WBCs. In one single WBC it was detected the point mutation TP53 S110P (VAF = 16%), with neutral pathogenicity score and not present in the CTCs from the same patient (supplementary table 1).

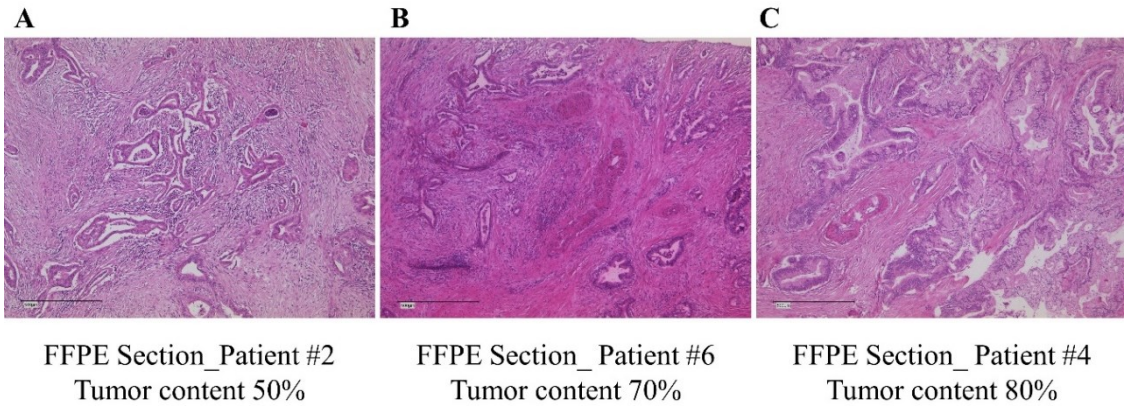

Figure 28. Histology sections of pancreatic tumor tissue. The sections were stained with hematoxylin and eosin and examined for the tumor content by a specialized pathologist. The pictures are representative of pancreatic sections with different tumor contents: (A) 50% (patient #2), (B) 70% (patient #6), (C) 80%. (patient #4). All the images were acquired at 50X and the scale bar represents 500 µm. *Images were kindly provided by the Institute of Pathology, Heinrich-Heine-University and University Hospital of Düsseldorf*

4.3.1.1. Validation of mutation screening with single cells from cell lines

The target NGS assay was validated in single cells form four cell lines with a known mutation profile (MDA-MB-231, CAPAN-1, SK-BR-3 and MIA PaCa-2). The profiling approach involving WGA, library preparation and NGS allowed us to detect in each cell line, point mutations in the expected position. However, in MDA-MB-321 cell line, we detected a point mutation that translated in a R280A substitutions instead that the reported R280K. Moreover, surprisingly, MDA-MB-231 cell line showed homozygous mutation G13D instead of the expected heterozygous mutation. To understand if this result was due to an allele loss, the sequencing library from bulk MDA-MB-231 WGA DNA was also sequenced. The VAF for G13D in this case was 65%, which could indicate that an allelic imbalance might have occurred during the whole genome amplification, deviating from the expected 50%.

Table 12. Overview of the point mutations in KRAS and TP53 detected in single cells and bulk material from cell lines. The percentages represent the VAF values. The right columns show the expected mutation and zygosity according to the literature (Cosmic, www.cancer.sanger.ac.uk, (250)). *Data are part of Stoecklein, N.H., Fluegen, G., Guglielmi, R. et al.,* Mol Cancer (2023) (238).

	KRAS			TP53					Expected Mutation	Expected zygosity
	Exon 2			Exon 5		Exon 7	Exon 8			
	G12C	G12V	G13D	A159V	R175H	R248W	R273C	R280A		
MDA-MB-231 bulk	0%	0%	65%	0%	0%	0%	0%	100%	G13D; R280K	Het; Hom
MDA-MB-231 #1	0%	0%	100%	0%	0%	0%	0%	100%	G13D; R280K	Het; Hom
MDA-MB-231 #2	0%	0%	100%	0%	0%	0%	0%	100%	G13D; R280K	Het; Hom
MDA-MB-231 #3	0%	0%	100%	0%	0%	0%	0%	100%	G13D; R280K	Het; Hom
CAPAN-1 #1	0%	100%	0%	100%	0%	0%	0%	0%	G12V; A159V	Hom; Hom
CAPAN-1 #2	0%	100%	0%	100%	0%	0%	0%	0%	G12V; A159V	Hom; Hom
Sk-Br-3 #1	0%	0%	0%	0%	100%	0%	0%	0%	R175H	Hom
Sk-Br-3 #2	0%	0%	0%	0%	100%	0%	0%	0%	R175H	Hom
MIAPaCa-2 #1	100%	0%	0%	0%	0%	100%	0%	0%	G12C;R248W	Hom; Hom
MIAPaCa-2 #2	100%	0%	0%	0%	0%	100%	0%	0%	G12C;R248W	Hom; Hom

4.3.2 Analysis of copy number alteration profiles in patient derived cells and matched tumor tissues

Genomic instability is a characteristic of most cancer cells and it contributes to originate somatically acquired CNAs, which play a major role in the cancer progression (251, 252). Due to tumor genetic heterogeneity, somatic CNAs might be masked by bulk genomic analysis, and can be best investigated analyzing individual cells. Therefore, here we assessed PDAC genome instability analyzing whole-genome CNAs in patient-derived single CTCs and matched tumor.

From the 31 cells screened, four potential tumor cells were discarded due to the low quality of the obtained profiles (dLRS >0.30 and number of reads <200k) (supplementary table 2). On the profiles with good quality obtained from tumor derived DNA and in single cell DNA, the percentage of aberrant genome (PAG) was calculated. To better evaluate if a single cell profile was aberrant or not, PAG was calculated also for matched single WBCs (figure 29A, supplementary table 3). The mean and highest value (mean = 0.7%; range 0-4.6%) of WBC-PAG (n=7) helped to interpret the CNA profiles from candidate CTCs, and all the patient derived cells with a PAG below than 4.6% were considered as non-aberrant cells. A total number of 13 cells from 5 patients (Pt#1, Pt#6, Pt#7, Pt#8, Pt#10) were confirmed as aberrant CTCs with an average PAG of 27.38% (range: 2.16-53.34%) (figure 29A). It was observed that 11 out of these 13 aberrant cells were also mutated for at least one pathogenic nucleotide substitutions in KRAS and/or TP53 genes (red rectangles, figure 32B), while two aberrant cells (from patient #8 and #10) did not show any investigated point mutations (grey rectangles, figure 29B). In one patient case (patient#1) aberrant profiles were observed in both CTCs and tumor (figure 29B, figure 30A). In patient #6 and #8, only CTCs showed aberrant profiles. On the contrary, only the tumor tissue DNA from patient #3 and #4 harbored CNAs.

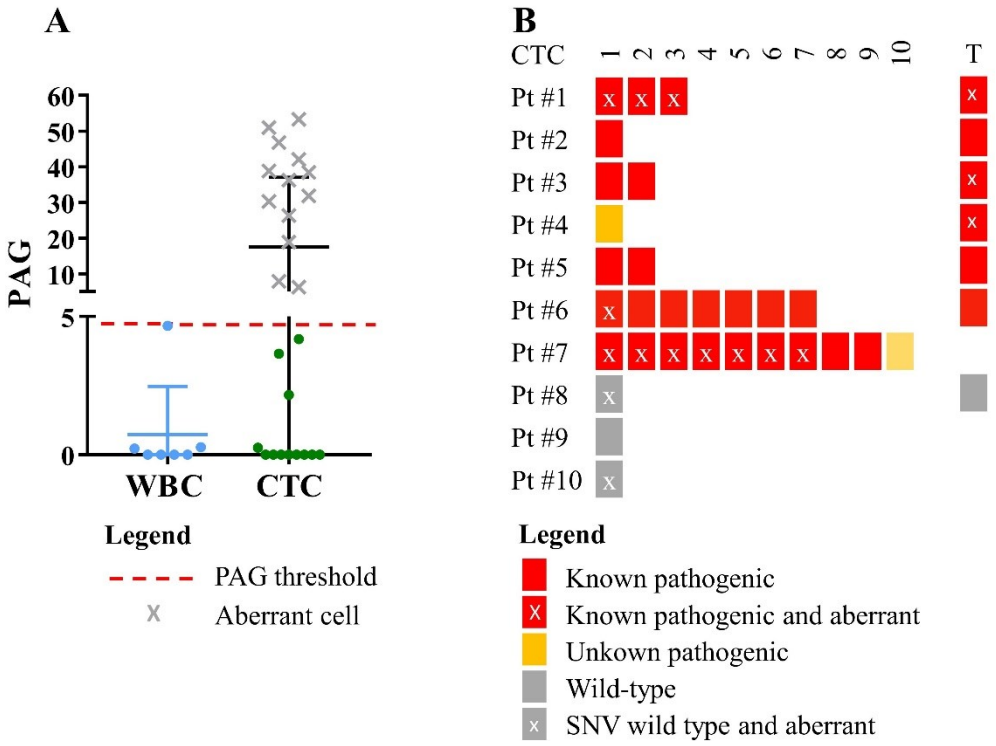

Figure 29. Mutational status from single patient derived cells and matched tumor tissue (A) Percentage of altered genome (PAG) in WBCs and CTCs. WBCs were isolated from 6 different patients, while CTCs from 10 patients. Line represents mean with standard deviation. Red dashed line represents the threshold determined by the highest PAG values obtained in WBCs. **(B) Summary of the mutational and CNA analysis.** Data were collected from 10 patients. Tumor was not available for 3 patients.
Data are part of Stoecklein, N.H., Fluegen, G., Guglielmi, R. et al., Mol Cancer (2023) (238).

Differences in gain and losses of chromosomal regions were observed between CTCs from different patients, as well as in CTCs from the same patient (figure 30A). CNAs were visualized via the progenetix plotting tool (https://progenetix.org/service-collection/uploader). The most frequent gains were observed in chromosome 1q, 1p, 2q, 5q, 6p, 7q, 7p, 8q, 11q, 11p, 12p and 19q; while the most frequent losses were observed in chromosomes 3p, 8p, 9p, 10q and 17p (frequency ≥ 50%). Notably, several known oncogenes and tumor suppressors are located in the same regions where more frequent aberrations were detected (e.g., EGFR in chromosome 7p, CDKN2A in chromosome 9p and TP53 in chromosome 17p) (figure 30B).
Although several differences in gains and losses were detected among CTCs, the CNA patterns revealed a high clonality among different CTCs of the same patient indicating a common origin of those cells, as shown by hierarchical cluster analysis performed for patient #1 and #7 (figure 30C). This analysis was performed only for those patients who displayed

the highest number of aberrant CTCs. Furthermore, in patient #1 CTC CNA profiles genomically resembled the pancreatic tumor (#T727) (Figure 30A and C).

Short tandem repeat (STR) analysis was used for the authentication both of CTC derived DNA and FFPE tumor derived DNA. Because the STR-PCR was not optimized for characterization of WGA products obtained with the MseI PCR, only partial STR profiles were obtained from such WGA-originated samples. However, the comparison between the patterns from patient derived single cells- and matching tumor- DNA was sufficient to confirm the same genetic origin in patient #2, #3, #4, #5 and #6 (supplementary table 3). In patient #1, #7, #8, #9 and #10, the tumor was not available for STR analysis.

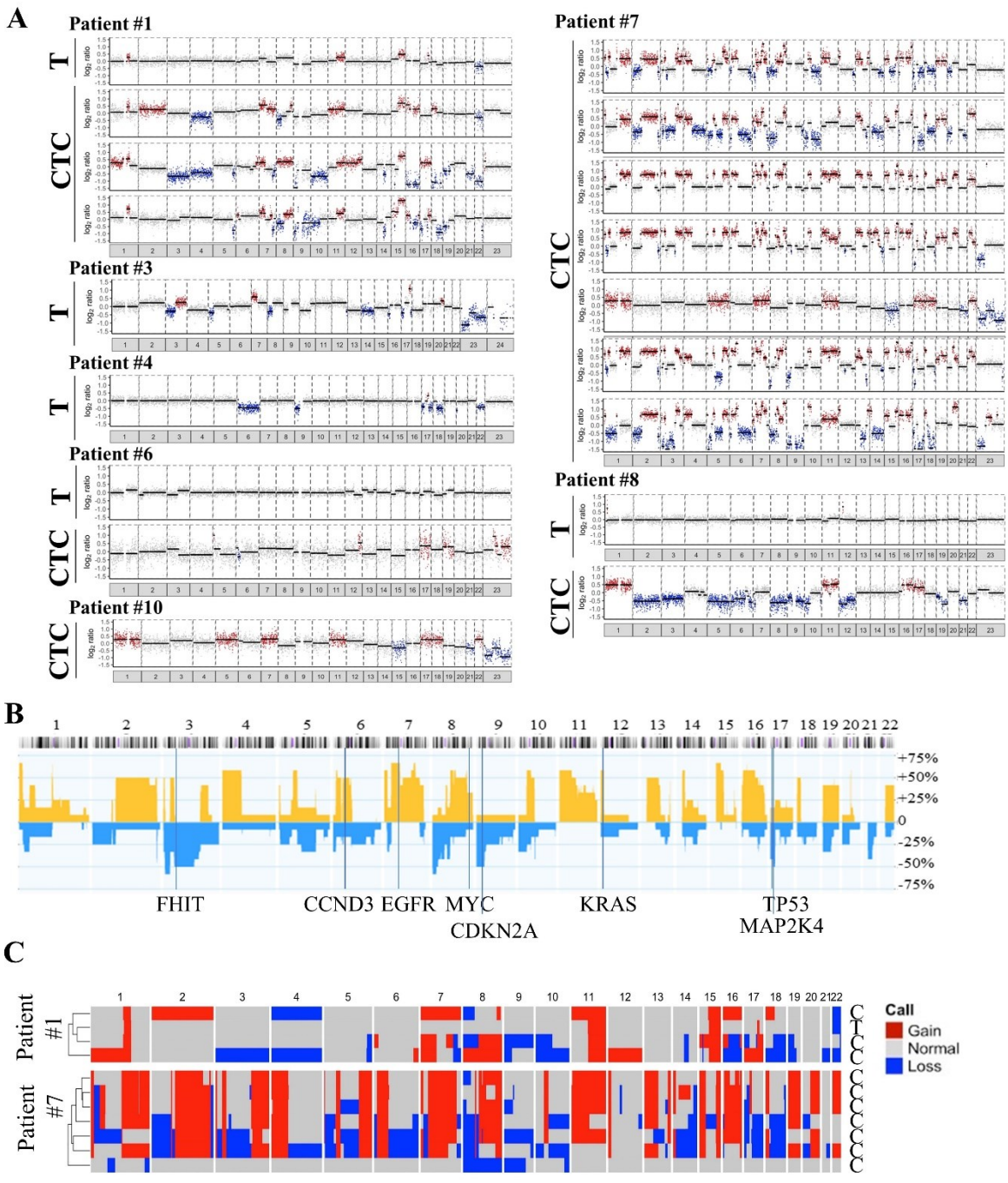

Figure 30. CNA analysis in CTCs and matched tumors. (A) Patterns of CNAs in the entire genome for single CTCs and matched tumors. The estimated CNA is reported on the y-axis as log2Ratio value; red and blue spots represent genomic gains and losses, respectively. CNA profiles are grouped for individual patient and solely patient profiles with aberration in CTCs and/or tumors are shown. Tumors are labelled with "T". **(B) Frequency of gain and losses in the isolated CTCs.** Gains are represented in yellow, while losses are in blue. **(C) Unsupervised hierarchical clustering heat maps depicting tumor clonality among CTCs in patient #7 and among CTCs and matched tumor in patient #1.** Tumor was not available in patient #7. Red represents gains while blue represents losses. CTCs are labelled with "C" and tumors are labelled with "T".
Data are part of Stoecklein, N.H., Fluegen, G., Guglielmi, R. et al., Mol Cancer (2023) (238).

4.4 Marker-independent enrichment of CTCs: DLA biochip

The use of CellSearch® system to analyze the whole DLA product would require multiple runs, due to the high load of WBCs (typically around 40 mL with $200x10^6$ WBCs/mL), and it would require high amount of expensive antibody cocktails, resulting inefficient in terms of load of work and costs. Therefore, alternative methods to process the entire DLA volumes are needed. A new label-free spiral chip was optimized to process DLA products and its performance was compared with the one of another commercialized label-free spiral chip (176).

4.4.1 Size of the tumor cell line cells

The efficiency of the cell enrichment within the spiral microfluidics chips is ultimately dependent on the size of the cells. Therefore, the cell diameter was calculated for three cell lines used for testing the device. A mean diameter of 13.7 ± 1.4 µm (range 10.5 to 15.9 µm) was measured for Sk-BR-3, a mean diameter of 15.1 ± 2.4 µm (range 11.8 to 20.5) was measured for Hup-T4, and a mean diameter of 15.9 ± 3.4 µm (range 12.3 to 26.4) for LNCaP (figure 31). The mean diameter of the WBCs was 8.5 ± 0.9 µm (range 6.4 to 10 µm), significantly smaller than the diameter of the cell line cells (P <0.0001).

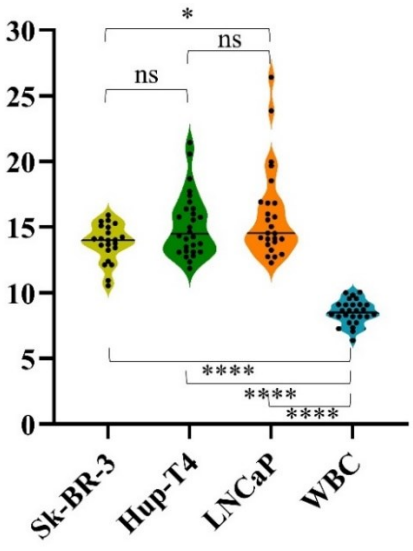

Figure 31. Cell diameter of the Sk-BR-3, LNCaP, Hup-T4 cells used for testing the microfluidic chips and of WBC isolated from mDLAs. Diameter was measured in randomly selected n = 22 Sk-BR-3 cells, n = 28 Hup-T4 cells, n = 25 LNCaP cells and n = 28 WBCs. Horizontal lines represent median value. Statistically significant differences. * indicates p = 0.0194 by Mann-Whitney U test.
Adapted from Guglielmi et al. (176), Creative Commons Attribution 4.0 International License.

4.4.2 Tumor cell recovery rates after mDLA enrichment with ClearCell® FX system and the DLA biochip

The three different cell lines were pre-labelled with different fluorescent dyes and were spiked in mDLA samples containing $50x100^6$, $200x10^6$ and $400x10^6$ WBCs (experimental condition 1, 2 and 3 respectively), and these resulting samples were used to test both the commercially available ClearCell® FX platform (CTChip FR1) and the new DLA biochip. For each of the tumor cell type used, it was observed a higher tumor cell recovery rate after DLA biochip enrichment than after CTChip FR1 enrichment (figure 32). By processing mDLA samples with $50x10^6$ WBCs (equivalent to ~15 mL PB), the mean tumor cell recovery rate was 30% in ClearCell® FX (n = 3 for each cell line, n_{tot} = 9) and 47% in DLA biochip (n = 6 for each cell line, n_{tot} = 18). By processing mDLAs containing $200x10^6$ WBCs (equivalent to ~60 mL PB), the mean tumor cell recovery rate was 23% in ClearCell® FX (n = 4 for each cell line, n_{tot} = 12) and 47% in DLA biochip (n = 6 for each cell line, n_{tot} = 18). By processing mDLAs containing $400x10^6$ WBCs (equivalent to ~120 mL PB, experimental condition 3) the output straw of the ClearCell® FX system clogged and did not allow sample enrichment, while it was calculated a mean tumor cell recovery rate of 50% (n=6 for each cell line, n_{tot} = 18) in the DLA biochip.

The global mean tumor cell recovery rate after CTChip FR1 enrichment, calculated considering all data collected with the different cell types, was 25% (n = 21) (data from experimental conditions 1 and 2), while the global mean tumor cell recovery rate with the DLA biochip was 48% (n = 54) and significantly higher ($p < 0.0001$) than the recovery calculated for the FR1 chip.

Although the difference in tumor cell sizes, the recoveries were not significantly different between the different cell lines across the three experimental conditions. An exception was observed only in the case of a higher recovery rate of LNCaP, the largest measured cell line, enriched from mDLA samples with $400x10^6$ WBCs.

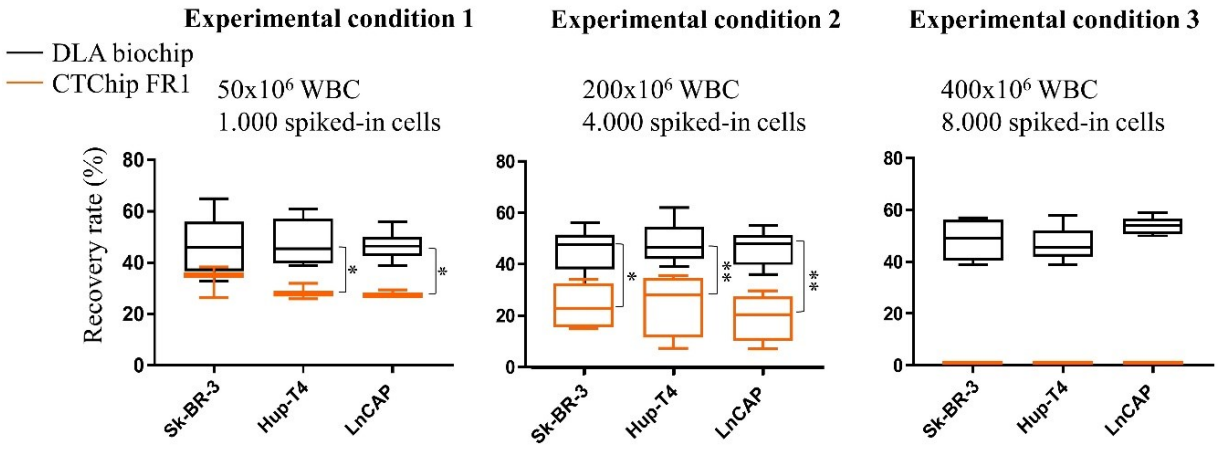

Figure 32. Tumor cell recovery rates after enrichment with the CTChipFR1 and DLA biochip. *p <0.05; **p <0.01, by Mann-Whitney U test.
Adapted from Guglielmi at al. (176), Creative Commons Attribution 4.0 International License.

4.4.3 WBC contamination after DLA biochip enrichment.

The CTC count and isolation can be difficult if the sample still contains a high WBC fraction after the enrichment step. Therefore, an efficient CTC enrichment technology should allow an effective CTC capture with low WBC contamination (i.e. high CTC purity). This can be difficult to achieve when the initial sample has an extremely high WBC load, as the case of DLA products. For this reason, it was measured the average WBC carryover after one (S1, n = 3) and two (S2, n = 6) enrichment cycles of mDLA products containing $50x10^6$, $200x10^6$ and $400x10^6$ WBCs. As expected, it was observed that the higher the cellular content of the processed mDLA, the higher the number of WBC contaminants counted in S1 and S2 (right panel, figure 33). Also not surprisingly, the number of contaminating WBCs decreased substantially after performing the second round of enrichment in all three experimental conditions.

Respect to $S1_{50x10^6}$, $S1_{200x10^6}$ and $S1_{400x10^6}$, the second enrichment cycle alone led to a WBC depletion of 75%, 94% and 99.7% respectively (right panel, figure 33). In the enriched sample initially containing $400x10^6$ WBCs, an average of 60,000 WBCs was observed after the two cycles (S2).

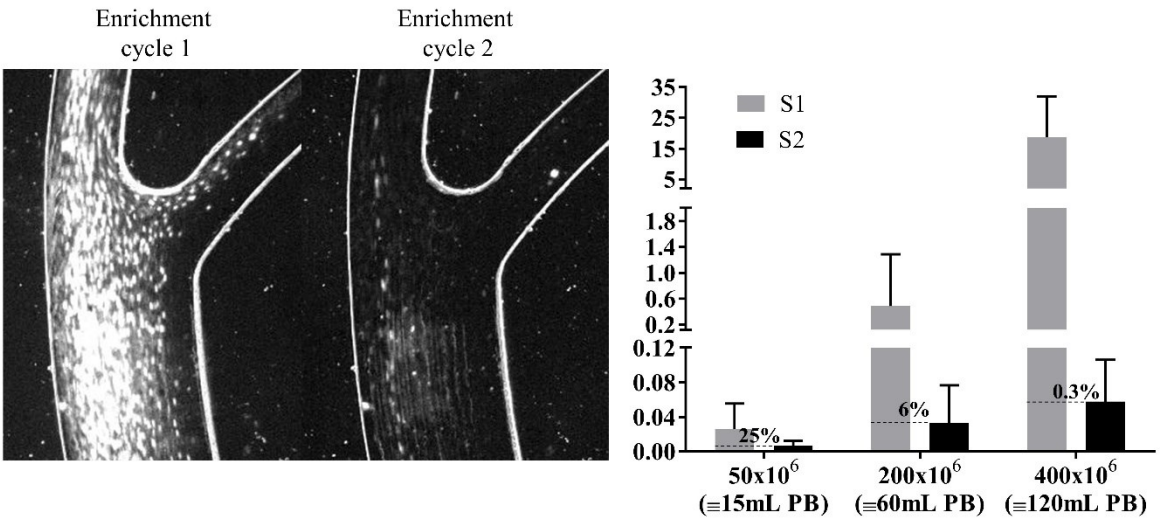

Figure 33. WBC carryover after one and two DLA biochip enrichment cycles. Left panel shows a representative snapshot taken at the branching point close to the outlets showing the WBCs flow in the DLA biochip during the first and the second enrichment cycle, tracked using the Photron Fastcam SA3 (MEC, Indiana) connected to the Olympus IX71 inverted microscope (Olympus, US). Right panel shows the mean number of WBCs counted after one enrichment cycle (S1, analyzed with hematology analyzer), and two enrichment cycles (S2, analyzed with flow cytometry), starting from mDLA products containing $50x10^6$, $200x10^6$ and $400x10^6$ WBCs. *Adapted from Guglielmi et al. (176), under a creative Commons Attribution 4.0 International.*

5. DISCUSSION

The goal of the present work was to increase the chance to detect and isolate pancreatic CTCs, with particular interest to obtain a sufficient number of cells that allows to stratify patients at high risk of metastasis and to perform genomic characterization.

5.1 Detection of CTCs in DLAs and prognostic impact

A first attempt to reach the research goal of this work was to test the value of screening a larger blood volume to increase the chance of detecting pancreatic CTCs. Recent studies demonstrated the value of increasing the blood volume for CTC analysis (223-226). Based on this strategy, DLA was used for the purpose of this work. In fact, DLA was introduced with the aim to increase the detection of CTCs (227, 232) by the screening of liters of blood and the analysis of only 5% of a DLA product using CellSearch® resulted already in a 250% increase of the CTC detection frequency and a 30-fold escalation of CTC count compared to a 7.5 mL PB sample (227).

In this study, the DLA procedure was performed in a cohort of 46-patients without any noticeable side effects and without any clinically relevant effect on vital parameters (figure 16), which is in line with previous reports (231, 233, 253). Using MNCs as a reference, the mean efficiency of the procedure was higher than 30% in 41 patients, indicating a highly efficient pre-enrichment process according to previous studies (231). Although the MNC collection efficiency was below 30% cut-off in 5 patients, the PB-equivalent volume was within the expected range and therefore, we decided to further process those samples as well.
The CellSearch® analysis of a median of 3 mL DLA/patient (containing approximately $200x10^6$ WBCs) significantly increased the chance to detect CTCs compared to the analysis of 7.5 mL of matched PB (figure 19 B) and the mean CTC count in 1 mL DLA was 16-folds higher than the mean CTC count in 1 mL PB (figure 19 A). These results demonstrated that the small sample volume dramatically affects the CTC detection in PDAC and that the analysis of around 6% of DLA product increases the CTC yield, in line with recent findings that emerged from a European prospective multicenter study in metastatic breast and prostate cancer (230). Noteworthy, it is the fact that extrapolating the mean number of CTCs in the whole DLA product results in a 90-fold higher mean number of CTCs compared to in 7.5 mL PB sample. This data emphasizes the advantages of screening a DLA entirely and the need of efficient methods to do it.

An additional relevant aspect of our study was the choice of a strategy to help the operator with DLA-CTC selection, by using a semi-automated image analysis software, ACCEPT (254). The ACCEPT pre-selected events were anyhow reviewed by a trained operator for the final cell selection. A comparative analysis between fully manual- and ACCEPT-classification of target cells was performed to evaluate the differences in terms of CTC count and detection frequency. Notably, the ACCEPT algorithm includes a more effective image segmentation to separate the relevant objects from the background cells compared to the older CellSearch® algorithm, which is especially relevant for cartridges with high density as observed in DLA samples (255). These different image processing tools can account for the differences observed in CTC detection frequencies between the original CellSearch® analysis and the reviewed ACCEPT detection (figure 18) of the same images. Indeed, although in the 72% of the cases, ACCEPT and the operator agreed to score a patient as CTC+ or CTC- (figure 18A), the use of ACCEPT allowed to detect CTCs in a significantly higher number of patients compared to the manual classification, for a total of 26 patients scored as CTC+ (≥1 CTC) by ACCEPT and 17 scored as CTC+ by operator. On the contrary, only two samples that were scored as CTC+ by the reviewer were not scored as CTC+ by ACCEPT. However, the CTC count was statistically not significantly different between CTC+ samples scored with ACCEPT and CTC+ samples scored by the original CellSearch® classification (figure 18 B). The differences observed for CTC detection highlight that a higher variability in the CTC selection might occur when a full manual scoring is adopted and the potential benefit to use a more standardized CTC count approach, which might facilitate the detection of relevant objects from the background cells (255), enable comparison of different reviewers and facilitate the achievement of a consensus on assigning objects (254).

The use of DLA products, which allowed to detect higher numbers of CTCs compared to PB offered the chance to explore the clinical value of pancreatic CTC count as tool for the risk stratification of operable PDAC patients. A positive correlation was found between DLA-CTC count and disease progression, as suggested by the higher CTC detection frequency ($p = 0.0314$) and CTC count ($p = 0.005$) in patients with advance disease (M1) compared to patients with localized tumor (M0) (figure 20 A, B). Similar associations were not found with the PB-CTC count, although this result might be biased by the low number of CTC detected, highlighting further the importance to detect a significant number of CTCs.

Furthermore, Kaplan-Mayer analysis in the entire cohort and in the subgroup of patients treated with curative intent showed that the presence of at least one DLA-CTC correlated with

poor survival, suggesting their potential as prognostic biomarkers. This observation is supported by the prognostic role described for CellSearch® CTCs in PB (198, 199, 201, 202, 205), although CTCs were less frequently detected. However, low frequent events detected in PB might limit Kaplan-Mayer analysis, making the analysis less robust. Interestingly, M0 patients in the DLA cohort without CTCs showed a significantly better OS compared to M0_CTC+ patients, showing that the presence of CTCs might also help to predict the risk of disease progression in patients with localized tumor, when the metastasis is at a subclinical stage and treatments might be more efficient (256). The data also showed that the absence of PDAC CTCs in M1 stage might also help to select M1 patients that could profit from combined chemotherapy (78, 80), as highlighted by the similar OS observed between M0_CTC+ and M1_CTC- patients. Of course, the potential of PDAC CTCs to drive therapeutic decisions would be unlocked once technical solutions for their detection are available for clinical routine.

5.2 Molecular characterization of CTCs from cryopreserved and fresh PDAC DLAs.

Besides CTC enumeration that has the potential to refine tumor staging in PDAC, the value of CTC profiling is gaining lot of interest for diagnostic tests in the context of targeted therapies but also for basic research questions (235-237).

In the present work, the genetic profiling was performed on cells isolated both from fresh and frozen DLA samples. Indeed, only 6% of the whole DLA product/patient was processed immediately after collection by CellSearch® system, while the remaining sample fraction was frozen and represented a precious source to isolate and characterize CTCs. A thawing protocol was adapted for DLA products (257) and the thawed samples were processed by CellSearch® similarly to fresh DLA samples.

In this work, the detection of typical SNVs in KRAS and TP53, the mutated genes in PDAC, helped to confirm the tumor identity in isolated CTCs. A total of 24 cells from six patients (four patients of the FR_DLA cohort and two patients of the DLA cohort) showed at least one pathogenic mutation in the target regions, while two additional cells showed mutations with unknown pathogenicity.

Genomic instability is considered as a hallmark of cancer (251, 258). Therefore, with the aim to identify pancreatic CTCs, single cell CNA profiling was performed in addition to SNV detection. The isolation of single CTCs and the generation of WGA libraries enabled low-

resolution NGS to assess the CNA profile from cells isolated from 10 patients. A total of 13 cells from five patients harbored multiple genomic aberrations, with a mean PAG of around 27%. The results (summarized in figure 29 and table 11) showed that 10 out of these 13 aberrant cells harbored also point mutations in KRAS and/or TP53 genes, providing additional evidence for their malignant origin. Indeed, two cells (from patient #8 and #10) which showed an aberrant profile did not harbor any of the SNVs investigated. The lack of SNVs in well-known tumor associated genes was already observed in CTCs with copy number altered regions involving the tumor suppressor gene PTEN and the oncogene MYC (258). Also, it must be considered that KRAS and TP53 mutations are not detectable in 100% of PDAC tumors (259). Surprisingly, 15 cells that harbored at least one pathogenic mutation did not show an aberrant profile. The absence of CNAs in the PDAC CTCs cast thus doubt on their malignant origin and their nature remains unclear at this point. It is possible that these cells are CECs (260), pre-malignant epithelial cells co-mobilized with the cancer cells or, potentially, false-CK-positive endothelial cells. On the other hand, the absence of mutations in the tested WBCs corroborates that the detected pathogenic SNVs in the CNA-negative cells are not sequencing artifacts. In summary, low-pass NGS allowed to detect similar CNA profiles in CTCs isolated from the same patient proving the common origin of the cells and allowed to show that CTC CNA profiles genomically resemble generally the tumor tissue (figure 30 A, C). Moreover, the method allowed to detect frequent aberrations in chromosomes 8q and 9p, consistent with previously reported CNAs in PDAC (54, 57) (figure 30 B). Additionally, our analysis revealed aberrations at chromosome arms 6p, 12p, 9p and 17p, which are not known as most frequent aberrant regions in PDAC. The CNAs were localized in regions where known oncogenes and tumor suppressors are located. In particular, CNAs were observed in chromosome arms where genes as CCND3 (cyclin D3), KRAS, CDKN2A and TP53 are located. Interestingly, these genes are known for their role in PDAC (124).

By showing that the genetic characterization of CellSearch-detected CTCs from DLA products was technically feasible, it was provided a proof of concept that the analysis of a whole DLA product might offer the chance for pancreatic CTC profiling. CTC profiling is gaining interest as a promising approach to dissect tumor heterogeneity and detect new potential therapeutic targets (235-237) and might be a useful approach in PDAC management. PDAC is characterized by a high degree of intra-tumoral heterogeneity with often multiple subclones displaying different genotypes and biological characteristics (261, 262) and therapeutic failure is often attributed to such heterogeneity (263). The formation of subclones

with distinct genotypes is explained by the clonal evolution model as the stochastic accumulation of mutations over time (264, 265). NGS studies of bulk tumor samples showed that metastasis is initiated by a subclone of the primary tumor (founder clone), but also revealed that there are many mutations represented in higher frequencies in metastatic tumor than in the paired primary tumor (264, 266). However, although sophisticated statistical and mathematical models have been developed, bulk data did not result sufficient to extrapolate single-cell genotypes or identify rare subclones to infer tumor heterogeneity (264, 267). Indeed, a tumor biopsy is limited in space and is usually sampled at a single time point, providing only a snapshot in location and time (268). In this context, the analysis at single cell level of CTCs which are released from the tumor into the bloodstream and can be repeatedly collected by a liquid biopsy, might better represent the whole tumor allowing to reveal subclonal mutations and monitoring the cancer evolution (natural or due to the pressure of therapy) (133, 269-271).

Several studies showed that mutations in CTCs reflect the spectrum of mutations in the primary tumor and distant metastases (272-274). On the other side, other studies highlighted that SNVs as well as CNAs can be divergent between CTCs and tumor tissue (275, 276) and that CTCs represent a genetically heterogeneous population of cells (215, 277). However, in PDAC not many studies used single cell analysis to deeply investigate this aspect, mainly due to the difficulties to obtain sufficient pancreatic tumor cells.

A recent study which analyzed KRAS mutations in pancreatic CTCs and tumor showed that KRAS mutations in CTCs were only partially concordant with those detected in matched tumor (278). In this study, 6 mL PB/patient was processed to capture the target cells using a size-based method and discriminating malignant CTCs based on their cytomorphological features. Although this method yielded a detection frequency higher than 70%, it relied on a less validated assay compared to the CellSearch® technology used in the present work. The processing of DLA samples using an EpCAM-based enrichment proved to be advantageous for the detection of pancreatic CTCs and allowed downstream profiling. The genetic analysis revealed that CTCs from the same patient harbored both common and unique SNVs, and that CTCs and matching tumor showed discordant SNVs in every patient, supporting the hypothesis that CTCs represent only a subpopulation of a heterogeneous tumor (216). For example, in patient #1 we could detect the mutation KRAS G12V (exon 2) in 2 out of 3 CTCs, while the mutation KRAS G12R was detected in the tumor. Similar observations emerged for TP53 SNVs. For example, patient #6 showed concordant TP53 Y87H (exon 5) and TP53 T230A (exon 7) mutations in the CTCs, but TP53 Y87H was not detected in the

tumor (exon 7 was not covered by target sequencing). Being aware that sample contamination can falsely inflate sample heterogeneity, STR analysis was performed to confirm the common origin of CTC and tumor (supplementary table 3).

As observed for SNVs, some differences in gain and losses emerged in CTCs from the same patient and between CTCs from different patients, supporting previous findings (276).

A comparison of CNA profiles between CTCs and matched tumor tissue was not always possible, because tumor DNA content was not sufficient (patient #7), or biopsy was not available (patient #10). Excluding these cases, comparative CNA profile analysis highlighted that in two patients (patient #6 and #8) only CTCs showed aberrant profiles. FFPE samples weren't always informative, because they showed either flat (patient #2, #5, #6 and #8) or low-aberrant profiles (patient #4). Considering that we processed FFPE samples stored for a long time, one possibility to explain this result might be connected to a low DNA quality. In fact, the DNA integrity of FFPE tissue can be affected by formalin fixation which induces molecular crosslinking, nucleotide changes and DNA degradation (279, 280). Another possible explanation is stromal contamination (281). Although tissue samples were accurately pre-selected by qualified pathologist and only slices with tumor content ≥ 50% were chosen, one cannot exclude that normal stromal cell DNA was amplified and thus, the method did not allow CNAs detection. The presented proof of concept sets the stage for deeper clinical studies that might use DLA-enriched CTCs as an interesting alternative to invasive endoscopic ultrasound guided biopsy, to enable pancreatic CTC profiling.

5.3 Technical validation of a new microfluidic device for enrichment of CTCs from large volumes of blood by using mimicking DLA products.

In this study, CellSearch® analysis of around 6% of DLA products helped to detect a sufficient number of pancreatic CTCs to demonstrate their correlation with the disease progression and the clinical outcome, supporting their potential clinical utility as prognostic biomarkers. Furthermore, PDAC DLA allowed to obtain pancreatic CTCs for molecular characterization, even from cryopreserved aliquots. Taken together, these findings highlight the value that CTCs might have for the clinical management of PDAC and for unravelling important mechanisms of the disease. Despite the promising results collected in this study, the potential of DLA has not been fully exploited, due to the small fraction of product analyzed. Indeed, the analysis of the whole DLA would allow to obtain higher number of CTCs and

thus increase the sensitivity for further CTC studies in PDAC.

However, the analysis of the whole DLA requires methods that efficiently deplete the high load of WBCs typical of this product (around $100x10^6$/mL), within reasonable processing time and costs. So far, CellSearch® analysis allowed to efficiently process at once up to 5% DLA ($200x10^6$ WBCs) (230, 231). This means that multiple CellSearch® runs would be necessary to process the whole DLA product from one patient, with a considerable impact on costs and time. Different strategies have been tested to process higher DLA volume. Interesting results have been recorded using enrichment methods based on biophysical properties as size, deformability and inertial focusing. For example, ISET allowed to process up to 10 mL NSCLC DLA, containing between 3- and 8-fold as many leukocytes as could be handled by CellSearch® (253). However, the ISET protocol adapted for DLA is quite labor intensive and the rescue of the cells from the filter might be challenging. Another recent promising research showed that the microfluidic based device ^{LP}CTC-iChip allowed to process the entire DLA volume (65 mL) (282). However, this method is also labor intensive because it requires multiple steps (RBCs and platelet inertial separation, magnetic depletion of antibody-tagged leukocytes) and cell loss might occur during the transfer of the sample between the two fluidically unconnected compounds of the device. Moreover, the need of an antibody cocktail used for the negative depletion might not be economically convenient.

Although many interesting methods have been reported (234, 253, 257, 282), the need of volume-scalable, time- and cost-effective methods are still required to process high DLA volumes. As part of this thesis work, a new label-free spiral chip (DLA biochip) was tested and the results were compared with those from a similar label-free spiral chip (CTChip FR1) commercialized with the purpose to enrich CTC from 7.5 mL of blood (176). DLA biochip was manufactured by Biolidics Ltd (Singapore) specifically to process DLA products. It is based on a spiral microchannel technology as the CTChip FR1, but the geometry of the cross-section is different between the two chips: rectangular for the CTChip FR1 and trapezoidal for DLA biochip (172) (figure 5 and 14 A). The trapezoidal geometry of the cross-section facilitates the cell separation based on their sizes upon a Dean Vortex Trapping (DVT) process. Large tumor cells migrate and can equilibrate in positions near the inner wall (figure 14 A, right panel), while the secondary dean flow acts as a “cell trapper” preferentially on the small blood cells, which are entrapped within the dean-vortexes near the outer wall (172). Compared the cell separation performed within the rectangular cross-section chip, the physical proprieties of this chip allow that larger sample volumes can be enriched at faster

rates with potentially higher tumor cell recoveries, although a lower CTC purity might be observed. However, two enrichment cycles through the same chip are considered a good compromise to increase the purity, as we also demonstrated. Similar size-based resolution obtained by trapezoidal geometry already showed promising results to efficiently separate WBCs and RBCs (172, 283). Although this design was not new, the DLA biochip was optimized to process DLA with the maximal CTC retention and WBC depletion possible.

Here, the technical performances of the spiral chips were tested using cell line tumor cells from three major cancer entities and mDLAs. Because DLA represents a precious sample, it was thought about using a surrogate for technical validations. Therefore, we proved that the hematological composition of patient-derived DLA was similar to BC after density gradient centrifugations (figure 22) and used these processed BC as mDLA product.

The data showed that DLA biochip performed better than CearCell FX system to enrich tumor cells from three different cell lines spiked-in mDLAs. ClearCell® FX system showed immediately limits to operate outside its intended use. In fact, the recovery rate of tumor cells from mDLAs containing just $50x10^6$ WBCs (equivalent to ~15 mL PB) was in average 30% (figure 32), which was much lower compared to the expected performance of the chip when processing standard 7.5 mL PB (171). Additionally, the recovery rate decreased when mDLA samples containing $200x10^6$ WBCs were processed and the system clogged while processing mDLAs with $400x10^6$ WBCs.

Indeed, DLA biochip efficiently processed up to $400x10^6$ WBCs per run (equivalent to ~120 mL PB) with a mean recovery rate of 50%. Differently to what we reported in the CTChip FR1, as well as to what was reported in filtration devices (284), DLA biochip never clogged, probably also due to the larger size of the channels compared to the CTChip FR1.

The performance of the chip was also evaluated in terms of WBC depletion. Because a high WBC carryover might interfere with downstream analysis, an efficient enrichment method should also remove a consistent fraction of WBCs. In order to guarantee the maximal WBC depletion, the DLA biochip workflow was designed as a two-cycle enrichment process through the same chip. The processing of samples containing $400x10^6$ WBCs with DLA biochip resulted in the 99.98% of WBCs depletion after two cycles and the second enrichment cycle alone removed approximately the 5% of the initial WBCs (around $18.6x10^6$ WBCs), confirming the importance of this step to improve the depletion.

In summary, the results of this study suggest that the DLA biochip might be a promising technology to enrich CTCs from DLA products with an acceptable WBC carryover. Although

we tested the performance of the chip with samples containing up to $400x10^6$ WBCs, the scalability of the method might allow to process further DLA aliquots either on the same chip or on more chips in parallel, preserving the simplicity of the system. Furthermore, since the technology separate the cells based on biophysical properties, it does not require expensive antibody cocktails for CTC capturing. Taken together, these observations suggest that this chip could represent an easy and cost-efficient tool to potentially screen a complete patient derived DLA. The potential of this technology meets our interest to increase the sensitivity for pancreatic CTCs, increasing the value that CTCs might have for the clinical management of PDAC and for unravelling unknown mechanisms of the disease.

6. CONCLUSIONS AND OUTLOOK

In this study it was demonstrated that DLA is a promising tool to increase the detection frequency and the yield of PDAC CTCs, offering the chance to establish CellSearch®-CTCs as prognostic biomarkers in this entity. The observed increase of analyzable cancer cells contributed to the potential value as a tool for improving patient selection and to guide treatment choice, setting the stage for future prospective clinical trials. Additionally, the feasibility of frozen DLA for pancreatic CTC detection and downstream analysis was demonstrated. Overall, it has been shown that DLA offers the possibility to analyze pancreatic CTCs at single-cell level, disclosing genomic feature that might contribute to explore the systemic disease and identify molecular targets for future targeted therapies in PDAC patients with advanced inoperable disease. Based on these findings, it is conceivable that the possibility to screen whole DLA products might provide the clinical relevance of CTCs in PDAC patients. Therefore, with the purpose to find an easy and cost-efficient tool to screen higher DLA volumes and increase the sensitivity for pancreatic CTCs, we tested a spiral microfluidic DLA biochip. The chip efficiently screened up to 4 mL mDLAs with a cell recovery rate of 50%. Although the processed volume represented only around 10% of a whole DLA product, the process can be repeated on the chip with further portions of the same DLA product, or several chips might be run in parallel. The scalability of the approach and the promising results might encourage to test DLA biochip for processing samples with higher cell load and patient derived DLAs, in combination, for example, with “in suspension” immunostaining protocols. A similar workflow could allow to isolate higher numbers of pancreatic CTCs, a prerequisite for future clinical use.

7. REFERENCES

1. Sung H, Ferlay J, Siegel RL, Laversanne M, Soerjomataram I, Jemal A, et al. Global Cancer Statistics 2020: GLOBOCAN Estimates of Incidence and Mortality Worldwide for 36 Cancers in 185 Countries. CA Cancer J Clin. 2021;71(3):209-49.
2. Mattiuzzi C, Lippi G. Cancer statistics: a comparison between World Health Organization (WHO) and Global Burden of Disease (GBD). Eur J Public Health. 2020;30(5):1026-7.
3. Erratum to "Cancer statistics, 2021". CA Cancer J Clin. 2021;71(4):359.
4. Orth M, Metzger P, Gerum S, Mayerle J, Schneider G, Belka C, et al. Pancreatic ductal adenocarcinoma: biological hallmarks, current status, and future perspectives of combined modality treatment approaches. Radiat Oncol. 2019;14(1):141.
5. Fischer R, Breidert M, Keck T, Makowiec F, Lohrmann C, Harder J. Early recurrence of pancreatic cancer after resection and during adjuvant chemotherapy. Saudi J Gastroenterol. 2012;18(2):118-21.
6. Le Large TYS, Bijlsma MF, Kazemier G, van Laarhoven HWM, Giovannetti E, Jimenez CR. Key biological processes driving metastatic spread of pancreatic cancer as identified by multi-omics studies. Semin Cancer Biol. 2017;44:153-69.
7. Hidalgo M, Cascinu S, Kleeff J, Labianca R, Lohr JM, Neoptolemos J, et al. Addressing the challenges of pancreatic cancer: future directions for improving outcomes. Pancreatology. 2015;15(1):8-18.
8. Rawla P, Sunkara T, Gaduputi V. Epidemiology of Pancreatic Cancer: Global Trends, Etiology and Risk Factors. World J Oncol. 2019;10(1):10-27.
9. Pandol SJ. The Exocrine Pancreas. Colloquium Series on Integrated Systems Physiology: From Molecule to Function to Disease. San Rafael (CA)2010.
10. Pishvaian MJ, Brody JR. Therapeutic Implications of Molecular Subtyping for Pancreatic Cancer. Oncology (Williston Park). 2017;31(3):159-66, 68.
11. Rhim AD, Stanger BZ. Molecular biology of pancreatic ductal adenocarcinoma progression: aberrant activation of developmental pathways. Prog Mol Biol Transl Sci. 2010;97:41-78.
12. Schawkat K, Manning MA, Glickman JN, Mortele KJ. Pancreatic Ductal Adenocarcinoma and Its Variants: Pearls and Perils. Radiographics. 2020;40(5):1219-39.
13. Fukuda A, Chiba T. Sox9-dependent acinar-to-ductal reprogramming is critical for pancreatic intraepithelial neoplasia formation. Gastroenterology. 2013;145(4):904-7.
14. Hruban RH, Adsay NV, Albores-Saavedra J, Compton C, Garrett ES, Goodman SN, et al. Pancreatic intraepithelial neoplasia: a new nomenclature and classification system for pancreatic duct lesions. Am J Surg Pathol. 2001;25(5):579-86.
15. Delpu Y, Hanoun N, Lulka H, Sicard F, Selves J, Buscail L, et al. Genetic and epigenetic alterations in pancreatic carcinogenesis. Curr Genomics. 2011;12(1):15-24.
16. Cannon A, Thompson C, Hall BR, Jain M, Kumar S, Batra SK. Desmoplasia in pancreatic ductal adenocarcinoma: insight into pathological function and therapeutic potential. Genes Cancer. 2018;9(3-4):78-86.
17. Miquel M, Zhang S, Pilarsky C. Pre-clinical Models of Metastasis in Pancreatic Cancer. Front Cell Dev Biol. 2021;9:748631.
18. Rhim AD, Mirek ET, Aiello NM, Maitra A, Bailey JM, McAllister F, et al. EMT and dissemination precede pancreatic tumor formation. Cell. 2012;148(1-2):349-61.
19. Waddell N, Pajic M, Patch AM, Chang DK, Kassahn KS, Bailey P, et al. Whole genomes redefine the mutational landscape of pancreatic cancer. Nature. 2015;518(7540):495-501.
20. Wood LD, Hruban RH. Pathology and molecular genetics of pancreatic neoplasms. Cancer J. 2012;18(6):492-501.
21. Bailey JM, Hendley AM, Lafaro KJ, Pruski MA, Jones NC, Alsina J, et al. p53 mutations cooperate with oncogenic Kras to promote adenocarcinoma from pancreatic ductal cells. Oncogene. 2016;35(32):4282-8.

22. Witkiewicz AK, McMillan EA, Balaji U, Baek G, Lin WC, Mansour J, et al. Whole-exome sequencing of pancreatic cancer defines genetic diversity and therapeutic targets. Nat Commun. 2015;6:6744.
23. Jones S, Zhang X, Parsons DW, Lin JC, Leary RJ, Angenendt P, et al. Core signaling pathways in human pancreatic cancers revealed by global genomic analyses. Science. 2008;321(5897):1801-6.
24. Cancer Genome Atlas Research Network. Electronic address aadhe, Cancer Genome Atlas Research N. Integrated Genomic Characterization of Pancreatic Ductal Adenocarcinoma. Cancer Cell. 2017;32(2):185-203 e13.
25. Tate JG, Bamford S, Jubb HC, Sondka Z, Beare DM, Bindal N, et al. COSMIC: the Catalogue Of Somatic Mutations In Cancer. Nucleic Acids Res. 2019;47(D1):D941-D7.
26. Pantsar T. The current understanding of KRAS protein structure and dynamics. Comput Struct Biotechnol J. 2020;18:189-98.
27. Bryant KL, Mancias JD, Kimmelman AC, Der CJ. KRAS: feeding pancreatic cancer proliferation. Trends Biochem Sci. 2014;39(2):91-100.
28. Eser S, Schnieke A, Schneider G, Saur D. Oncogenic KRAS signalling in pancreatic cancer. Br J Cancer. 2014;111(5):817-22.
29. Caldas C, Kern SE. K-ras mutation and pancreatic adenocarcinoma. Int J Pancreatol. 1995;18(1):1-6.
30. Maitra A, Fukushima N, Takaori K, Hruban RH. Precursors to invasive pancreatic cancer. Adv Anat Pathol. 2005;12(2):81-91.
31. Kanda M, Matthaei H, Wu J, Hong SM, Yu J, Borges M, et al. Presence of somatic mutations in most early-stage pancreatic intraepithelial neoplasia. Gastroenterology. 2012;142(4):730-3 e9.
32. Hingorani SR, Petricoin EF, Maitra A, Rajapakse V, King C, Jacobetz MA, et al. Preinvasive and invasive ductal pancreatic cancer and its early detection in the mouse. Cancer Cell. 2003;4(6):437-50.
33. Izeradjene K, Combs C, Best M, Gopinathan A, Wagner A, Grady WM, et al. Kras(G12D) and Smad4/Dpc4 haploinsufficiency cooperate to induce mucinous cystic neoplasms and invasive adenocarcinoma of the pancreas. Cancer Cell. 2007;11(3):229-43.
34. Collins MA, Bednar F, Zhang Y, Brisset JC, Galban S, Galban CJ, et al. Oncogenic Kras is required for both the initiation and maintenance of pancreatic cancer in mice. J Clin Invest. 2012;122(2):639-53.
35. Soussi T, Hjortsberg L. When mutant p53 plays hide and seek: a new challenge for diagnosis and therapy? Trends Mol Med. 2009;15(1):1-4.
36. Evans T, Faircloth M, Deery A, Thomas V, Turner A, Dalgleish A. Analysis of K-ras gene mutations in human pancreatic cancer cell lines and in bile samples from patients with pancreatic and biliary cancers. Oncol Rep. 1997;4(6):1373-81.
37. Yu J, Sadakari Y, Shindo K, Suenaga M, Brant A, Almario JAN, et al. Digital next-generation sequencing identifies low-abundance mutations in pancreatic juice samples collected from the duodenum of patients with pancreatic cancer and intraductal papillary mucinous neoplasms. Gut. 2017;66(9):1677-87.
38. Yachida S, White CM, Naito Y, Zhong Y, Brosnan JA, Macgregor-Das AM, et al. Clinical significance of the genetic landscape of pancreatic cancer and implications for identification of potential long-term survivors. Clin Cancer Res. 2012;18(22):6339-47.
39. Casey G, Yamanaka Y, Friess H, Kobrin MS, Lopez ME, Buchler M, et al. p53 mutations are common in pancreatic cancer and are absent in chronic pancreatitis. Cancer Lett. 1993;69(3):151-60.
40. Mafficini A, Amato E, Fassan M, Simbolo M, Antonello D, Vicentini C, et al. Reporting tumor molecular heterogeneity in histopathological diagnosis. PLoS One. 2014;9(8):e104979.
41. Hingorani SR, Wang L, Multani AS, Combs C, Deramaudt TB, Hruban RH, et al. Trp53R172H and KrasG12D cooperate to promote chromosomal instability and widely metastatic pancreatic ductal adenocarcinoma in mice. Cancer Cell. 2005;7(5):469-83.
42. Freed-Pastor WA, Prives C. Mutant p53: one name, many proteins. Genes Dev. 2012;26(12):1268-86.

43. Hwang RF, Gordon EM, Anderson WF, Parekh D. Gene therapy for primary and metastatic pancreatic cancer with intraperitoneal retroviral vector bearing the wild-type p53 gene. Surgery. 1998;124(2):143-50; discussion 50-1.
44. Morton JP, Timpson P, Karim SA, Ridgway RA, Athineos D, Doyle B, et al. Mutant p53 drives metastasis and overcomes growth arrest/senescence in pancreatic cancer. Proc Natl Acad Sci U S A. 2010;107(1):246-51.
45. Aubrey BJ, Strasser A, Kelly GL. Tumor-Suppressor Functions of the TP53 Pathway. Cold Spring Harb Perspect Med. 2016;6(5).
46. Joerger AC, Fersht AR. Structural biology of the tumor suppressor p53 and cancer-associated mutants. Adv Cancer Res. 2007;97:1-23.
47. Kruse JP, Gu W. Modes of p53 regulation. Cell. 2009;137(4):609-22.
48. Sun H, Zhang B, Li H. The Roles of Frequently Mutated Genes of Pancreatic Cancer in Regulation of Tumor Microenvironment. Technol Cancer Res Treat. 2020;19:1533033820920969.
49. Olivier M, Hollstein M, Hainaut P. TP53 mutations in human cancers: origins, consequences, and clinical use. Cold Spring Harb Perspect Biol. 2010;2(1):a001008.
50. Takeuchi S, Doi M, Ikari N, Yamamoto M, Furukawa T. Mutations in BRCA1, BRCA2, and PALB2, and a panel of 50 cancer-associated genes in pancreatic ductal adenocarcinoma. Sci Rep. 2018;8(1):8105.
51. Kamaraj B, Bogaerts A. Structure and Function of p53-DNA Complexes with Inactivation and Rescue Mutations: A Molecular Dynamics Simulation Study. PLoS One. 2015;10(8):e0134638.
52. Aguirre AJ, Bardeesy N, Sinha M, Lopez L, Tuveson DA, Horner J, et al. Activated Kras and Ink4a/Arf deficiency cooperate to produce metastatic pancreatic ductal adenocarcinoma. Genes Dev. 2003;17(24):3112-26.
53. Wolfgang CL, Herman JM, Laheru DA, Klein AP, Erdek MA, Fishman EK, et al. Recent progress in pancreatic cancer. CA Cancer J Clin. 2013;63(5):318-48.
54. Harada T, Chelala C, Bhakta V, Chaplin T, Caulee K, Baril P, et al. Genome-wide DNA copy number analysis in pancreatic cancer using high-density single nucleotide polymorphism arrays. Oncogene. 2008;27(13):1951-60.
55. Willis JA, Mukherjee S, Orlow I, Viale A, Offit K, Kurtz RC, et al. Genome-wide analysis of the role of copy-number variation in pancreatic cancer risk. Front Genet. 2014;5:29.
56. Redon R, Ishikawa S, Fitch KR, Feuk L, Perry GH, Andrews TD, et al. Global variation in copy number in the human genome. Nature. 2006;444(7118):444-54.
57. Du Y, Zhao B, Liu Z, Ren X, Zhao W, Li Z, et al. Molecular Subtyping of Pancreatic Cancer: Translating Genomics and Transcriptomics into the Clinic. J Cancer. 2017;8(4):513-22.
58. Di Marco M, Astolfi A, Grassi E, Vecchiarelli S, Macchini M, Indio V, et al. Characterization of pancreatic ductal adenocarcinoma using whole transcriptome sequencing and copy number analysis by single-nucleotide polymorphism array. Mol Med Rep. 2015;12(5):7479-84.
59. Murphy SJ, Hart SN, Halling GC, Johnson SH, Smadbeck JB, Drucker T, et al. Integrated Genomic Analysis of Pancreatic Ductal Adenocarcinomas Reveals Genomic Rearrangement Events as Significant Drivers of Disease. Cancer Res. 2016;76(3):749-61.
60. Lee JH, Giovannetti E, Hwang JH, Petrini I, Wang Q, Voortman J, et al. Loss of 18q22.3 involving the carboxypeptidase of glutamate-like gene is associated with poor prognosis in resected pancreatic cancer. Clin Cancer Res. 2012;18(2):524-33.
61. Wood LD, Canto MI, Jaffee EM, Simeone DM. Pancreatic Cancer: Pathogenesis, Screening, Diagnosis, and Treatment. Gastroenterology. 2022;163(2):386-402 e1.
62. Soreide K. Sweet Predictions Speak Volumes for Early Detection of Pancreatic Cancer. Gastroenterology. 2018;155(2):265-8.
63. Winter K, Talar-Wojnarowska R, Dabrowski A, Degowska M, Durlik M, Gasiorowska A, et al. Diagnostic and therapeutic recommendations in pancreatic ductal adenocarcinoma. Recommendations of the Working Group of the Polish Pancreatic Club. Prz Gastroenterol. 2019;14(1):1-18.

64. Tempero MA, Malafa MP, Al-Hawary M, Asbun H, Bain A, Behrman SW, et al. Pancreatic Adenocarcinoma, Version 2.2017, NCCN Clinical Practice Guidelines in Oncology. J Natl Compr Canc Netw. 2017;15(8):1028-61.
65. Evans DB. What Makes a Pancreatic Cancer Resectable? American Society of Clinical Oncology Educational Book. 2018(38):300-5.
66. Trisolini E, Armellini E, Paganotti A, Veggiani C, Bozzola C, Frattini M, et al. KRAS mutation testing on all non-malignant diagnosis of pancreatic endoscopic ultrasound-guided fine-needle aspiration biopsies improves diagnostic accuracy. Pathology. 2017;49(4):379-86.
67. Sekita-Hatakeyama Y, Nishikawa T, Takeuchi M, Morita K, Takeda M, Hatakeyama K, et al. K-ras mutation analysis of residual liquid-based cytology specimens from endoscopic ultrasound-guided fine needle aspiration improves cell block diagnosis of pancreatic ductal adenocarcinoma. PLoS One. 2018;13(3):e0193692.
68. Brand RE, Persson J, Bratlie SO, Chung DC, Katona BW, Carrato A, et al. Detection of Early-Stage Pancreatic Ductal Adenocarcinoma From Blood Samples: Results of a Multiplex Biomarker Signature Validation Study. Clin Transl Gastroenterol. 2022;13(3):e00468.
69. Strobel O, Neoptolemos J, Jager D, Buchler MW. Optimizing the outcomes of pancreatic cancer surgery. Nat Rev Clin Oncol. 2019;16(1):11-26.
70. Kamyabi N, Bernard V, Maitra A. Liquid biopsies in pancreatic cancer. Expert Rev Anticancer Ther. 2019;19(10):869-78.
71. Law EW, Settell ML, Kurani SS, Eckert EC, Liu MC, Greenberg-Worisek AJ. Liquid Biopsy: Emergence of an Alternative Cancer Detection Method. Clin Transl Sci. 2020;13(5):845-7.
72. Duffy MJ, Sturgeon C, Lamerz R, Haglund C, Holubec VL, Klapdor R, et al. Tumor markers in pancreatic cancer: a European Group on Tumor Markers (EGTM) status report. Ann Oncol. 2010;21(3):441-7.
73. Poruk KE, Gay DZ, Brown K, Mulvihill JD, Boucher KM, Scaife CL, et al. The clinical utility of CA 19-9 in pancreatic adenocarcinoma: diagnostic and prognostic updates. Curr Mol Med. 2013;13(3):340-51.
74. Chan A, Prassas I, Dimitromanolakis A, Brand RE, Serra S, Diamandis EP, et al. Validation of biomarkers that complement CA19.9 in detecting early pancreatic cancer. Clin Cancer Res. 2014;20(22):5787-95.
75. Sefrioui D, Blanchard F, Toure E, Basile P, Beaussire L, Dolfus C, et al. Diagnostic value of CA19.9, circulating tumour DNA and circulating tumour cells in patients with solid pancreatic tumours. Br J Cancer. 2017;117(7):1017-25.
76. Steinberg W. The clinical utility of the CA 19-9 tumor-associated antigen. Am J Gastroenterol. 1990;85(4):350-5.
77. Karakas Y, Lacin S, Yalcin S. Recent advances in the management of pancreatic adenocarcinoma. Expert Rev Anticancer Ther. 2018;18(1):51-62.
78. Jentzsch V, Davis JAA, Djamgoz MBA. Pancreatic Cancer (PDAC): Introduction of Evidence-Based Complementary Measures into Integrative Clinical Management. Cancers (Basel). 2020;12(11).
79. Conroy T, Hammel P, Hebbar M, Ben Abdelghani M, Wei AC, Raoul JL, et al. FOLFIRINOX or Gemcitabine as Adjuvant Therapy for Pancreatic Cancer. N Engl J Med. 2018;379(25):2395-406.
80. Sohal DPS, Kennedy EB, Khorana A, Copur MS, Crane CH, Garrido-Laguna I, et al. Metastatic Pancreatic Cancer: ASCO Clinical Practice Guideline Update. J Clin Oncol. 2018;36(24):2545-56.
81. Ramanathan RK, McDonough SL, Philip PA, Hingorani SR, Lacy J, Kortmansky JS, et al. Phase IB/II Randomized Study of FOLFIRINOX Plus Pegylated Recombinant Human Hyaluronidase Versus FOLFIRINOX Alone in Patients With Metastatic Pancreatic Adenocarcinoma: SWOG S1313. J Clin Oncol. 2019;37(13):1062-9.
82. Riva F, Dronov OI, Khomenko DI, Huguet F, Louvet C, Mariani P, et al. Clinical applications of circulating tumor DNA and circulating tumor cells in pancreatic cancer. Mol Oncol. 2016;10(3):481-93.

83. Pappalardo A, Giunta EF, Tirino G, Pompella L, Federico P, Daniele B, et al. Adjuvant Treatment in Pancreatic Cancer: Shaping the Future of the Curative Setting. Front Oncol. 2021;11:695627.
84. O'Kane GM, Ladak F, Gallinger S. Advances in the management of pancreatic ductal adenocarcinoma. CMAJ. 2021;193(23):E844-E51.
85. Satoi S. Surgical Treatment of Pancreatic Ductal Adenocarcinoma. Cancers (Basel). 2021;13(16).
86. Wei K, Hackert T. Surgical Treatment of Pancreatic Ductal Adenocarcinoma. Cancers (Basel). 2021;13(8).
87. Du J, Gu J, Li J. Mechanisms of drug resistance of pancreatic ductal adenocarcinoma at different levels. Biosci Rep. 2020;40(7).
88. Vaupel P, Hockel M, Mayer A. Detection and characterization of tumor hypoxia using pO2 histography. Antioxid Redox Signal. 2007;9(8):1221-35.
89. Cros J, Raffenne J, Couvelard A, Pote N. Tumor Heterogeneity in Pancreatic Adenocarcinoma. Pathobiology. 2018;85(1-2):64-71.
90. Pompella L, Tirino G, Pappalardo A, Caterino M, Ventriglia A, Nacca V, et al. Pancreatic Cancer Molecular Classifications: From Bulk Genomics to Single Cell Analysis. Int J Mol Sci. 2020;21(8).
91. Collisson EA, Sadanandam A, Olson P, Gibb WJ, Truitt M, Gu S, et al. Subtypes of pancreatic ductal adenocarcinoma and their differing responses to therapy. Nat Med. 2011;17(4):500-3.
92. Johnson BA, 3rd, Yarchoan M, Lee V, Laheru DA, Jaffee EM. Strategies for Increasing Pancreatic Tumor Immunogenicity. Clin Cancer Res. 2017;23(7):1656-69.
93. Li KY, Yuan JL, Trafton D, Wang JX, Niu N, Yuan CH, et al. Pancreatic ductal adenocarcinoma immune microenvironment and immunotherapy prospects. Chronic Dis Transl Med. 2020;6(1):6-17.
94. Qian Y, Gong Y, Fan Z, Luo G, Huang Q, Deng S, et al. Molecular alterations and targeted therapy in pancreatic ductal adenocarcinoma. J Hematol Oncol. 2020;13(1):130.
95. Almoguera C, Shibata D, Forrester K, Martin J, Arnheim N, Perucho M. Most human carcinomas of the exocrine pancreas contain mutant c-K-ras genes. Cell. 1988;53(4):549-54.
96. Waters AM, Der CJ. KRAS: The Critical Driver and Therapeutic Target for Pancreatic Cancer. Cold Spring Harb Perspect Med. 2018;8(9).
97. Ostrem JM, Peters U, Sos ML, Wells JA, Shokat KM. K-Ras(G12C) inhibitors allosterically control GTP affinity and effector interactions. Nature. 2013;503(7477):548-51.
98. Smania MA. Liquid biopsy for cancer screening, diagnosis, and treatment. J Am Assoc Nurse Pract. 2020;32(1):5-7.
99. Rofi E, Vivaldi C, Del Re M, Arrigoni E, Crucitta S, Funel N, et al. The emerging role of liquid biopsy in diagnosis, prognosis and treatment monitoring of pancreatic cancer. Pharmacogenomics. 2019;20(1):49-68.
100. Mattox AK, Bettegowda C, Zhou S, Papadopoulos N, Kinzler KW, Vogelstein B. Applications of liquid biopsies for cancer. Sci Transl Med. 2019;11(507).
101. Tivey A, Church M, Rothwell D, Dive C, Cook N. Circulating tumour DNA - looking beyond the blood. Nat Rev Clin Oncol. 2022;19(9):600-12.
102. Heredia-Soto V, Rodriguez-Salas N, Feliu J. Liquid Biopsy in Pancreatic Cancer: Are We Ready to Apply It in the Clinical Practice? Cancers (Basel). 2021;13(8).
103. El Rassy E, Khaled H, Pavlidis N. Liquid biopsy: a new diagnostic, predictive and prognostic window in cancers of unknown primary. Eur J Cancer. 2018;105:28-32.
104. Lozar T, Gersak K, Cemazar M, Kuhar CG, Jesenko T. The biology and clinical potential of circulating tumor cells. Radiol Oncol. 2019;53(2):131-47.
105. Palmirotta R, Lovero D, Cafforio P, Felici C, Mannavola F, Pelle E, et al. Liquid biopsy of cancer: a multimodal diagnostic tool in clinical oncology. Ther Adv Med Oncol. 2018;10:1758835918794630.
106. Lin D, Shen L, Luo M, Zhang K, Li J, Yang Q, et al. Circulating tumor cells: biology and clinical significance. Signal Transduct Target Ther. 2021;6(1):404.

107. Menyailo ME, Tretyakova MS, Denisov EV. Heterogeneity of Circulating Tumor Cells in Breast Cancer: Identifying Metastatic Seeds. Int J Mol Sci. 2020;21(5).
108. Aceto N, Bardia A, Miyamoto DT, Donaldson MC, Wittner BS, Spencer JA, et al. Circulating tumor cell clusters are oligoclonal precursors of breast cancer metastasis. Cell. 2014;158(5):1110-22.
109. Szczerba BM, Castro-Giner F, Vetter M, Krol I, Gkountela S, Landin J, et al. Neutrophils escort circulating tumour cells to enable cell cycle progression. Nature. 2019;566(7745):553-7.
110. Tao L, Zhang L, Peng Y, Tao M, Li L, Xiu D, et al. Neutrophils assist the metastasis of circulating tumor cells in pancreatic ductal adenocarcinoma: A new hypothesis and a new predictor for distant metastasis. Medicine (Baltimore). 2016;95(39):e4932.
111. Micalizzi DS, Maheswaran S, Haber DA. A conduit to metastasis: circulating tumor cell biology. Genes Dev. 2017;31(18):1827-40.
112. Neophytou CM, Kyriakou TC, Papageorgis P. Mechanisms of Metastatic Tumor Dormancy and Implications for Cancer Therapy. Int J Mol Sci. 2019;20(24).
113. Fidler IJ. The pathogenesis of cancer metastasis: the 'seed and soil' hypothesis revisited. Nat Rev Cancer. 2003;3(6):453-8.
114. Miller MC, Doyle GV, Terstappen LW. Significance of Circulating Tumor Cells Detected by the CellSearch System in Patients with Metastatic Breast Colorectal and Prostate Cancer. Journal of oncology. 2010;2010:617421.
115. Cristofanilli M, Budd GT, Ellis MJ, Stopeck A, Matera J, Miller MC, et al. Circulating tumor cells, disease progression, and survival in metastatic breast cancer. N Engl J Med. 2004;351(8):781-91.
116. Moreno JG, Miller MC, Gross S, Allard WJ, Gomella LG, Terstappen LW. Circulating tumor cells predict survival in patients with metastatic prostate cancer. Urology. 2005;65(4):713-8.
117. Cohen SJ, Punt CJ, Iannotti N, Saidman BH, Sabbath KD, Gabrail NY, et al. Prognostic significance of circulating tumor cells in patients with metastatic colorectal cancer. Ann Oncol. 2009;20(7):1223-9.
118. Wang J, Wang K, Xu J, Huang J, Zhang T. Prognostic significance of circulating tumor cells in non-small-cell lung cancer patients: a meta-analysis. PLoS One. 2013;8(11):e78070.
119. Keller L, Pantel K. Unravelling tumour heterogeneity by single-cell profiling of circulating tumour cells. Nat Rev Cancer. 2019;19(10):553-67.
120. Alix-Panabieres C, Pantel K. [The circulating tumor cells: liquid biopsy of cancer]. Klin Lab Diagn. 2014(4):60-4.
121. Banko P, Lee SY, Nagygyorgy V, Zrinyi M, Chae CH, Cho DH, et al. Technologies for circulating tumor cell separation from whole blood. J Hematol Oncol. 2019;12(1):48.
122. Ferreira MM, Ramani VC, Jeffrey SS. Circulating tumor cell technologies. Mol Oncol. 2016;10(3):374-94.
123. Low WS, Wan Abas WA. Benchtop technologies for circulating tumor cells separation based on biophysical properties. BioMed research international. 2015;2015:239362.
124. Marrinucci D, Bethel K, Bruce RH, Curry DN, Hsieh B, Humphrey M, et al. Case study of the morphologic variation of circulating tumor cells. Hum Pathol. 2007;38(3):514-9.
125. Pan L, Yan G, Chen W, Sun L, Wang J, Yang J. Distribution of circulating tumor cell phenotype in early cervical cancer. Cancer Manag Res. 2019;11:5531-6.
126. Barriere G, Fici P, Gallerani G, Fabbri F, Zoli W, Rigaud M. Circulating tumor cells and epithelial, mesenchymal and stemness markers: characterization of cell subpopulations. Ann Transl Med. 2014;2(11):109.
127. Kalluri R, Weinberg RA. The basics of epithelial-mesenchymal transition. J Clin Invest. 2009;119(6):1420-8.
128. Thiery JP, Acloque H, Huang RY, Nieto MA. Epithelial-mesenchymal transitions in development and disease. Cell. 2009;139(5):871-90.
129. Wu S, Liu S, Liu Z, Huang J, Pu X, Li J, et al. Classification of circulating tumor cells by epithelial-mesenchymal transition markers. PloS one. 2015;10(4):e0123976.

130. Lu M, Jolly MK, Levine H, Onuchic JN, Ben-Jacob E. MicroRNA-based regulation of epithelial-hybrid-mesenchymal fate determination. Proc Natl Acad Sci U S A. 2013;110(45):18144-9.
131. Liu X, Fan D. The epithelial-mesenchymal transition and cancer stem cells: functional and mechanistic links. Curr Pharm Des. 2015;21(10):1279-91.
132. Mani SA, Guo W, Liao MJ, Eaton EN, Ayyanan A, Zhou AY, et al. The epithelial-mesenchymal transition generates cells with properties of stem cells. Cell. 2008;133(4):704-15.
133. Agnoletto C, Corra F, Minotti L, Baldassari F, Crudele F, Cook WJJ, et al. Heterogeneity in Circulating Tumor Cells: The Relevance of the Stem-Cell Subset. Cancers (Basel). 2019;11(4).
134. Rushton AJ, Nteliopoulos G, Shaw JA, Coombes RC. A Review of Circulating Tumour Cell Enrichment Technologies. Cancers (Basel). 2021;13(5).
135. Miltenyi S, Muller W, Weichel W, Radbruch A. High gradient magnetic cell separation with MACS. Cytometry. 1990;11(2):231-8.
136. Drucker A, Teh EM, Kostyleva R, Rayson D, Douglas S, Pinto DM. Comparative performance of different methods for circulating tumor cell enrichment in metastatic breast cancer patients. PLoS One. 2020;15(8):e0237308.
137. Hayes DF, Cristofanilli M, Budd GT, Ellis MJ, Stopeck A, Miller MC, et al. Circulating tumor cells at each follow-up time point during therapy of metastatic breast cancer patients predict progression-free and overall survival. Clin Cancer Res. 2006;12(14 Pt 1):4218-24.
138. de Bono JS, Scher HI, Montgomery RB, Parker C, Miller MC, Tissing H, et al. Circulating tumor cells predict survival benefit from treatment in metastatic castration-resistant prostate cancer. Clinical cancer research : an official journal of the American Association for Cancer Research. 2008;14(19):6302-9.
139. Cohen SJ, Terstappen LW, Punt CJ, Mitchell EP, Fynan TM, Li T, et al. Circulating endothelial cells (CEC) and circulating tumor cells (CTC) in patients (pts) with metastatic colorectal cancer (mCRC). Journal of Clinical Oncology. 2006;24(18_suppl):3531-.
140. Swennenhuis JF, van Dalum G, Zeune LL, Terstappen LW. Improving the CellSearch(R) system. Expert Rev Mol Diagn. 2016;16(12):1291-305.
141. Harouaka RA, Nisic M, Zheng SY. Circulating tumor cell enrichment based on physical properties. J Lab Autom. 2013;18(6):455-68.
142. Nagrath S, Sequist LV, Maheswaran S, Bell DW, Irimia D, Ulkus L, et al. Isolation of rare circulating tumour cells in cancer patients by microchip technology. Nature. 2007;450(7173):1235-9.
143. Sequist LV, Nagrath S, Toner M, Haber DA, Lynch TJ. The CTC-chip: an exciting new tool to detect circulating tumor cells in lung cancer patients. J Thorac Oncol. 2009;4(3):281-3.
144. Sheng W, Ogunwobi OO, Chen T, Zhang J, George TJ, Liu C, et al. Capture, release and culture of circulating tumor cells from pancreatic cancer patients using an enhanced mixing chip. Lab Chip. 2014;14(1):89-98.
145. Ozkumur E, Shah AM, Ciciliano JC, Emmink BL, Miyamoto DT, Brachtel E, et al. Inertial focusing for tumor antigen-dependent and -independent sorting of rare circulating tumor cells. Sci Transl Med. 2013;5(179):179ra47.
146. Harb W, Fan A, Tran T, Danila DC, Keys D, Schwartz M, et al. Mutational Analysis of Circulating Tumor Cells Using a Novel Microfluidic Collection Device and qPCR Assay. Transl Oncol. 2013;6(5):528-38.
147. Kallergi G, Papadaki MA, Politaki E, Mavroudis D, Georgoulias V, Agelaki S. Epithelial to mesenchymal transition markers expressed in circulating tumour cells of early and metastatic breast cancer patients. Breast Cancer Res. 2011;13(3):R59.
148. Horimoto Y, Tokuda E, Murakami F, Uomori T, Himuro T, Nakai K, et al. Analysis of circulating tumour cell and the epithelial mesenchymal transition (EMT) status during eribulin-based treatment in 22 patients with metastatic breast cancer: a pilot study. J Transl Med. 2018;16(1):287.
149. Dobrzynska I, Skrzydlewska E, Figaszewski ZA. Changes in electric properties of human breast cancer cells. J Membr Biol. 2013;246(2):161-6.

150. Gutowski KA, Hudson JL, Aminoff D. Flow cytometric analysis of human erythrocytes: I. Probed with lectins and immunoglobulins. Exp Gerontol. 1991;26(4):315-26.
151. Hofman VJ, Ilie MI, Bonnetaud C, Selva E, Long E, Molina T, et al. Cytopathologic detection of circulating tumor cells using the isolation by size of epithelial tumor cell method: promises and pitfalls. Am J Clin Pathol. 2011;135(1):146-56.
152. Hass R, Bertram C. Characterization of human breast cancer epithelial cells (HBCEC) derived from long term cultured biopsies. J Exp Clin Cancer Res. 2009;28:127.
153. Shapiro HM, Schildkraut ER, Curbelo R, Laird CW, Turner B, Hirschfeld T. Combined blood cell counting and classification with fluorochrome stains and flow instrumentation. J Histochem Cytochem. 1976;24(1):396-401.
154. Khoja L, Backen A, Sloane R, Menasce L, Ryder D, Krebs M, et al. A pilot study to explore circulating tumour cells in pancreatic cancer as a novel biomarker. British journal of cancer. 2012;106(3):508-16.
155. Hofman V, Long E, Ilie M, Bonnetaud C, Vignaud JM, Flejou JF, et al. Morphological analysis of circulating tumour cells in patients undergoing surgery for non-small cell lung carcinoma using the isolation by size of epithelial tumour cell (ISET) method. Cytopathology. 2012;23(1):30-8.
156. Zabaglo L, Ormerod MG, Parton M, Ring A, Smith IE, Dowsett M. Cell filtration-laser scanning cytometry for the characterisation of circulating breast cancer cells. Cytometry A. 2003;55(2):102-8.
157. Zheng S, Lin HK, Lu B, Williams A, Datar R, Cote RJ, et al. 3D microfilter device for viable circulating tumor cell (CTC) enrichment from blood. Biomed Microdevices. 2011;13(1):203-13.
158. Zhou MD, Hao S, Williams AJ, Harouaka RA, Schrand B, Rawal S, et al. Separable bilayer microfiltration device for viable label-free enrichment of circulating tumour cells. Sci Rep. 2014;4:7392.
159. Lara O, Tong X, Zborowski M, Chalmers JJ. Enrichment of rare cancer cells through depletion of normal cells using density and flow-through, immunomagnetic cell separation. Exp Hematol. 2004;32(10):891-904.
160. Coumans FA, van Dalum G, Beck M, Terstappen LW. Filter characteristics influencing circulating tumor cell enrichment from whole blood. PLoS One. 2013;8(4):e61770.
161. Li X, Li Y, Shao W, Li Z, Zhao R, Ye Z. Strategies for enrichment of circulating tumor cells. Transl Cancer Res. 2020;9(3):2012-25.
162. Gertler R, Rosenberg R, Fuehrer K, Dahm M, Nekarda H, Siewert JR. Detection of circulating tumor cells in blood using an optimized density gradient centrifugation. Recent Results Cancer Res. 2003;162:149-55.
163. Rosenberg R, Gertler R, Friederichs J, Fuehrer K, Dahm M, Phelps R, et al. Comparison of two density gradient centrifugation systems for the enrichment of disseminated tumor cells in blood. Cytometry. 2002;49(4):150-8.
164. Hvichia GE, Parveen Z, Wagner C, Janning M, Quidde J, Stein A, et al. A novel microfluidic platform for size and deformability based separation and the subsequent molecular characterization of viable circulating tumor cells. Int J Cancer. 2016;138(12):2894-904.
165. Lee Y, Guan G, Bhagat AA. ClearCell(R) FX, a label-free microfluidics technology for enrichment of viable circulating tumor cells. Cytometry A. 2018;93(12):1251-4.
166. Gossett DR, Tse HT, Lee SA, Ying Y, Lindgren AG, Yang OO, et al. Hydrodynamic stretching of single cells for large population mechanical phenotyping. Proc Natl Acad Sci U S A. 2012;109(20):7630-5.
167. Hur SC, Henderson-MacLennan NK, McCabe ER, Di Carlo D. Deformability-based cell classification and enrichment using inertial microfluidics. Lab Chip. 2011;11(5):912-20.
168. Cohen EN, Jayachandran G, Moore RG, Cristofanilli M, Lang JE, Khoury JD, et al. A Multi-Center Clinical Study to Harvest and Characterize Circulating Tumor Cells from Patients with Metastatic Breast Cancer Using the Parsortix((R)) PC1 System. Cancers (Basel). 2022;14(21).
169. Dong Y, Skelley AM, Merdek KD, Sprott KM, Jiang C, Pierceall WE, et al. Microfluidics and circulating tumor cells. J Mol Diagn. 2013;15(2):149-57.

170. Khoo BL, Warkiani ME, Tan DS, Bhagat AA, Irwin D, Lau DP, et al. Clinical validation of an ultra high-throughput spiral microfluidics for the detection and enrichment of viable circulating tumor cells. PLoS One. 2014;9(7):e99409.
171. Hou HW, Warkiani ME, Khoo BL, Li ZR, Soo RA, Tan DS, et al. Isolation and retrieval of circulating tumor cells using centrifugal forces. Sci Rep. 2013;3:1259.
172. Guan G, Wu L, Bhagat AA, Li Z, Chen PC, Chao S, et al. Spiral microchannel with rectangular and trapezoidal cross-sections for size based particle separation. Sci Rep. 2013;3:1475.
173. Lee Y, Guan GF, Bhagat AA. ClearCell (R) FX, a label-free microfluidics technology for enrichment of viable circulating tumor cells. Cytom Part A. 2018;93a(12):1251-4.
174. Wu A, Bhagat AA, Leong MC, Lim CT. ClearCell FX: A microfluidic system for label-free circulating tumor cell enrichment. J Clin Oncol. 2014;32(15).
175. Hou HW, Warkiani ME, Khoo BL, Li ZR, Soo RA, Tan DSW, et al. Isolation and retrieval of circulating tumor cells using centrifugal forces. Sci Rep-Uk. 2013;3.
176. Guglielmi R, Lai Z, Raba K, van Dalum G, Wu J, Behrens B, et al. Technical validation of a new microfluidic device for enrichment of CTCs from large volumes of blood by using buffy coats to mimic diagnostic leukapheresis products. Sci Rep. 2020;10(1):20312.
177. Descamps L, Le Roy D, Deman AL. Microfluidic-Based Technologies for CTC Isolation: A Review of 10 Years of Intense Efforts towards Liquid Biopsy. Int J Mol Sci. 2022;23(4).
178. Thiele JA, Bethel K, Kralickova M, Kuhn P. Circulating Tumor Cells: Fluid Surrogates of Solid Tumors. Annu Rev Pathol. 2017;12:419-47.
179. Alshareef M, Metrakos N, Juarez Perez E, Azer F, Yang F, Yang X, et al. Separation of tumor cells with dielectrophoresis-based microfluidic chip. Biomicrofluidics. 2013;7(1):11803.
180. Kallergi G, Agelaki S, Kalykaki A, Stournaras C, Mavroudis D, Georgoulias V. Phosphorylated EGFR and PI3K/Akt signaling kinases are expressed in circulating tumor cells of breast cancer patients. Breast Cancer Res. 2008;10(5):R80.
181. Spizzo G, Fong D, Wurm M, Ensinger C, Obrist P, Hofer C, et al. EpCAM expression in primary tumour tissues and metastases: an immunohistochemical analysis. J Clin Pathol. 2011;64(5):415-20.
182. Moll R. [Epithelial tumor markers]. Verh Dtsch Ges Pathol. 1986;70:28-50.
183. Lindberg K, Rheinwald JG. Suprabasal 40 kd keratin (K19) expression as an immunohistologic marker of premalignancy in oral epithelium. Am J Pathol. 1989;134(1):89-98.
184. Chu PG, Weiss LM. Keratin expression in human tissues and neoplasms. Histopathology. 2002;40(5):403-39.
185. Pantel K, Alix-Panabieres C. Detection methods of circulating tumor cells. J Thorac Dis. 2012;4(5):446-7.
186. Mikolajczyk SD, Millar LS, Tsinberg P, Coutts SM, Zomorrodi M, Pham T, et al. Detection of EpCAM-Negative and Cytokeratin-Negative Circulating Tumor Cells in Peripheral Blood. J Oncol. 2011;2011:252361.
187. Andratschke M, Hagedorn H, Nerlich A. Expression of the Epithelial Cell Adhesion Molecule and Cytokeratin 8 in Head and Neck Squamous Cell Cancer: A Comparative Study. Anticancer Res. 2015;35(7):3953-60.
188. Hong B, Zu Y. Detecting circulating tumor cells: current challenges and new trends. Theranostics. 2013;3(6):377-94.
189. Po JW, Ma Y, Balakrishna B, Brungs D, Azimi F, de Souza P, et al. Immunomagnetic isolation of circulating melanoma cells and detection of PD-L1 status. PLoS One. 2019;14(2):e0211866.
190. Kasimir-Bauer S, Hoffmann O, Wallwiener D, Kimmig R, Fehm T. Expression of stem cell and epithelial-mesenchymal transition markers in primary breast cancer patients with circulating tumor cells. Breast Cancer Res. 2012;14(1):R15.
191. Shen Z, Wu A, Chen X. Current detection technologies for circulating tumor cells. Chem Soc Rev. 2017;46(8):2038-56.
192. Lemma S, Perrone AM, De Iaco P, Gasparre G, Kurelac I. Current methodologies to detect circulating tumor cells: a focus on ovarian cancer. Am J Cancer Res. 2021;11(9):4111-26.

193. Bidard FC, Peeters DJ, Fehm T, Nole F, Gisbert-Criado R, Mavroudis D, et al. Clinical validity of circulating tumour cells in patients with metastatic breast cancer: a pooled analysis of individual patient data. Lancet Oncol. 2014;15(4):406-14.
194. Goodman OB, Jr., Fink LM, Symanowski JT, Wong B, Grobaski B, Pomerantz D, et al. Circulating tumor cells in patients with castration-resistant prostate cancer baseline values and correlation with prognostic factors. Cancer epidemiology, biomarkers & prevention : a publication of the American Association for Cancer Research, cosponsored by the American Society of Preventive Oncology. 2009;18(6):1904-13.
195. Cohen SJ, Punt CJ, Iannotti N, Saidman BH, Sabbath KD, Gabrail NY, et al. Relationship of circulating tumor cells to tumor response, progression-free survival, and overall survival in patients with metastatic colorectal cancer. Journal of clinical oncology : official journal of the American Society of Clinical Oncology. 2008;26(19):3213-21.
196. Gazzaniga P, Raimondi C, Gradilone A, Biondi Zoccai G, Nicolazzo C, Gandini O, et al. Circulating tumor cells in metastatic colorectal cancer: do we need an alternative cutoff? J Cancer Res Clin Oncol. 2013;139(8):1411-6.
197. Han L, Chen W, Zhao Q. Prognostic value of circulating tumor cells in patients with pancreatic cancer: a meta-analysis. Tumour Biol. 2014;35(3):2473-80.
198. Kurihara T, Itoi T, Sofuni A, Itokawa F, Tsuchiya T, Tsuji S, et al. Detection of circulating tumor cells in patients with pancreatic cancer: a preliminary result. J Hepatobiliary Pancreat Surg. 2008;15(2):189-95.
199. Bidard FC, Huguet F, Louvet C, Mineur L, Bouche O, Chibaudel B, et al. Circulating tumor cells in locally advanced pancreatic adenocarcinoma: the ancillary CirCe 07 study to the LAP 07 trial. Annals of oncology : official journal of the European Society for Medical Oncology / ESMO. 2013;24(8):2057-61.
200. Bissolati M, Sandri MT, Burtulo G, Zorzino L, Balzano G, Braga M. Portal vein-circulating tumor cells predict liver metastases in patients with resectable pancreatic cancer. Tumour biology : the journal of the International Society for Oncodevelopmental Biology and Medicine. 2015;36(2):991-6.
201. Okubo K, Uenosono Y, Arigami T, Mataki Y, Matsushita D, Yanagita S, et al. Clinical impact of circulating tumor cells and therapy response in pancreatic cancer. Eur J Surg Oncol. 2017;43(6):1050-5.
202. Earl J, Garcia-Nieto S, Martinez-Avila JC, Montans J, Sanjuanbenito A, Rodriguez-Garrote M, et al. Circulating tumor cells (Ctc) and kras mutant circulating free Dna (cfdna) detection in peripheral blood as biomarkers in patients diagnosed with exocrine pancreatic cancer. BMC cancer. 2015;15:797.
203. Dotan E, Alpaugh RK, Ruth K, Negin BP, Denlinger CS, Hall MJ, et al. Prognostic Significance of MUC-1 in Circulating Tumor Cells in Patients With Metastatic Pancreatic Adenocarcinoma. Pancreas. 2016;45(8):1131-5.
204. Negin BP, Cohen SJ. Circulating tumor cells in colorectal cancer: past, present, and future challenges. Curr Treat Options Oncol. 2010;11(1-2):1-13.
205. Khoja L, Lorigan P, Zhou C, Lancashire M, Booth J, Cummings J, et al. Biomarker utility of circulating tumor cells in metastatic cutaneous melanoma. J Invest Dermatol. 2013;133(6):1582-90.
206. Martini V, Timme-Bronsert S, Fichtner-Feigl S, Hoeppner J, Kulemann B. Circulating Tumor Cells in Pancreatic Cancer: Current Perspectives. Cancers (Basel). 2019;11(11).
207. Brychta N, Drosch M, Driemel C, Fischer JC, Neves RP, Esposito I, et al. Isolation of circulating tumor cells from pancreatic cancer by automated filtration. Oncotarget. 2017;8(49):86143-56.
208. Akita H, Nagano H, Takeda Y, Eguchi H, Wada H, Kobayashi S, et al. Ep-CAM is a significant prognostic factor in pancreatic cancer patients by suppressing cell activity. Oncogene. 2011;30(31):3468-76.

209. Jolly MK, Somarelli JA, Sheth M, Biddle A, Tripathi SC, Armstrong AJ, et al. Hybrid epithelial/mesenchymal phenotypes promote metastasis and therapy resistance across carcinomas. Pharmacol Ther. 2019;194:161-84.
210. Catenacci DV, Chapman CG, Xu P, Koons A, Konda VJ, Siddiqui UD, et al. Acquisition of Portal Venous Circulating Tumor Cells From Patients With Pancreaticobiliary Cancers by Endoscopic Ultrasound. Gastroenterology. 2015;149(7):1794-803 e4.
211. Colombano SP, Reese PA. The cascade theory of metastatic spread: are there generalizing sites? Cancer. 1980;46(10):2312-4.
212. Rahbari NN, Bork U, Kircher A, Nimitz T, Scholch S, Kahlert C, et al. Compartmental differences of circulating tumor cells in colorectal cancer. Ann Surg Oncol. 2012;19(7):2195-202.
213. Jiao LR, Apostolopoulos C, Jacob J, Szydlo R, Johnson N, Tsim N, et al. Unique localization of circulating tumor cells in patients with hepatic metastases. J Clin Oncol. 2009;27(36):6160-5.
214. Tien YW, Kuo HC, Ho BI, Chang MC, Chang YT, Cheng MF, et al. A High Circulating Tumor Cell Count in Portal Vein Predicts Liver Metastasis From Periampullary or Pancreatic Cancer: A High Portal Venous CTC Count Predicts Liver Metastases. Medicine (Baltimore). 2016;95(16):e3407.
215. Castro-Giner F, Aceto N. Tracking cancer progression: from circulating tumor cells to metastasis. Genome Med. 2020;12(1):31.
216. Miyamoto DT, Ting DT, Toner M, Maheswaran S, Haber DA. Single-Cell Analysis of Circulating Tumor Cells as a Window into Tumor Heterogeneity. Cold Spring Harb Symp Quant Biol. 2016;81:269-74.
217. Nelep C, Eberhardt J. Automated rare single cell picking with the ALS cellcelector. Cytometry A. 2018;93(12):1267-70.
218. Rossi E, Zamarchi R. Single-Cell Analysis of Circulating Tumor Cells: How Far Have We Come in the -Omics Era? Front Genet. 2019;10:958.
219. Lampignano R, Yang L, Neumann MHD, Franken A, Fehm T, Niederacher D, et al. A Novel Workflow to Enrich and Isolate Patient-Matched EpCAM(high) and EpCAM(low/negative) CTCs Enables the Comparative Characterization of the PIK3CA Status in Metastatic Breast Cancer. Int J Mol Sci. 2017;18(9).
220. Neumann MH, Schneck H, Decker Y, Schomer S, Franken A, Endris V, et al. Isolation and characterization of circulating tumor cells using a novel workflow combining the CellSearch((R)) system and the CellCelector(). Biotechnol Prog. 2017;33(1):125-32.
221. Di Trapani M, Manaresi N, Medoro G. DEPArray system: An automatic image-based sorter for isolation of pure circulating tumor cells. Cytometry A. 2018;93(12):1260-6.
222. Neves RP, Raba K, Schmidt O, Honisch E, Meier-Stiegen F, Behrens B, et al. Genomic high-resolution profiling of single CKpos/CD45neg flow-sorting purified circulating tumor cells from patients with metastatic breast cancer. Clin Chem. 2014;60(10):1290-7.
223. Tamminga M, Andree KC, van den Bos H, Hiltermann TJN, Mentink A, Spierings DCJ, et al. Leukapheresis increases circulating tumour cell yield in non-small cell lung cancer, counts related to tumour response and survival. Br J Cancer. 2022;126(3):409-18.
224. Tibbe AG, Miller MC, Terstappen LW. Statistical considerations for enumeration of circulating tumor cells. Cytometry A. 2007;71(3):154-62.
225. Coumans FA, Ligthart ST, Uhr JW, Terstappen LW. Challenges in the enumeration and phenotyping of CTC. Clin Cancer Res. 2012;18(20):5711-8.
226. Edd JF, Mishra A, Dubash TD, Herrera S, Mohammad R, Williams EK, et al. Microfluidic concentration and separation of circulating tumor cell clusters from large blood volumes. Lab Chip. 2020;20(3):558-67.
227. Fischer JC, Niederacher D, Topp SA, Honisch E, Schumacher S, Schmitz N, et al. Diagnostic leukapheresis enables reliable detection of circulating tumor cells of nonmetastatic cancer patients. Proceedings of the National Academy of Sciences of the United States of America. 2013;110(41):16580-5.

228. Greze V, Chambon F, Merlin E, Rochette E, Isfan F, Demeocq F, et al. Leukapheresis in management of hyperleukocytosis in children's leukemias. J Pediatr Hematol Oncol. 2014;36(8):e513-7.
229. Hutt D, Bielorai B, Baturov B, Z'Orbinski I, Ilin N, Adam E, et al. Feasibility of leukapheresis for CAR T-cell production in heavily pre-treated pediatric patients. Transfus Apher Sci. 2020;59(4):102769.
230. Andree KC, Mentink A, Zeune LL, Terstappen L, Stoecklein NH, Neves RP, et al. Toward a real liquid biopsy in metastatic breast and prostate cancer: Diagnostic LeukApheresis increases CTC yields in a European prospective multicenter study (CTCTrap). Int J Cancer. 2018;143(10):2584-91.
231. Fehm TN, Meier-Stiegen F, Driemel C, Jager B, Reinhardt F, Naskou J, et al. Diagnostic leukapheresis for CTC analysis in breast cancer patients: CTC frequency, clinical experiences and recommendations for standardized reporting. Cytometry Part A : the journal of the International Society for Analytical Cytology. 2018;93(12):1213-9.
232. Stoecklein NH, Fischer JC, Niederacher D, Terstappen LW. Challenges for CTC-based liquid biopsies: low CTC frequency and diagnostic leukapheresis as a potential solution. Expert Rev Mol Diagn. 2016;16(2):147-64.
233. Lambros MB, Seed G, Sumanasuriya S, Gil V, Crespo M, Fontes M, et al. Single-Cell Analyses of Prostate Cancer Liquid Biopsies Acquired by Apheresis. Clin Cancer Res. 2018;24(22):5635-44.
234. Mout L, van Dessel LF, Kraan J, de Jong AC, Neves RPL, Erkens-Schulze S, et al. Generating human prostate cancer organoids from leukapheresis enriched circulating tumour cells. Eur J Cancer. 2021;150:179-89.
235. Habli Z, AlChamaa W, Saab R, Kadara H, Khraiche ML. Circulating Tumor Cell Detection Technologies and Clinical Utility: Challenges and Opportunities. Cancers (Basel). 2020;12(7).
236. Deng G, Krishnakumar S, Powell AA, Zhang H, Mindrinos MN, Telli ML, et al. Single cell mutational analysis of PIK3CA in circulating tumor cells and metastases in breast cancer reveals heterogeneity, discordance, and mutation persistence in cultured disseminated tumor cells from bone marrow. BMC Cancer. 2014;14:456.
237. Gerlinger M, Rowan AJ, Horswell S, Math M, Larkin J, Endesfelder D, et al. Intratumor heterogeneity and branched evolution revealed by multiregion sequencing. N Engl J Med. 2012;366(10):883-92.
238. Stoecklein NH, Fluegen G, Guglielmi R, Neves RPL, Hackert T, Birgin E, et al. Ultra-sensitive CTC-based liquid biopsy for pancreatic cancer enabled by large blood volume analysis. Mol Cancer. 2023;22(1):181.
239. Sobin LH, Compton CC. TNM seventh edition: what's new, what's changed: communication from the International Union Against Cancer and the American Joint Committee on Cancer. Cancer. 2010;116(22):5336-9.
240. Zeune L, van Dalum G, Decraene C, Proudhon C, Fehm T, Neubauer H, et al. Quantifying HER-2 expression on circulating tumor cells by ACCEPT. PLoS One. 2017;12(10):e0186562.
241. de Wit S, Zeune LL, Hiltermann TJN, Groen HJM, Dalum GV, Terstappen L. Classification of Cells in CTC-Enriched Samples by Advanced Image Analysis. Cancers (Basel). 2018;10(10).
242. Klein CA, Schmidt-Kittler O, Schardt JA, Pantel K, Speicher MR, Riethmuller G. Comparative genomic hybridization, loss of heterozygosity, and DNA sequence analysis of single cells. Proc Natl Acad Sci U S A. 1999;96(8):4494-9.
243. Stoecklein NH, Erbersdobler A, Schmidt-Kittler O, Diebold J, Schardt JA, Izbicki JR, et al. SCOMP is superior to degenerated oligonucleotide primed-polymerase chain reaction for global amplification of minute amounts of DNA from microdissected archival tissue samples. Am J Pathol. 2002;161(1):43-51.
244. Mohlendick B, Bartenhagen C, Behrens B, Honisch E, Raba K, Knoefel WT, et al. A robust method to analyze copy number alterations of less than 100 kb in single cells using oligonucleotide array CGH. PLoS One. 2013;8(6):e67031.

245. Franken A, Honisch E, Reinhardt F, Meier-Stiegen F, Yang L, Jaschinski S, et al. Detection of ESR1 Mutations in Single Circulating Tumor Cells on Estrogen Deprivation Therapy but Not in Primary Tumors from Metastatic Luminal Breast Cancer Patients. J Mol Diagn. 2020;22(1):111-21.
246. Afgan E, Baker D, Batut B, van den Beek M, Bouvier D, Cech M, et al. The Galaxy platform for accessible, reproducible and collaborative biomedical analyses: 2018 update. Nucleic Acids Res. 2018;46(W1):W537-W44.
247. Thorvaldsdottir H, Robinson JT, Mesirov JP. Integrative Genomics Viewer (IGV): high-performance genomics data visualization and exploration. Brief Bioinform. 2013;14(2):178-92.
248. Ferrarini A, Forcato C, Buson G, Tononi P, Del Monaco V, Terracciano M, et al. A streamlined workflow for single-cells genome-wide copy-number profiling by low-pass sequencing of LM-PCR whole-genome amplification products. PLoS One. 2018;13(3):e0193689.
249. Zipursky A, Bow E, Seshadri RS, Brown EJ. Leukocyte density and volume in normal subjects and in patients with acute lymphoblastic leukemia. Blood. 1976;48(3):361-71.
250. Bamford S, Dawson E, Forbes S, Clements J, Pettett R, Dogan A, et al. The COSMIC (Catalogue of Somatic Mutations in Cancer) database and website. British journal of cancer. 2004;91(2):355-8.
251. Yao Y, Dai W. Genomic Instability and Cancer. J Carcinog Mutagen. 2014;5.
252. Esteves L, Caramelo F, Ribeiro IP, Carreira IM, de Melo JB. Probability distribution of copy number alterations along the genome: an algorithm to distinguish different tumour profiles. Sci Rep. 2020;10(1):14868.
253. Tamminga M, Andree KC, Hiltermann TJN, Jayat M, Schuuring E, van den Bos H, et al. Detection of Circulating Tumor Cells in the Diagnostic Leukapheresis Product of Non-Small-Cell Lung Cancer Patients Comparing CellSearch((R)) and ISET. Cancers (Basel). 2020;12(4).
254. Zeune LL, de Wit S, Berghuis AMS, MJ IJ, Terstappen L, Brune C. How to Agree on a CTC: Evaluating the Consensus in Circulating Tumor Cell Scoring. Cytometry A. 2018;93(12):1202-6.
255. Stevens M, Nanou A, Terstappen L, Driemel C, Stoecklein NH, Coumans FAW. StarDist Image Segmentation Improves Circulating Tumor Cell Detection. Cancers (Basel). 2022;14(12).
256. Sarantis P, Koustas E, Papadimitropoulou A, Papavassiliou AG, Karamouzis MV. Pancreatic ductal adenocarcinoma: Treatment hurdles, tumor microenvironment and immunotherapy. World J Gastrointest Oncol. 2020;12(2):173-81.
257. Franken A, Driemel C, Behrens B, Meier-Stiegen F, Endris V, Stenzinger A, et al. Label-Free Enrichment and Molecular Characterization of Viable Circulating Tumor Cells from Diagnostic Leukapheresis Products. Clinical chemistry. 2019;65(4):549-58.
258. Gao Y, Ni X, Guo H, Su Z, Ba Y, Tong Z, et al. Single-cell sequencing deciphers a convergent evolution of copy number alterations from primary to circulating tumor cells. Genome Res. 2017;27(8):1312-22.
259. Luchini C, Paolino G, Mattiolo P, Piredda ML, Cavaliere A, Gaule M, et al. KRAS wild-type pancreatic ductal adenocarcinoma: molecular pathology and therapeutic opportunities. J Exp Clin Cancer Res. 2020;39(1):227.
260. Chemi F, Rothwell DG, McGranahan N, Gulati S, Abbosh C, Pearce SP, et al. Pulmonary venous circulating tumor cell dissemination before tumor resection and disease relapse. Nat Med. 2019;25(10):1534-9.
261. Edil BH, Luo W, Li M. Genomic and single cell sequencing facilitate the dissection of heterogeneity of pancreatic tumors. BMC Med. 2020;18(1):177.
262. Hasanain A, Blanco BA, Yu J, Wolfgang CL. The importance of circulating and disseminated tumor cells in pancreatic cancer. Surg Open Sci. 2019;1(2):49-55.
263. Evan T, Wang VM, Behrens A. The roles of intratumour heterogeneity in the biology and treatment of pancreatic ductal adenocarcinoma. Oncogene. 2022;41(42):4686-95.
264. Lawson DA, Kessenbrock K, Davis RT, Pervolarakis N, Werb Z. Tumour heterogeneity and metastasis at single-cell resolution. Nat Cell Biol. 2018;20(12):1349-60.
265. Greaves M, Maley CC. Clonal evolution in cancer. Nature. 2012;481(7381):306-13.

266. Yachida S, Jones S, Bozic I, Antal T, Leary R, Fu B, et al. Distant metastasis occurs late during the genetic evolution of pancreatic cancer. Nature. 2010;467(7319):1114-7.
267. Gawad C, Koh W, Quake SR. Single-cell genome sequencing: current state of the science. Nat Rev Genet. 2016;17(3):175-88.
268. Gilson P, Merlin JL, Harle A. Deciphering Tumour Heterogeneity: From Tissue to Liquid Biopsy. Cancers (Basel). 2022;14(6).
269. Massague J, Obenauf AC. Metastatic colonization by circulating tumour cells. Nature. 2016;529(7586):298-306.
270. Dai Z, Gu XY, Xiang SY, Gong DD, Man CF, Fan Y. Research and application of single-cell sequencing in tumor heterogeneity and drug resistance of circulating tumor cells. Biomark Res. 2020;8(1):60.
271. Yeo D, Bastian A, Strauss H, Saxena P, Grimison P, Rasko JEJ. Exploring the Clinical Utility of Pancreatic Cancer Circulating Tumor Cells. Int J Mol Sci. 2022;23(3).
272. Mohamed Suhaimi NA, Foong YM, Lee DY, Phyo WM, Cima I, Lee EX, et al. Non-invasive sensitive detection of KRAS and BRAF mutation in circulating tumor cells of colorectal cancer patients. Mol Oncol. 2015;9(4):850-60.
273. Tellez-Gabriel M, Heymann MF, Heymann D. Circulating Tumor Cells as a Tool for Assessing Tumor Heterogeneity. Theranostics. 2019;9(16):4580-94.
274. Ankeny JS, Court CM, Hou S, Li Q, Song M, Wu D, et al. Circulating tumour cells as a biomarker for diagnosis and staging in pancreatic cancer. British journal of cancer. 2016;114(12):1367-75.
275. Pestrin M, Salvianti F, Galardi F, De Luca F, Turner N, Malorni L, et al. Heterogeneity of PIK3CA mutational status at the single cell level in circulating tumor cells from metastatic breast cancer patients. Mol Oncol. 2015;9(4):749-57.
276. Baslan T, Kendall J, Volyanskyy K, McNamara K, Cox H, D'Italia S, et al. Novel insights into breast cancer copy number genetic heterogeneity revealed by single-cell genome sequencing. Elife. 2020;9.
277. Bednarz-Knoll N, Alix-Panabieres C, Pantel K. Clinical relevance and biology of circulating tumor cells. Breast Cancer Res. 2011;13(6):228.
278. Kulemann B, Rosch S, Seifert S, Timme S, Bronsert P, Seifert G, et al. Pancreatic cancer: Circulating Tumor Cells and Primary Tumors show Heterogeneous KRAS Mutations. Sci Rep. 2017;7(1):4510.
279. Van der Linden M, Raman L, Vander Trappen A, Dheedene A, De Smet M, Sante T, et al. Detection of Copy Number Alterations by Shallow Whole-Genome Sequencing of Formalin-Fixed, Paraffin-Embedded Tumor Tissue. Arch Pathol Lab Med. 2019.
280. Koshiba M, Ogawa K, Hamazaki S, Sugiyama T, Ogawa O, Kitajima T. The effect of formalin fixation on DNA and the extraction of high-molecular-weight DNA from fixed and embedded tissues. Pathol Res Pract. 1993;189(1):66-72.
281. Yost SE, Smith EN, Schwab RB, Bao L, Jung H, Wang X, et al. Identification of high-confidence somatic mutations in whole genome sequence of formalin-fixed breast cancer specimens. Nucleic Acids Res. 2012;40(14):e107.
282. Mishra A, Dubash TD, Edd JF, Jewett MK, Garre SG, Karabacak NM, et al. Ultrahigh-throughput magnetic sorting of large blood volumes for epitope-agnostic isolation of circulating tumor cells. Proc Natl Acad Sci U S A. 2020;117(29):16839-47.
283. Wu L, Guan G, Hou HW, Bhagat AA, Han J. Separation of leukocytes from blood using spiral channel with trapezoid cross-section. Anal Chem. 2012;84(21):9324-31.
284. Ji HM, Samper V, Chen Y, Heng CK, Lim TM, Yobas L. Silicon-based microfilters for whole blood cell separation. Biomed Microdevices. 2008;10(2):251-7.

8. APPENDIX

8.1 Supplementary tables

Supplementary table 1. Mutation analysis of targeted gene sequences in patient derived WBCs. The same genomic regions as for matching patient derived tumor cells have been sequenced and analyzed. Any pathogenic mutation was detected in CTCs. Only one cell (from patient #4) showed a SNV, but with neutral pathogenicity.
Data are part of Stoecklein, N.H., Fluegen, G., Guglielmi, R. et al., Mol Cancer (2023) (238).

Pt ID	WBC analyzed (n)	Mutation status		Pathogenicity prediction
		Mutations (Y/N)	Cell (n)	
Pt #1	3	N		
Pt #2	3	N		
Pt #3	2	N		
Pt #4	4	Y (TP53 S110P)	1	neutral
Pt #5	3	N		
Pt #6	3	N		
Pt #7	4	N		
Pt #8	4	N		
Pt #9	1	N		
Pt #10	1	N		

Supplementary table 2. Summary of sequencing data quality analysis.
Values below the acceptance criteria are labelled in red; PAG values referring to CTCs that passed the quality check analysis are pointed out (orange).
Data are part of Stoecklein, N.H., Fluegen, G., Guglielmi, R. et al., Mol Cancer (2023) (238).

Patient	Cell ID	Cell type	DLRS	IQR	total.reads	used.reads	genome_altered
patient_1	**727**	PT	0,1816154	0,1751073	389425	321727	4,87776922151732
patient_1	**C9917**	CTC	0,2181884	0,1744741	1572645	1315352	42,0890518162297
patient_1	**C9918**	CTC	0,2048953	0,1791397	1048036	876140	18,8998131953938
patient_1	**C16328**	CTC	0,2119652	0,2192597	1290529	1070246	26,3226400412809
patient_1	**W2585**	WBC	0,1430425	0,1367745	1301521	1081753	0,27457641313177
patient_1	**W4023**	WBC	0,1351795	0,1260478	6080433	5054451	0
patient_2	**723**	PT	0,1428482	0,1289831	562907	467388	0
patient_2	**C10597**	CTC	0,2296235	0,2185181	285743	236736	0
patient_3	**728**	PT	0,1688063	0,1443904	589769	487482	18,332013464974
patient_3	**C10602**	CTC	na	na	na	na	0
patient_3	**C10603**	CTC	0,2271428	0,2137900	290469	240100	4,1832524118311
patient_3	**W4016**	WBC	0,1413596	0,1206641	3699323	3065838	0
patient_4	**725**	PT	0,1507993	0,1277659	592057	491638	9,04487007963477
patient_4	**C11123**	CTC	0,1935925	0,1803388	680650	564674	0
patient_4	**W3134**	WBC	0,1341928	0,1273579	3077239	2559097	0
patient_5	**724**	PT	0,1119385	0,0954982	1194235	988202	4,15094930440381
patient_5	**C11351**	CTC	0,4859273	0,3330477	292701	239178	41,544291501908
patient_5	**C11352**	CTC	2,6033214	1,5593992	213541	174490	28,1234454412203
patient_5	**W3086**	WBC	0,1570890	0,1413595	2894794	2409113	0
patient_6	**730**	PT	0,1253089	0,1117687	735333	610741	0
patient_6	**C11569**	CTC	0,2243689	0,2135501	346587	287982	0
patient_6	**C11570**	CTC	0,2287544	0,2150931	332077	275169	0,258424859418136
patient_6	**C11571**	CTC	0,2416802	0,2278155	288238	238789	0,629910594831707
patient_6	**C11572**	CTC	0,2503451	0,2243192	261056	216387	0
patient_6	**C11573**	CTC	0,3230420	0,3202109	295258	234053	6,26680284088981
patient_6	**C11575**	CTC	0,1375590	0,1286252	7379328	6157842	2,16430819762689
patient_6	**C11576**	CTC	0,2249632	0,2104948	343698	285320	0
patient_7	**12201**	CTC	0,1792991	0,1999746	4407622	3625212	38,7809755417759
patient_7	**12202**	CTC	0,2157045	0,1939702	352955	289485	50,9562548050145
patient_7	**12204**	CTC	0,1590123	0,1653878	3163384	2602126	31,8681105523407
patient_7	**12207**	CTC	0,2022738	0,1910846	391023	323879	0
patient_7	**12214**	CTC	0,2303374	0,2095322	270454	224715	0
patient_7	**12219**	CTC	0,2485680	0,2467178	223011	185734	0
patient_7	**12222**	CTC	0,1739216	0,1736244	3028820	2489822	36,2315254054643
patient_7	**12226**	CTC	0,2701912	0,2586315	282748	234922	7,92602036145231
patient_7	**12228**	CTC	0,1741843	0,1948186	3707604	3045027	38,4256413600759
patient_7	**12229**	CTC	0,2342492	0,1865784	693440	566684	53,3360207882022
patient_7	**W3351**	WBC	0,1269200	0,1180768	3747377	3117295	0
patient_8	**726**	PT	0,1414311	0,1316677	553034	459721	0,145363983422702
patient_8	**C10589**	CTC	0,1778747	0,1783086	1397226	1159227	46,7705070427409
patient_8	**W3192**	WBC	0,1447158	0,1299038	2913565	2425187	0,226121751990869
patient_9	**C11105**	CTC	0,2318783	0,2219128	331715	273074	3,65025113928117
patient_10	**C11116**	CTC	0,2848057	0,2537113	214513	176886	4,74855679180825
patient_10	**C11117**	CTC	0,2453763	0,2502895	351154	289916	30,2866585635054
patient_10	**C11118**	CTC	0,3430098	0,2684839	125464	103397	22,3052956785279

Supplementary table 3. **Illustrative results of STR analysis.** STR-System column shows the target STR loci amplified. Squares with the same color indicate that same allele/alleles were amplified for a specific STR locus; white squares indicate that the allele/alleles were unique for the specific cell or tumor; the symbol minus is used to indicate the non-amplification of the alleles for a specific locus. Tumor was not available for patient 1 and 7. **(A) Patient 1, 2 and 3. (B) Patient 4, 5 and 6. (C) Patient 7.** CTCs are labelled with "C", tumors are labelled with "T".

A

STR-System	Patient1			Patient 2		Patient3		
	C1	C2	C3	C1	T	C1	C2	T
D3S1358	-	-						
D1S1656	-		-	-		-	-	
D6S1043	-							
D13S317	-	-	-	-		-	-	-
PENTA E	-							-
D16S539	-							
D18S51	-	-	-					
D2S1338	-	-	-	-		-	-	
CSF1PO	-	-	-	-		-	-	-
PENTA D	-	-	-	-		-	-	-
TH01								
VWA	-	-						
D21S11	-	-						
D7S820	-	-	-	-		-	-	
D5S818	-	-	-	-		-	-	-
TPOX	-	-	-			-	-	-
D8S1S391	-	-	-					
D12S391	-	-						
D19S433	-	-						
FGA	-	-	-					
AMEL	-	X	-	X	X	X Y	X Y	X Y

B

STR-System	Patient 4		Patient 5			Patient 6							
	C1	T	C1	C2	T	C1	C2	C3	C4	C5	C6	C7	T
D3S1358			-	na						-			
D1S1656	-		-	na		-	-		-	-	-		
D6S1043			-	n		-				-			
D13S317	-		-	na		-	-	-	-	-	-	-	
PENTA E		-	-	na						-			
D16S539			-	na						-			
D18S51			-	na						-			
D2S1338	-		-	na		-	-	-		-	-	-	
CSF1PO	-		-	na		-	-	-	-	-	-	-	
PENTA D	-	-	-	na		-	-	-	-	-	-	-	
TH01			-	na						-			
VWA			-	na						-			
D21S11			-	na						-			
D7S820	-		-	na		-	-	-	-	-	-	-	
D5S818	-		-	na		-	-	-	-	-	-	-	
TPOX	-		-	na		-	-	-	-	-	-	-	
D8S1S391				na						-			
D12S391			-	na						-			
D19S433			-	na		-				-			
FGA	-			na		-	-	-	-	-	-		
AMEL	-	X X	-	na	X Y	X	X	-	X	-	X	X	X X

C

STR-System	Patient 7										
	C1	C2	C3	C4	C5	C6	C7	C8	C9	C 10	C 11
D3S1358											
D1S1656	-	-	-	-	-	-	-	-	-	-	-
D6S1043			-	-							
D13S317	-	-	-	-	-	-	-	-	-	-	-
PENTA E		-									
D16S539											
D18S51		-	-			-					-
D2S1338	-	-	-	-	-	-	-	-	-	-	-
CSF1PO	-	-	-	-	-	-	-	-	-	-	-
PENTA D	-	-	-	-	-	-	-	-	-	-	-
TH01		-									
VWA											
D21S11											
D7S820	-	-	-	-	-	-	-	-	-	-	-
D5S818	-	-	-	-	-	-	-	-	-	-	-
TPOX	-	-	-	-	-	-	-	-	-	-	-
D8S1S391											
D12S391											
D19S433											
FGA											
AMEL	X	-	X	X	X	X	X	X	X	X	X

8.2 List of illustrations

8.3 List of tables

8.4 List of chemicals and kits

Chemicals/Kit	**Manifacturer**
Agarose	Sigma-Aldrich
Agencourt AMPure XP beads	Beckmann Coulter
Ampli1TM LowPass Kit for Illumina®	Menarini Silicon Biosystems
ATP	Roche Diagnostic
Broad Range Quant-iT dsDNA Assay Kit	Thermo Fisher Scientific Inc.
BSA	GE Healthcare
CellTrackerDeepRed	Invitrogen
CellTrackerGreen	Invitrogen
CellTrackerOrange	Invitrogen
ClearCell® FX Resuspension Buffer	Biolidics
CountBright™ absolute counting beads	Invitrogen
DEPArray FFPE QC Kit	Menarini Silicon Biosystems
DEPArray LibPrep kit	Menarini Silicon Biosystems
Diluent Additive	Biolidics
DMSO	Sigma Aldrich
dNTPs	GE Healthcare
DPBS	Sigma-Aldrich
DRAQ5	Thermo Fisher Scientific Inc.
EDTA	Serva
FBS	Gibco
Ficoll-Paque^{TM} PLUS	GE Healthcare
Ficoll-Paque^{TM} PREMIUM	GE Healthcare
GelRed	Biotium
GeneRuler, 50 bp	Thermo Fisher Scientific Inc.
Hoechst 33342	Thermo Fisher Scientific Inc.
HSA	Albunorm
Igepal CA-630	Sigma-Aldrich
KAPA HiFi HotStart ReadyMix	Roche Diagnostic
KAPA Library Quantification Kit	Roche Diagnostic
KAPA2G Fast Multiplex Mix	Merck
Ladder	Thermo Fisher Scientific Inc.
Low TE Buffer	Menarini Silicon Biosystems
Nuclease-free water	Gibco
PEG NaCl solution	Menarini Silicon Biosystems
Penicillin-Streptomycin	Sigma-Aldrich
SPRIselect beads	Beckman Coulter
TBE Buffer pH 8.3	Thermo Fisher Scientific Inc.
TE Buffer pH 8.0	Promega
Trypsin 0.25%	Sigma-Aldrich

8.5 Scientific Curriculum vitae

Academic education

08/2016 - 05/2021	**Heinrich-Heine-University (HHU), Düsseldorf. Department of General, Visceral and Pediatric Surgery, University Hospital of Düsseldorf**. Prof. Dr. Nikolas Stoecklein (Supervisor). PhD in Biology. Final Degree: PhD. Main topic: the role of circulating tumor cells as novel biomarkers for patients suffering of different tumor entities.
04/2015 - 07/2015	**Aldo Moro University, Bari, Italy.** State Examination for Biologists. Final Degree: certified biologist.
03/2012 - 12/2014	**Aldo Moro University, Bari, Italy.** Master´s degree in Medical Biotechnology and Molecular Medicine. Final Degree: Master of Science.
10/2008 - 03/2012	**Aldo Moro University, Bari, Italy.** Bachelor´s degree in Medical and Pharmaceutical Biotechnology. Final Degree: Bachelor of Science.

Publications

Nikolas H. Stoecklein*, Georg Flügen*, **Rosa Guglielmi***, Rui P.L. Neves*, Thilo Hackert, Emrullah Birgin, Stefan A. Cieslik, Monica Sudarsanam, Christiane Driemel, Guus van Dalum, André Franken, Dieter Niederacher, Hans Neubauer, Tanja Fehm, Jutta M. Rox, Petra Böhme, Lena Häberle, Wolfgang Göring, Irene Esposito, Stefan A. Topp, Frank A.W. Coumans, Jürgen Weitz, Wolfram T. Knoefel, Johannes C. Fischer*, Ulrich Bork*, Nuh N. Rahbari*. **Ultra-sensitive CTC-based Liquid Biopsy for Pancreatic Cancer enabled by Large Blood Volume analysis.** Mol Cancer 22, 181 (2023).
*These authors contributed equally.

R. Guglielmi, Z. Lai, K. Raba, G. van Dalum, J. Wu, B. Behrens, A. A. S. Bhagat, W. T. Knoefel, R. P. L. Neves & N. H. Stoecklein. **Technical validation of a new microfluidic device for enrichment of CTCs from large volumes of blood by using buffy coats to mimic diagnostic leukapheresis products.** Sci Rep 10, 20312 (Nov 20, 2020).

J. Wu, K. Raba, **R. Guglielmi**, B. Behrens, G. Van Dalum, G. Flugen, A. Koch, S. Patel, W.T. Knoefel, N.H. Stoecklein, R.P.L. Neves. **Magnetic-Based Enrichment of Rare Cells from High Concentrated Blood Samples.** Cancers (Basel), 12 (Apr 10, 2020).

Poster at congresses

4th ACTC (Advances in Circulating Tumor Cells; 10/2019): **A label-free CTC-enrichment method to isolate CTC from mimicked-DLA products.** R. Guglielmi (presenter), Z. Lai, K. Raba, G. V. Dalum, B. Behrens, J. Wu, R. Neves, N. H. Stoecklein.

11th ISMRC (International Symposium on Minimal Residual Cancer; 05/2018): **Testing a label-free CTC-enrichment method to isolate viable pancreatic cancer CTC.** R. Guglielmi (presenter), R.P.L. Neves, K. Raba, B. Behrens, N. H. Stoecklein.

8.6 Statement

Hiermit erkläre ich, Rosa Guglielmi, dass ich die vorliegende Dissertation selbstständig verfasst und bei keiner anderen Universität bzw. Fakultät in der vorgelegten oder einer ähnlichen Form eingereicht habe. Für die Anfertigung der Dissertation habe ich keine anderen als die angegebenen Hilfsmittel verwendet. Die Stellen, die anderen Arbeiten dem Wortlaut oder dem Sinn nach entnommen sind, wurden unter Angabe der dazugehörigen Quelle kenntlich gemacht.

Düsseldorf, 30/03/2023

Rosa Guglielmi

ACKNOWLEDGMENTS

I want to express my gratitude to all the patients and the healthy volunteers who donated blood samples. The importance of their contribution is priceless.

I am grateful to my Supervisor, Prof. Dr. Stoecklein, who gave me the opportunity to join his team. I want to thank him for the mentoring, the constant encouragement and all the support.

I would like to thank the whole lab team. Each of my colleagues contributed to both my personal and academic development. They were a second family during my time away from home and they will always hold a special place in my heart.
A special thank goes to Rui and Bianca, who shared their precious knowledge with me and were my mentors, always ready to help and motivate me.

Thanks to Rita for all the professional help, advice, and support. She and Miryam have been part of my experience in Germany from the very beginning and with their friendship, they always made me feel at home.

I want to express my gratitude to my mum, my dad and my brother. Being far away is not easy, but their constant support, love and encouragement push me to always give my best. I know that distance is very hard for them too, but I hope to make them proud of me.

Last but not least, I want to thank my life partner, who is always by my side supporting my choices. I thank him for all the patience and the respect he has for me and my professional career.